Characterization and Properties of Sulfonated Chitosan Membrane for Direct Methanol Fuel Cell

By

Livhuwani Elsie Modau (12739634)

Submitted in accordance with the requirements for the degree of

Master of Engineering (MEng) (90121)

Submitted to

Department of Chemical Engineering, School of Engineering, College of Science, Engineering, and Technology

Supervisor: Dr Rudzani Sigwadi

Co-supervisor: Prof Touhami Mokrani

: Prof Fulufhelo Nemavhola

Declaration

I, Livhuwani Elsie Modau, Student number, 12739634, hereby certify that this dissertation, titled Characterization, and properties of sulfonated chitosan membrane for direct methanol fuel cell, is solely my original work. This dissertation is submitted in fulfillment of the requirements for the degree of Master of engineering: Chemical Engineering at the University of South Africa.

Signature……………………..

Livhuwani Elsie Modau

Date…11 April 2023….

Abstract

This dissertation examines the structure and properties of chitosan membranes regarding their applicability in fuel cells. The objective of this work is to synthesize a polymer membrane with improved properties such as high proton conductivity, low water uptake, low methanol permeability, and high efficiency. Membranes made of synthetic polymeric materials with enhanced functionality have been developed to compensate for Nafion® deficiency. Polymeric membranes have numerous benefits, including an excellent mechanism for pore-forming control, high mechanical strength, low cost, and greater flexibility.

The membrane properties such as identification of functional groups using Fourier Transform Infrared (FTIR), physical properties using Scanning Electron Microscope (SEM), water uptake, Ion Exchange Capacity (IEC), proton conductivity, methanol permeability, and tensile strength were evaluated. Silica is used as a filler, and it was synthesized through Sol-gel and Stober methods and was calcinated for 2h and 24h. Synthesized silica particles were categorized as pure and sulfonated.

The membranes showed successful modification with silica. It was found that the water uptake and proton conductivity of the unmodified and modified silica/chitosan membrane increase with an increase in filler content. The s-SiO$_2$/Cs membranes show improvement in membrane properties, particularly, the 4% s-SiO$_2$/Cs (Sol-gel 24h) which has superior proton conductivity of 0.238 Scm^{-1} which is higher than that of Nafion® of 1.43 x 10^{-2} Scm^{-1}. However, this membrane has a methanol permeability of 0.97×10^{-7} cm^{2}s^{-1} which is higher than 2.83 x10^{-6} cm^{2}s^{-1} of Nafion®. The selectivity of the fabricated membrane is 1.269 x 10^5 S.s/cm^{-3} which is higher compared to that of Nafion® of 3.71 x 10^4 S.s/cm^{-3}.

It was found that the incorporation of silica particles successfully improves the chitosan membrane's proton conductivity while suppressing its methanol permeability. The recommended synthesis method of silica is by Sol-gel, and it is significant to introduce sulfonic groups in the silica as to improve its suitability as a membrane filler.

Acknowledgments

List of abbreviation

AFC	Alkaline Fuel Cell
BET	Braeuer Emmert teller
CS	Chitosan
DMFC	Direct Methanol Fuel Cell
DMF	Dimethylformamide
FTIR	Fourier Transformed Infrared
FC	Fuel Cell
IEC	Ion Exchange Capacity
MCFC	Molten carbonate fuel cell
PAFC	Phosphoric Acid Fuel Cell
PEM	Proton Exchange Membrane
PEMFC	Proton Exchange Membrane Fuel Cell
SiO_2	Silica
s-SiO_2	Sulfonated Silica
SEM	Scanning Electron Microscopy
SOFC	Solid Oxide Fuel Cell
XRD	X-Ray Diffraction

Keywords

Characterization

Chitosan

Fuel cell

Ion exchange

Membrane

Methanol

Particles

Permeability

Proton conductivity

Silica

Sulfonated silica

Water-uptake

Table of content

Contents

List of figures

List of tables

Chapter 1 Introduction

1.1. Background

Interest in the fuel cell has been motivated by a lack of clean energy sources, as well as the energy crisis that is faced globally (Smitha, Sridhar, and Khan, 2005). Research has been done on investigating the use and suitability of fuel cells in energy generation. The first hydrogen-oxygen fuel cell was made by William Groove in the year 1839 (Wisniak, 2015). Groove's invention proved that combining oxygen and hydrogen produces electric current and water (Douglas and Liebhafsky, 1960). Later, in 1889 Charles Langer and Ludwig Mond constructed an alkaline type of cell that utilizes industrial coal gas and air, this cell was later modified in 1932 by Bacon (Douglas and Liebhafsky, 1960; Wisniak, 2015). Fuel cells come in a variety of forms, including proton exchange membrane fuel cells (PEMFCs), alkaline fuel cells (AFCs), solid oxide fuel cells (SOFCs), molten carbonate fuel cells (MCFCs), and phosphoric acid fuel cells (PACs) (Jawad *et al.*, 2022).

The most promising type of fuel cell is the direct methanol fuel cell (DMFC) compared to other types of fuel cells (Ahmed *et al.*, 2022). It utilizes a polymer electrolyte membrane (PEM) which is the most important material of this cell (Ahmed *et al.*, 2022). The membrane material act as a pathway for the anode's protons to the cathode compartment and it also inhibits direct contact by electric means between the cathode and anode (Ahmad *et al.*, 2010; Ahmed *et al.*, 2022). A good PEM must have high ionic conductivity, low fuel permeation, and must have good thermal stability for suitability in various applications (Zhu *et al.*, 2022). Perflurosulphonic membrane such as Nafion® 117, for example, it's been the most popularly utilized DMFC membrane as it possesses good thermal stability and excellent proton conductivity, however, is non-ecofriendly, and the production cost is expensive (Sigwadi, Dhlamini, Mokrani, Ņemavhola, *et al.*, 2019; Ng *et al.*, 2022; Selim, Szijjártó and Tompos, 2022; Zhu *et al.*, 2022). Many researchers have been trying to find a better substitute material that calls for biopolymer membranes such as chitosan as a substitute. Chitosan is a plant-based polymer that is derived from the deacetylation of chitin, it is a low-cost polymer and can operate at high temperatures and it is naturally abundant. The chitosan

materials also have some shortcomings such as high-water uptake (Ng *et al.*, 2022). To improve the ionic conductivity of the chitosan polymer, it's imperative to be modified, which can be achieved through chemical or physical modifications (Zhu *et al.*, 2022). The free amino and hydroxyl groups make it easy for the biopolymer to be modified. Improvements to chitosan proton conductivity are possible by chemically adding hygroscopic inorganic filler such as silicon dioxide to the polymer matrix (Li, Elango and Wu, 2020; Adiyar *et al.*, 2021a; Ding, 2022). Researchers have shown that the silica particles and their large surface area make the incorporation of silica into chitosan simple as it is easy for them to penetrate the membrane film (Kusumastuti *et al.*, 2016a).

The other advantage of adding nano-silica particles is that it limits the displacement of methanol on the membrane by closing pores of the membrane. Reports have indicated that it also minimizes the crystallinity of the membrane while increasing its mechanical toughness properties such as tensile strength, Resistant to water, and intensive stretching. The presence of nano-silica particles also assists in keeping the biopolymer hydration when the fuel cell is operated at elevated temperatures, by managing water absorption of the membrane (Hanna Rosli *et al.*, 2020). Also, fuel crossover on the chitosan-silica membrane decreases with a decrease in membrane swelling degree, which is believed to be affected by the ionic interaction that happens between chitosan chains (Hanna Rosli *et al.*, 2020). The ionic interaction is believed to be influenced by crosslink density. Furthermore, the swelling degree of chitosan decrease as the crosslink density increases. Sulfuric acid is the most used crosslinking agent for the modification of chitosan, it helps in reducing the swelling of the chitosan membrane (Gierszewska-Drużyńska and Ostrowska-Czubenko, 2011).

1.2.   Problem Statement

The negative impact posed on the environment by using fossil fuels as a source of energy calls for a better alternative. Fossil fuels emit greenhouse gases which are also non-renewable and pose a threat to the generation of power as well as the health of humans. Fuel cell technology has been identified as the best alternative for replacing fossil fuels as it is environmentally friendly. The hydrogen fuel cell was the most used ancient technology; however, its use is limited due to

hydrogen storage and safety. This has sparked research interest in DMFC as promising, when compared to other forms of fuel cells, this sort of fuel cell has a lot of advantages. Nafion® 117 has been the most commercially used polymer in DMFCs. However, the production cost of Nafion is high and it also has some limitations such as high methanol crossover. Much research has been done in improving properties of Nafion® 117 and it was a success in terms of lowering methanol permeability while keeping its proton conductivity high, however the biggest challenge is still the cost. A research gap exists in the development of a fuel cell that uses a cheap polymer that is naturally abundant like chitosan, and the other requirements of the polymer include, good water retention, proton conductivity, and good thermal and mechanical stabilities for application in the fuel cell. The chitosan polymer is only limited by its hydrophilic nature, however, if modified it exhibits great potential for application in the fuel cell.

- It is environmentally friendly and cheap.

    (i)   Advantages of using chitosan polymer:

- Can operate at high temperatures; and
- Functional groups on its backbone make it easy for modification.

    (ii)   Advantages of adding nano-silica fillers:

- Increase proton conductivity.
- Reduce methanol permeability; and
- Improved overall cell efficiency.

1.3.   Research Questions

- Will the modification of the chitosan membrane improve its chemical structure?
- What will happen to the water uptake, proton conductivity, ion exchange capacity, and methanol permeability of the modified chitosan membrane?
- What will the membrane morphology look like after modification?

- Will the mechanical strength of the membrane be improved after modification?

1.4. Aim

This research aims to improve the properties of chitosan membranes such as water uptake, proton conductivity, and permeability for its application in a fuel cell.

1.5. Specific Objectives

- To synthesize silica (silicon dioxide).

- To prepare silica/chitosan membrane.

- To evaluate the effects of silica content on membrane properties (water uptake, proton conductivity, permeability).

- To compare the mechanical properties of unmodified chitosan and modified chitosan.

1.6. Hypothesis

Modified chitosan membranes will show high proton conductivity with reduced fuel permeability compared to unmodified chitosan.

1.7. Research Scope: Overview

Chapter 1: Introduction, problem statement, research questions, aims, objective and specific objectives, and hypothesis.

Chapter 2: Types of fuel cells, types of membranes, different kinds of fillers, and application of fuel cells.

Chapter 3: Methodology and research procedures.

Chapter 4: Synthesis of silica particles, results, and discussion.

Chapter 5: Fabrication of chitosan membranes, results, and discussion.

Chapter 6: Conclusion and future work.

1.8. References

Adiyar, S.R., Satriyatama, A., Anjuba, A.N. and Sari, N.K.A.K. (2021) 'An overview of synthetic polymer-based membrane modified with chitosan for direct methanol fuel cell application', IOP Conference Series: Materials Science and Engineering, 1143(1).

Ahmad, H., Kamarudin, S.K., Hasran, U.A, and Daud, W.R.W. (2010) 'Overview of hybrid membranes for direct-methanol fuel-cell applications', International Journal of Hydrogen Energy,35(5), pp.2160–2175.

Ahmed, A.A., Labadi, M.A., Hamada, A.T. and Orhan, M.F. (2022) 'Design and Utilization of a Direct Methanol Fuel Cell', Membranes, 12(12).pp 1266.

Ding, N. (2022) 'Homogeneous Etherification Modification of Chitosan and Preparation of High-Strength Hydrogel', Journal of Physics: Conference Series, 2261(1).

Douglas, D.L. and Liebhafsky, H.A. (1960) 'Fuel cells: History, operation, and applications, Physics. 13(6), pp. 26–30.

Gierszewska-Drużyńska, M. and Ostrowska-Czubenko, J. (2011) 'Influence of Crosslinking Process Conditions on Molecular and Supermolecular Structure of Chitosan Hydrogel Membrane', Progress in the Chemistry and Application of Chitin and its Derivatives, pp. 15-22.

Hanna Rosli, N.A., Loh, K.S., Wong, W.Y., Lee, T.K., Ahmad, A. and Chong, S.T. (2020) 'Review of chitosan-based polymers as proton exchange membranes and roles of chitosan-supported ionic liquids', International Journal of Molecular Sciences. MDPI AG.

Jawad, N.H., Yahya, A., Al-Shathr, A.R., Salih, H.G., Rashid, K.T., Al-Saadi, S., Abdul Razak, A.A., Salih, I.K., Zreli, A. and Alsalhy, Q.F. (2022) 'Fuel Cell Types, Properties of Membrane, and Operating Conditions: A Review', Sustainability (Switzerland), 14(21).pp. 2-9.

Kusumastuti, E., Siniwi, W.T., Mahatmanti, F.W., Atmaja, J.L. and Widiastuti, N. (2016) 'Modification of chitosan membranes with nano silica particles as polymer electrolyte membranes', in AIP Conference Proceedings. American Institute of Physics Inc.

Li, B., Elango, J. and Wu, W. (2020) 'Recent advancement of molecular structure and biomaterial function of chitosan from marine organisms for pharmaceutical and nutraceutical application', Applied Sciences (Switzerland), 10(14), pp. 30–50.

Ng, W.W., Thiam, H.S., Pang, Y.L., Chong, K.C. and Lai, S.O. (2022) 'A State-of-Art on the Development of Nafion-Based Membrane for Performance Improvement in Methanol Fuel Cells', Membranes,12(5).

Selim, A., Szijjártó, G.P. and Tompos, A. (2022) 'Insights into the Influence of Different Pre-Treatments on Physicochemical Properties of Nafion XL Membrane and Fuel Cell Performance', Polymers, 14(16). pp 3385-3385

Sigwadi, R., Dlamimi, M.S., Mokraini, T., Nemavhola, F., Nonjola, P.F. and Msomi, P.F. (2019) 'The proton conductivity and mechanical properties of Nafion®/ ZrP nanocomposite membrane', Heliyon, 5(8).

Smitha, B., Sridhar, S. and Khan, A.A. (2005) 'Solid polymer electrolyte membranes for fuel cell applications - A review', Journal of Membrane Science, 259(1–2), pp. 10–26.

Wisniak, J. (2015) 'Historical Notes: Electrochemistry and Fuel Cells: The Contribution of William Robert Grove', Indian Journal of History of Science, 50(4), pp. 476-490.

Zhu, L.Y., Li, Y.C., Liu, J., He, L., Wang, L.W. and Lei, J.D. (2022) 'Recent developments in high-performance Nafion membranes for hydrogen fuel cells applications', Petroleum Science, 19(3), pp. 1371–1381.

Chapter 2 Literature review

2.1. Fuel Cell Technology

The use of electrochemical fuel cells is the most convenient method for replacing fossil fuels as an energy source (Shaari and Kamarudin, 2015; Hanna Rosli *et al.*, 2020). These cells convert electrochemical energy into electricity (Hanna Rosli *et al.*, 2020). Figure 2.1. indicate a typical fuel cell. The operation technique of fuel cell is like that of batteries, and a steady fuel supply is crucial (Winter and Brodd, 2004; Wisniak, 2015; Wang *et al.*, 2019). Fuel such as hydrogen, ethanol, and methanol are used as power sources (Hanna Rosli et al., 2020a). Fuel cells using polymeric membranes have been the most popular alternative means of energy generation due to them being environmentally friendly and having high effectiveness (Niakolas *et al.*, 2016; Goh *et al.*, 2021).
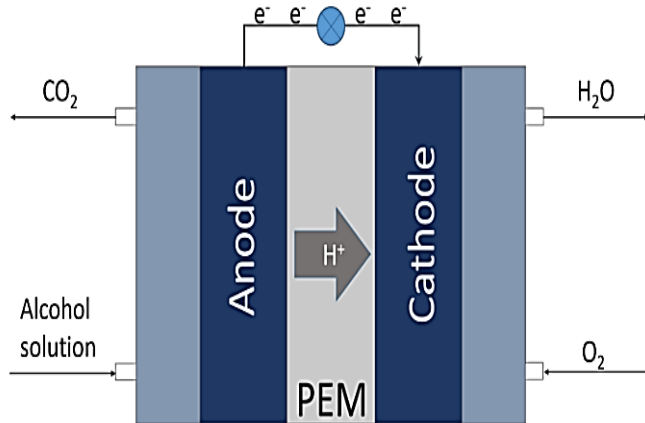
Figure 2.1. Fuel cell (Wala and Simka, 2021).

Polymer electrolyte membrane fuel cell (PEMFC) uses a polymer material such as Nafion[®], chitosan, and other polymers for ionic transport, hence ionic transport is a very crucial aspect of the membrane (Hlavatá *et al.*, 2014; Ghassemi and Slaughter, 2017; Myndrul *et al.*, 2022; Zhu *et al.*, 2022, 2022). Direct methanol fuel cell (DMFC) is one of the most favoured types of fuel cell

because it is simple to manage and simply distribute methanol and store fuel (Ramkrishna Joshi, 2014; Sajgure *et al.*, 2016; Ahmed *et al.*, 2022). The success of this type of cell is dependent on the polymer membrane, which is assigned for transport in the cell, the membrane polymer must possess exceptionally good proton conductivity, low fuel permeability, excellent thermal performance, and mechanical stability. (Ramkrishna Joshi, 2014; Baroutaji, Arjunan, Alaswad, *et al.*, 2021). The utilization of organic-inorganic composite membranes with improved proton conduction, mechanical properties, water retention, and added low-fuel crossover can be a cost-effective and practical solution to improve PEM performance (Alaswad, *et al.*, 2021).

2.2. Direct Methanol Fuel Cell

2.2.1. Principle of Operations

Recently, direct methanol fuel cells (DMFCs), because of their distinct characteristics (densely packed power, volume, and weight), have gotten a lot of attention (Scott and Xing, 2012; Weber, Balasubramanian and Das, 2012; Walkowiak-Kulikowska, Wolska and Koroniak, 2017; Sun *et al.*, 2019). DMFC utilizes electrolyte polymer film which is used for transport(Junoh *et al.*, 2015, 2020a). The conductive membrane in the cell is utilized for separating the cathode and anode (Hacquard, no date; Masdar *et al.*, 2017).

Methanol is used as a fuel in DMFC to produce protons. The methanol-based mixture and water are fed directly to the anode of DMFC. The methanol-based mixture is further oxidized to form carbon dioxide and other by-products like formic acid, formaldehyde, and carbon monoxide which influence the methanol oxidation reaction to have sluggish kinetics at the anode (Zhang and Pandalai, 2005; Awang *et al.*, 2015a; Junoh *et al.*, 2015, 2020b; Feng *et al.*, 2022). Protons are produced during the oxidation of methanol (MOR) and pass through a polymer membrane connecting the anode and cathode compartments, while electrons travel through the external circuit of the cell (Cho, Kim and Chang, 2009; Tafaoli-Masoule, Bahrami and Mohammadrezaei, 2013; Feng, Liu and Yang, 2017; Ahmed *et al.*, 2022). Furthermore, at the cathode, oxygen interacts with protons and electrons to make water. The operation differs from that of an alkaline DMFC as in this type of hydroxyl ions are utilized to oxidize the methanol and water is generated at the

anode (Ahmad *et al.*, 2010; Ramkrishna Joshi, 2014; Ng *et al.*, 2022). Below in Figure 2.6. is an illustration of DMFC and the redox-chemical reactions that occur in DMFCs (Junoh et al., 2015).
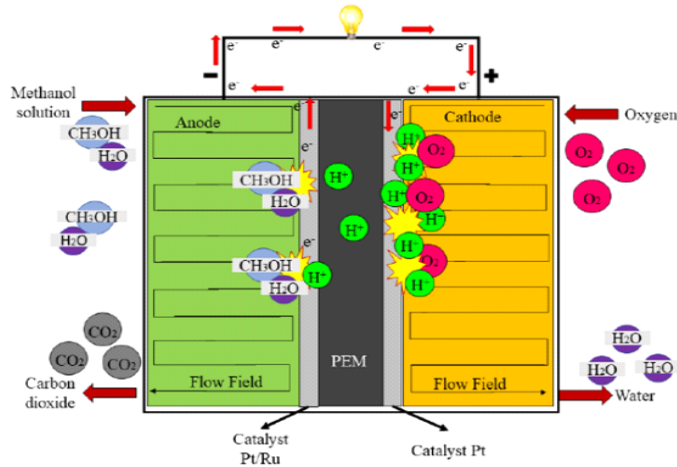
Figure 2.2. Direct methanol fuel cell (Junoh et al., 2020a).

Anode: $CH_3OH + H_2O \rightarrow 6H_2^+ + 6e^-$

Cathode: $\frac{3}{2}O_2 + 6H^+ + 6e^- \rightarrow 3H_2O$

Overall reaction: $CH_3OH + \frac{3}{2}O_2 \rightarrow 2H_2O + CO_2$
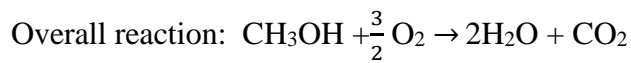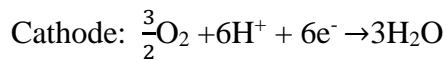
Direct methanol fuel cells are operated either in passive mode or active mode. In a passive mode of operation, there is the continuous feeding of methanol to the system. The system is operated automatically, therefore there is no need for pumping Methanol and blowing the air into stacks. When DMFCs are operated in a passive mode system, oxygen, and methanol are provided to the layer of the catalyst as reactants (Junoh *et al.*, 2020a).
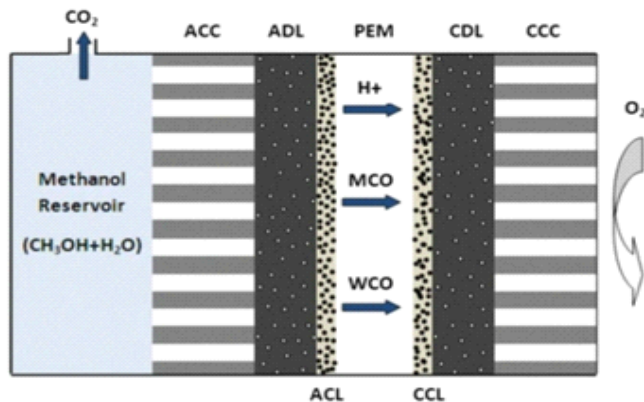
Figure 2.*3*. The passive mode of direct methanol fuel cell (Shrivastava, Thombre and Chadge, 2016).

During MOR, carbon dioxide and water are emitted from the system by passive means. The passive system is cheap, simple, and has a compact design. The passive mode is usually used in low-power systems, on the contrary, the active mode is used in high-power systems. In the active mode system of DMFC, methanol liquid is pumped from an external reservoir to the anode by a peristaltic pump while the cathode is supplied with oxygen through a blower (Halim *et al.*, 2012; Kong, Masdar and Zainoodin, 2015; Balasubramanian and Vijayakumar, 2017; Mallick, Moharana and Mohapatra, 2018). The output stream of the active mode system is recirculated through a closed control loop of methanol liquid (Kong, Masdar and Zainoodin, 2015).

Table 2.1. Summary of Fuel Cells

Type of fuel cell	Temperature range(^{0}C)	Mobile ion	Application
Direct methanol fuel cell (DMFC)	20-90	H^+	These uses include autonomous power for test and training instrumentation, battery chargers, and power for man-portable tactical equipment.

Proton exchange membrane (PEMFC)	30-100	H^+	Is a kind of fuel cell that is currently being developed for use in portable, stationary, and transportation applications.
Phosphoric fuel cell (PAFC)	150-200	H^+	Buses and other large vehicles, as well as stationary electric generators with output in the range of 100 kW to 400 kW
Alkaline fuel cell (AFC)	50-200	OH^-	They are used in controlled aerospace applications and underwater applications.
Molten carbonate fuel cell (MCFC)	600-700	CO_3^{2-}	For use in electrical utility, industrial, and military applications, (MCFCs) was created for biogas, natural gas, and coal-based power plants.
Solid oxide fuel cell (SOFC)	700-1000	O^{2-}	Cogeneration, combined cycle power plants, and residential applications are the three main uses of SOFC.

2.2.2. Components of DMFC

2.2.2.1. Polymer Membrane

Direct methanol fuel cell is classified as PEMFC. It uses a polymer film as an electrolyte. The membrane is the key component of the cell. It is mainly responsible for separating gases, charging carriers for protons, and serving as an electric insulator for preventing the migration of electrons through the membrane (Peighambardoust et al., 2010a). High ionic conductivity is desired in membrane materials, and also the membrane must inhibit electron transport and the cross-over of oxygen reactant from the cathode and methanol fuel from the anode (Shimpalee *et al.*, 2018;

Banerjee, Calay and Eregno, 2022). The polymer material must also be physically durable, thermally stable throughout the operational temperatures, and chemically stable in an environment containing HO$^-$ and HOO radicals (Peighambardoust, Rowshanzamir and Amjadi, 2010a; Shimpalee *et al.*, 2018; Banerjee, Calay and Eregno, 2022). Most of today's membranes are made of perflurosulphonic acid membrane popularly known as Nafion$^®$, which was created by the DuPont Company in the 1960s (Kim *et al.*, 2015; Olabi *et al.*, 2022).

2.2.2.2. Anode and Cathode Catalyst Layer

To carry out electrochemical reactions, the catalyst layers form a border with three phases between the catalyst, incomers, and reactants (Mukherjee et al., 2011). The pt-based electrocatalyst is usually used at the anode of DMFC due to its high reactivity (Ahmad *et al.*, 2010; Awang *et al.*, 2015b). There are three major drawbacks associated with the use of this catalyst, this includes slow kinetic oxidation, high cost, and the development of intermediates species (Neburchilov *et al.*, 2007; Sajgure *et al.*, 2016).

The formation and irreversible absorption of intermediate aldehyde and carbon monoxide species cause incomplete MOR activation when a pure Pt catalyst is used, this disrupts MOR kinetics on the catalyst (Basri et al., 2014). Pt catalyst used is usually coated with other metals such as nickel, cobalt, rubidium, and others to eliminate the effect that can be caused by the poisonous intermediate products (Mansor *et al.*, 2019; Shafer *et al.*, 2019). The elimination of these products is made possible by the ligand effect and bifunctional mechanisms. Platinum hybrid electrocatalysts such as Pt/Sn, Pt/Rb, PtMO, PtPbMnO, PtCo, and Pt-M are examples of hybrids used on the anodes of DMFC. However, PtRu is the most used (Mansor *et al.*, 2019; Baruah and Deb, 2021). The addition of Ru in the Pt catalyst enhances its electronic properties, and this reduces oxidation overpotential at the anode, thus preventing carbon monoxide adsorption on the Pt catalyst (Ahmed and Dincer, 2011; Shafer *et al.*, 2019; Baruah and Deb, 2021; Yuda, Ashok and Kumar, 2022).

2.2.2. 3. Gas Diffusion Layer

The most common material for gas diffusion layers is porous carbon paper or carbon cloth with a PTFE/microporous carbon powder coating on top. In addition, the gas layers are often wetproofed with a Teflon dispersion coating to prevent liquid from clogging the pores of the layer (Giorgi & Leccese, n.d.). The porous gas diffusion layer of DMFC acts as a conductor of electricity and it carries electrons from or to the catalytic layer. It is responsible for ensuring that the reactants diffuse effectively to the catalyst layer (El-kharouf & Pollet, 2012a).

The gas diffusion layer assists in the management of water by permitting an appropriate quantity of water to reach and remain in the membrane for hydration. This layer's primary function is to (i) act as a gas diffuser, (ii) provide an electrical conduit for electrons, (iii) provide mechanical support, and (iv) channel product water away from electrodes. Hence, ideal GDL should possess high electronic conductivity, mechanical strength, water permeability, gas permeability, and good electrochemical stability (Zhang *et al.*, 2007; Schröder *et al.*, 2010; Xue, Zhang and Liu, 2017).

2.2.2.4. Membrane Electrode Assembly (MEA)

Figure 2.4. demonstrate a typical illustration of membrane electrode assembly. The electrodes and the electrolyte layer are hot pressed together to form a membrane electrode assembly (MEA). Two gas diffusion layers and two catalyst layers make up the MEA. Individually produced components are typically pressed together at low temperatures and pressures (Giorgi and Leccese, no date; Haile, 2003).
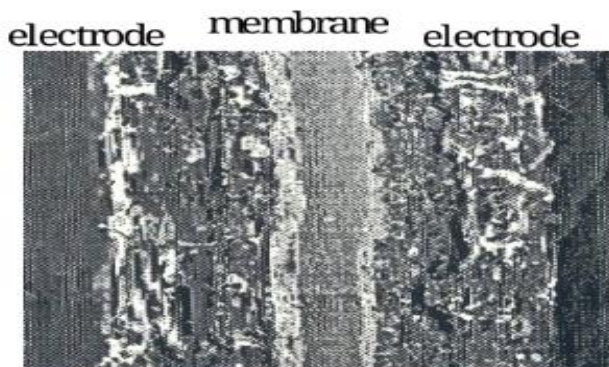
Figure 2.*4*. Membrane electrode assembly (Giorgi and Leccese, no date).

Advantages of DMFC:

A solid electrolyte is included in the DMFC which provides good methanol crossover resistance (Eriksson, no date). The ability of DMFC to operate at a low temperature, makes it start up quickly, and because there are no corrosive cell materials, it doesn't require the unusual materials used in various types of fuel cells (Guangul and Chala, 2020; Ahmed *et al.*, 2022). DMFCs are capable of large current densities (Xia *et al.*, 2019).

2.3. Types of Membrane

.

2.3.1. Perfluorinated Ionomers

Nafion® is one of the most used Perfluorinated membranes. Ionomers made of Perfluorinated sulfonic acid (PFSA) are part of a group of ion-conductive polymers renowned for their exceptional ionic conductivity and chemical-mechanical durability, however, fuel cross-over and cost are the most limiting factor for the utilization of these polymers (Amiinu *et al.*, 2013; Gloukhovski, Freger and Tsur, 2018).

15
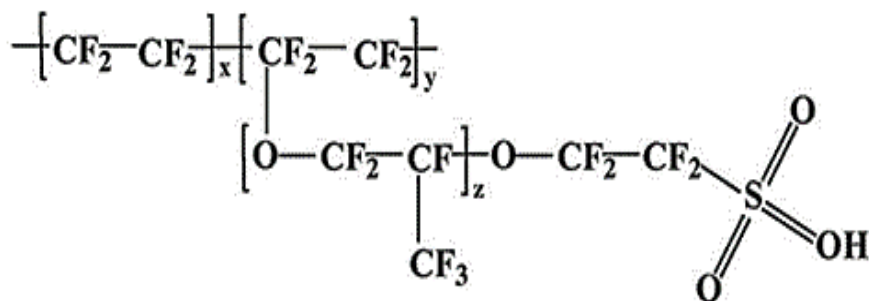
Figure 2.*5*. Perfluorinated ionomer (Amiinu *et al.*, 2013).

Figure 2.5. represent an example of perfluorinated ionomer. Nafion® is the most commercially used type of this membrane. The interior structure of Nafion® membranes is directly impacted by mechanical qualities' stability and longevity. Perfluorinated polymers comprise tiny size, limited polarization ability, and high electronegativity fluorine atoms, as well as a strong C–F link. The membranes are manufactured using the polymerization of monomers method, which uses a molecule's functional group or moiety, commonly a sulfonic group ($-CF_2SO_3H$), which can be turned cationic or anionic by additional treatment (Amiinu *et al.*, 2013; Wang, 2013; Karan, 2019). A hydrophilic channel can form when the sulfonic acid functional group self-organizes (Xia *et al.*, 2019). The membrane's channel provides good behavior in proton transport and prevents membrane swelling (Kusoglu and Weber, 2017; Zhu *et al.*, 2022). A hydrophobic polymer backbone is interspersed between the hydrophilic channels, ensuring that the Nafion® membrane is mechanically (Mayadevi *et al.*, 2022).

2.3.1. Fluorinated polymers

In PEM fuel cells, membranes that are commonly employed are fluorinated. The most prevalent variety is Du Point Chemical Company's Nafion® membranes, which are perfluoro-sulfonic polymers. The backbone of Fluorinated polymers has a sulfonic group attached to it (Ogungbemi et al., 2019).
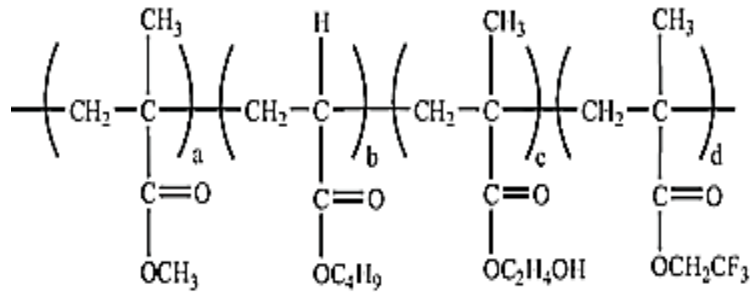
Figure 2.*6*. Fluorinated polymers (Mayadevi *et al.*, 2022).

2.3.3. Partially fluorinated membrane

Partially fluorinated membranes can yield membranes with increased stability and better mechanical qualities. The following are some examples of perfluorinated materials that are often used poly (chlorotrifluoroethylene), polyvinyl fluoride, and poly (vinylidene fluoride) (Maiyalagan and Pasupathi, 2010; Ogungbemi *et al.*, 2019). Even though partly fluorinated membranes have a high proton conductivity, they are costly and unaffordable due to the usage of expensive fluorinated materials (Ogungbemi et al., 2019).

2.3.4. Non-fluorinated membrane

Non-fluorinated membranes are a type of ionomeric polymer in which the proton conduction qualities are provided by ionogenic groups connected to a fluorine-free polymeric backbone (Roziére and Jones, 2003; Pica, 2014). Figure 2.7. indicate a non- fluorinated compound. Non-fluorinated organic compound ionomers have distinct environmental, technical, and cost benefits (Hertel, 2005; Luo, 2005). In comparison the incumbent perfluorinated acid-based ionomers have better thermo-mechanical characteristics at temperatures above 90 °C, are less expensive to manufacture, and have reduced gas cross-over. Furthermore, because there are no (per) fluorinated precursors, ionomers of hydrocarbons with no fluorine such as sulfonated butadiene, sulfonated

polyimide, sulfonated styrene, and sulfonated polystyrene are less harmful to the environment (Roziére and Jones, 2003; Pica, 2014)
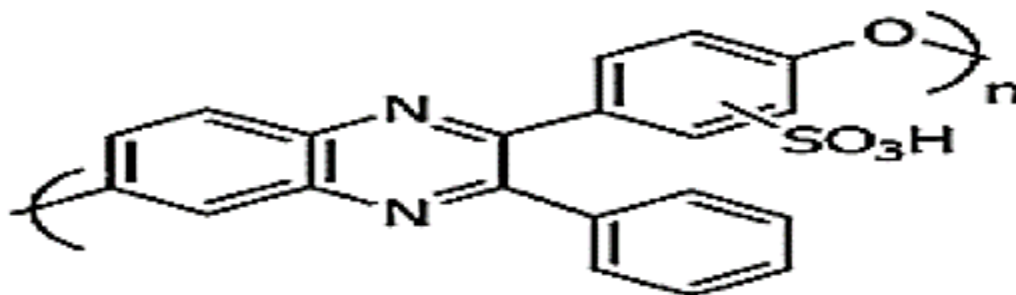
Figure 2.7. Non-fluorinated membrane (Roziére and Jones, 2003)

2.3.5. Acid-Base membranes

The acid-base membrane is less expensive than other types of membranes. It absorbs more water, has a broader temperature range, and is recyclable. This is environmentally friendly (Zuo, Fu and Manthiram, 2012a; Mack *et al.*, 2015). Heat conductivity and chemical compatibility, on the other hand, are a difficulty. Acid-base membranes, which are made up of acidic polymers and basic additives that might be inorganic, organic, or polymeric, were primarily designed for high-temperature PEMFCs (Ogungbemi et al., 2019). Figure 2.8. indicate chemical structure of polybenzimidazole as an example of acid-base membrane.
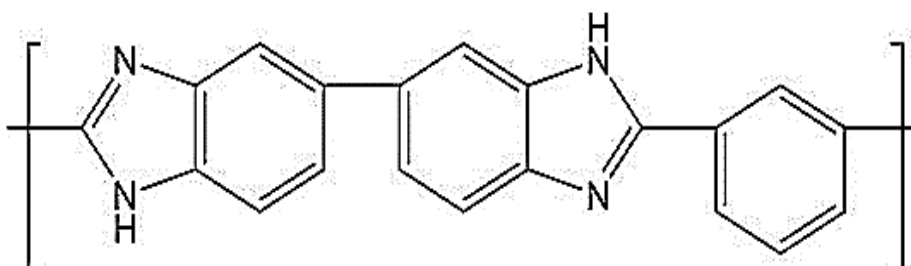
Figure 2.8. Acid-base membrane (Ogungbemi et al., 2019)

2.4. Chitin and chitosan

Chitin is the second most prevalent polysaccharide in nature, after cellulose(Mukoma, Jooste and Vosloo, 2004a). It is crystalline in form, and it is contained poly (1,4) -linked N acetyl -2-amino 2- deoxy-*B* -D glucose and some remains of 2-amino-2-deoxy-B-D glucose. Chitin is mostly mistaken for cellulose because of their similar chemical backbone However, Chitin, on the other hand, has an acetamide group on the C2 position rather than a hydroxyl group (Rinaudo, 2006; Szliszka *et al.*, 2009; Osifo and Masala, 2010). Chitin can be obtained by two techniques which are chemical and biological methods (Pighinelli, 2019). The chemical method is eco-friendly, uneconomical, and has an impact on the physiochemical characteristic of chitin negatively. The biological method is cheaper and safe (Pal *et al.*, 2014, 2014; Kozma, Acharya and Bissessur, 2022).

There are three types of chitin crystals: namely the alpha (α), beta(*β*), and the y form (Younes and Rinaudo, 2015). The most prevalent type is the alpha allomorph crystal form of chitin, which is derived from crabs, fungi, krill, shrimps, lobsters, and fungi, it possesses strong intramolecular and intermolecular bonds that inhibit diffusion of macromolecules into crystal phase making it suitable for industrial application (Robertson, 2004; Hou, Aydemir and Dumanli, 2021). The orthorhombic unit of alpha chitin is made up of antiparallel sheets or chain stacks (Hou, Aydemir and Dumanli, 2021). The β type has weak intramolecular hydrogen bonds which require their solubility, reactivity, and swelling to be monitored (Robertson, 2004). Chitosan is an N-derivative of chitin. Chitin is a naturally abundant material that is found mainly in fungi, invertebrates, and yeast (Osifo & Masala, 2010). Figure 2.9. is a systematic summarized illustration of how chitosan is synthesized from chitin.
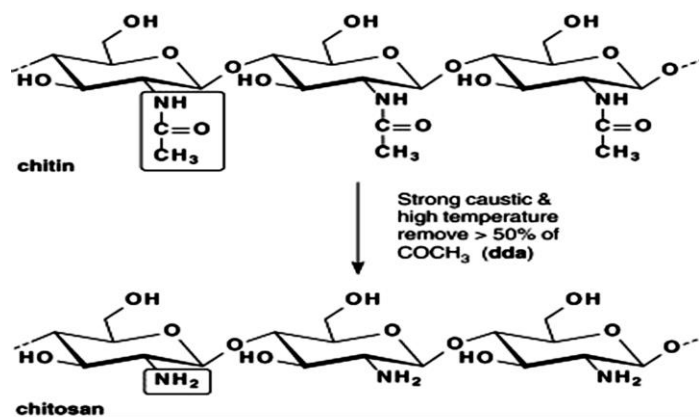
Figure 2.*9*. Chitin and chitosan (Mukoma, Jooste and Vosloo, 2004a).

When the degree of N-deacetylate of chitin makes it soluble in aqueous acidic solutions it is referred to as chitosan (Aranaz et al., 2021). Chitosan is a cationic linear biopolymer. It is non-hazardous, has power-solid or white flakes, and is slightly pearlescent. It entails biocompatible and biodegradable capacities, and it is soluble in some inorganic acids (Jiménez-Gómez & Cecilia, 2020). Organic acids dissolve chitosan and inorganic acids like formic acid, hydrochloric acid, and acetic acid (Li *et al.*, 1992; Romanazzi *et al.*, 2009). Free hydroxyl and amino group on the chitosan backbone makes it easy for modification through sulfonation, tosylation, carboxylation, alkylation, quaternary salt, and Schiff base (Jain *et al.*, 2013; Argüelles-Monal *et al.*, 2018). Free amino ions on swollen hydrated chitosan may experience protonation while leaving free hydroxyl ions in water which will lead to ionic conductivity (Li *et al.*, 1992; Aranaz *et al.*, 2021). The electrical conductivity of chitosan in a normal state is very low (Permana, Ahmad and Ramadhan, 2016). Even though the shape of the chitosan monomer consists of three hydrogen atoms, it is not possible to be mobilized by the influence of a proton conductor created by an electric field due to its strong bonded structure. Chitosan can be utilized in various industries such as cement, paper production, wastewater treatment, heavy metal chelation, and others (Permana, Ahmad and Ramadhan, 2016; Wang *et al.*, 2019; Adiyar *et al.*, 2021b).

2.5. Membrane Morphologies

A membrane is a solid matrix with discrete pore sizes and distinct pore size nomenclatures. The membranes that are utilized in DMFC are categorized according to their morphological structure: thin, thick, dense, sandwiched, layered, porous, or pore-filled membranes (Aricò et al., 2015a).

2.5.1. Thin and Thick Membranes

The phrases thin and thick membranes refer to the thickness of the membrane, not the micro pores. This membrane has the same structure as a dense membrane. The influence of membrane thickness on proton conductivity has been studied extensively, particularly in the context of DMFC applications. The thickness of the membrane is one of the most crucial variables that can affect DMFC performance (Aricò et al., 2015a).

2.5.2. Dense Membranes

At the limitations of electron microscopy, dense membranes are distinguished by their lack of holes and homogeneity. The membranes have pores with a diameter of less than 0.2 nm, according to the IPUC nomenclature (Junoh *et al.*, 2020b). The main driving forces of pressure electrical gradient potential and concentration are covered by the dense membrane transport mechanism. Nonetheless, the electrical potential gradient is largely used in electrolyte membrane processing to induce the passage of anions or cations from the supply stream through the membrane's sides (Junoh *et al.*, 2020a; Jawad *et al.*, 2022).

2.5.3. Layered Membranes

A layered membrane is one in which another substance is present on the membrane's upper layer. The multilayer construction tries to keep or increase proton conductivity while blocking methanol crossing (Kannan *et al.*, 2020; Tjiptowidjojo *et al.*, 2022).

2.5.4. Pore-filling Membranes

A pore-filling electrolyte membrane is made up of two components: a porous substrate, as well as a polymer to fill the pores in the substrate. Proton migration can be aided by the presence of water in the filling polymer electrolyte despite the porous substrate being completely inert to liquid fuels or gases. The filling electrolyte polymer was used to achieve proton conductivity (Yamaguchi, Miyata and Nakao, 2003). The swelling of the membranes regulated methanol permeation. The substrate sustained a high temperature from a strong proton conductivity was demonstrated in this concept occurs in membranes with a decreased permeability to methanol. Proton conductivity is exhibited by the filling (Kang, 2013; Kim *et al.*, 2017).
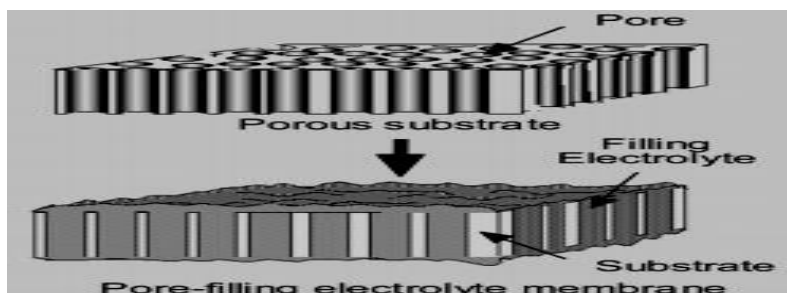
Figure 2.10. Pore-filling process (Yamaguchi, Miyata and Nakao, 2003).

Figure 2.10. indicate pore filling membrane. To produce a pore-filling electrolyte membrane, the electrically charged electrolyte is injected into the pores of a porous substrate as indicated in Figure 2.10.(Yamaguchi, Miyata and Nakao, 2003). Pore-filling membranes have a high affinity for aromatic chemicals and can withstand considerable swelling (Z. Li et al., 2011). The substrate or host membrane should have a stronger mechanical strength to prevent swelling during the impregnation process. However, the production of porous membranes using the phase inversion approach is largely dependent on both the thermodynamics and kinetic factors of the polymer, as well as solvent and non-solvent properties. Different solvents/non-solvents produce various morphologies (Yamaguchi, Miyata and Nakao, 2003; Z. Li et al., 2011).

2.5.5. Sandwiched

Sandwiched membranes, unlike layered membranes, are created by squeezing one membrane between two different-material membranes. To increase the parent membranes' performance in DMFC applications, the material to be squeezed is chosen carefully (Junoh *et al.*, 2020a).Below in Figure 2.15. is a structural representation of sand-wiched membrane.
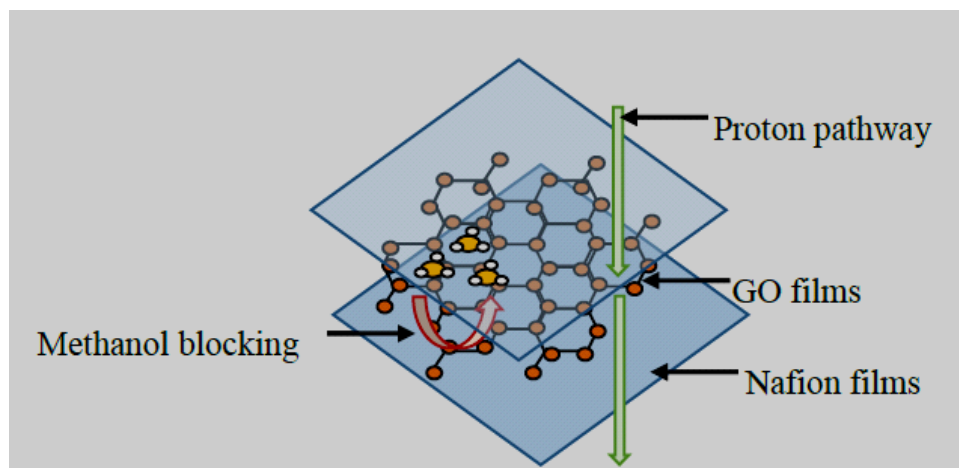
Figure 2.*11*. Sandwiched membrane (Junoh *et al.*, 2020a)

2.6. Modification of Chitosan

2.6.1. Chemical Modification

It is important to modify the chitosan polymer to enhance its chemical and mechanical properties. Chemical modification is often used to enhance chitosan solubility, not only that it also improves physiochemical properties such as its bacterial properties, oxidation resistance, thermal stability, and rheological properties (Vaghari *et al.*, 2013a; Szymańska and Winnicka, 2015). The chitosan structure consists of hydroxyl and amino groups which makes it easy for chemical modification. The modification can occur either on the hydroxyl or amino group or both. However, the hydroxyl

primary group reacts actively to the secondary hydroxyl group, but it is less reactive compared to the amino group. When chemical modification occurs on the amino group it will be N-modified, on the hydroxyl group it will be O-modified. If the chemical modification was done on both groups, it will be N, O modified (Vaghari *et al.*, 2013a; Kyzas and Bikiaris, 2015; Casadidio *et al.*, 2019).

2.6.1.1. Carboxylation

The carboxylation of chitosan is accomplished by adding acidic groups to the chitosan chain. It improves film-forming, solubility, and moisturizing properties. Carboxymethylation occurs mostly at C-6 the NH_2 moiety or hydroxyl groups, resulting in Compounds of N, O–carboxymethyl chitosan that is water soluble and that comprises a primary ($-NH_2$) or secondary ($-NH_3$) amino group. Carboxylation of chitosan is done through Carboxymethylation which can be classified into three categories, O-Carboxymethylation, N-Carboxymethylation, and N, O Carbo-methylation. N-Carboxymethylation usually occurs under high-temperature conditions whereas O-Carboxylation takes place amid monochloroacetic acid sodium hydroxide and isopropanol-water solution under room temperature conditions (Jain *et al.*, 2013; Chen *et al.*, 2022).

2.6.1.2. Cross-linking

Chemical alteration through cross-linking is a widespread practice. It is the purpose of cross-linking to ensure that chitosan and insoluble chitosan in the aqueous media is chemically and mechanically stable (Hanna Rosli et al., 2020b). Cross-linking happens when the chitosan membrane's sulfuric acid concentration is combined with protonation (Z. Yang et al., 2010). Cross-linking of chitosan is the best way of modification as it stabilizes its chemical properties, making it to be insoluble in acids and bases. Crosslinking can happen within molecules. Sulfuric acid can also be utilized as a cross-linker agent.(Wan Ngah et al., 2011) reported that cross-linked chitosan shows stability and insolubility to bases and acids. Several cross-linkers, for example, glutaraldehyde, epichlorohydrin, sulfuric acid, and glyoxal, are used in the traditional synthesis of chitosan. These cross-linkers can both stabilize and improve the mechanical characteristics of chitosan (L. Xu et al., 2015). Crosslinking increases dimensional stability and dodges permanent

enlargement of the chitosan polymer; it also reduces the swelling property of the membrane enabling its suitability in fuel cell application (Wan Ngah et al., 2011).

2.6.2. Physical Modification

A rising study on the usage of chitosan polymer encouraged interest in the physical modification of chitosan, while the chemical modification is still the most common method. The modification of chitosan by physical means can be done through ultrasonic treatment, ionizing radiation, and mechanical grinding for its suitability in a different application (W. Wang et al., 2020)

2.6.2.1. Ultrasonic Treatment

Ultrasonic treatment involves transferring of waves to the liquid material causing bubbles to be formed in the medium. This causes an increase in pressure and temperature which leads to deformation and vibration (Kasaai, Arul and Charlet, 2008; Vallejo-Domínguez *et al.*, 2021).
Ultrasonic energy is transmitted to the polymer utilizing holed effect producing energy like that of a hydrogen bond (Kasaai, Arul and Charlet, 2008; Vallejo-Domínguez *et al.*, 2021). Polysaccharide polymer's intramolecular and intermolecular hydrogen bonds can be destroyed successfully using the whole effect, this also leads to a reduction of polymer molecular weight. It is reported that the effects of an ultrasonic cavity on chitosan lead to its degradation. However, chitosan nanoparticles and nanogels can be prepared by ultrasonic treatment liquid (H. Liu et al., 2006).

2.6.2.2. Ionizing Radiation

The ionizing radiation process has shown to be one of the most effective creating techniques for various ranges of membranes with certain customized capabilities, allowing employed in several biological, environmental, and industrial applications (Abd El-Rehim *et al.*, 2015). The utilization of several commercially available kinds of accessible sources of high-energy radiation, such as X-ray, electron beam, and Co to launch energy-maintained polymerization or copolymerization techniques involving free radicals is the general premise of this clean and environmentally

acceptable technology (Mahmud *et al.*, 2014; García *et al.*, 2015). Resulting in the fabrication of flexible, functionalized, and structured membranes or the integrated chemical groups into a matrix made up of a cheap polymer (Mahmud *et al.*, 2014; Abd El-Rehim *et al.*, 2015; García *et al.*, 2015).

2.6.2. 3. Mechanical Grinding

Mechanical grinding of chitosan involves pulverizing chitosan flakes under mechanical force to alter their physicochemical characteristics, crystal structure, and structural makeup. This method yields a better, more consistent, and homogeneous composite material. Furthermore, thermomechanical processing can improve the mechanical traits of chitosan (Ibrahim *et al.*, 2019; Podgorbunskikh *et al.*, 2022).

2.7. Application of Chitosan

2.7.1. Wastewater Treatment

Wastewater contains hazardous materials such as aromatic materials, dye, heavy metals, and so on, these toxic materials in water bodies can be removed using chitosan. Chitosan is believed to remove toxins by adsorption. During the process, chitosan is utilized as a coagulant, adsorbent in the treatment of aquaculture effluent, and bactericide (Sandeep et al., 2013).

2.7.2. Biomedical Application

Chitosan and its nanoparticles can be utilized as carriers for nano-delivery systems and have a variety of biological uses, including medication delivery, vaccine delivery, antibacterial agents, and wound healing (Zhao et al., 2018). Over the last two decades, chitosan has been employed as a safe excipient in oral dosage forms. When compared to commercial goods, chitosan tablets can provide a longer-lasting medication release (Morin-Crini et al., 2019).

2.8. Membrane Hydroscopic Oxides Fillers

The improvement of membrane properties by organic-inorganic combination not only reduces fuel permeability but also improves physiochemical characteristics of the membrane-like ion exchange capacity, water management, and proton conductivity (Tran *et al.*, 2013a; Sugino and Kawaguchi, 2017; Mohammed Hello and Kadhim Hlial, 2019; Gorji *et al.*, 2021).

2.8.1. Silica (SiO$_2$)

Silica is the most popular hygroscopic oxide inorganic filler used mostly in proton exchange membranes. Silica is hydrophilic, and it provides support and improves thermal stability in proton exchange membranes (Hanna Rosli et al., 2020b). Hydrophilic silica has been rated an interesting material for proton exchange membrane fabrication due to its unique capabilities to offer reinforcement and thermal stability. With silica filler, (Al-Sagheer & Muslim, 2010) found that chitosan membranes were more thermally and mechanically stable. According to reports, silica added to the membrane reduces hydrophilic properties produced by the availability of free hydroxyl and amino groups at the carbon atom of the chitosan film's main chain (Handayani et al., 2012). (Kusumastuti et al., 2016) has reported that optimal performance of Nano-silica membrane was found when the 3% weight of silica to chitosan was used giving proton conductivity of 0.231 S/cm. When added to a polymer as organic filler silica particles provide interfacial interaction or response. According to current research, the formation of extra silica functional groups is caused by hydrogen covalent interactions and the interfacial connecting network. The interaction of hydroxyl groups embedded in the molecule of silica with key polymer functional groups causes hydrogen bonding between the polymer matrix and silica particles (Setiawan & Chiang, 2019). (Kusumastuti *et al.*, 2016a) shows that chitosan membrane which was incorporated with silica-based material showed improved proton conductivity, water retention ability, membrane selectivity, thermal, and mechanical for applications in DMFC.

2.8.2. Titanium Dioxide (TiO$_2$)

Titanium dioxide has a long history of being employed as a semiconductor photocatalyst for application in carbon dioxide reduction, water separation, bacterial disinfection, and degradation of pollutants (Baglio *et al.*, 2004; Simari *et al.*, 2020; Karim, 2021). It has been also utilized solar panels because of their water-loving as well as ultraviolet-resistance properties. Therefore, its utilization as a filler in the membrane will improve the chemical and thermal stabilities of the membrane, furthermore, increasing proton conductivity (Devrim *et al.*, 2013; Ahmed *et al.*, 2021). Proton groups on TiO$_2$'s surface can establish ongoing proton-conducting routes throughout the C/STiO$_2$ interface, improving the ionic conductivity of C/STiO$_2$ nanocomposites because the hydroxyl groups of TiO$_2$ and the sulphonic group of acid have a strong interfacial relationship. Furthermore, the –NH$_2$ groups on chitosan limit chitosan chains' mobility, enhancing the nanocomposite membranes' mechanical and thermal resilience. Proton exchange membrane fuel cells could benefit from these C/STiO$_2$ nanocomposite membranes (Mohsenpour, Kamgar and Esmaeilzadeh, 2018; Salarizadeh *et al.*, 2019; Thmaini *et al.*, 2022).

2.8.3. Zirconium Oxide (ZrO$_2$)

To improve mechanical and thermal durability and proton conductivity, the polymer matrix has been filled with inorganic fillers such as zirconium oxide during the manufacture of PEMs. Acid-grafted inorganic fillers can improve proton conductivity and interface composite membrane compatibility (S. Ahmed et al., 2021b). Chemical inertness, chemical strength, excellent electrical characteristics, corrosion resistance, excellent chemical stability, and water retention have all influenced people's interest in using zirconium oxide nanoparticles. Zirconium oxides can be used in the modification of PEM for application in the fuel cell. However, studies show that membranes will have low proton conductivity if the ZrO$_2$ is not modified with sulfates (Vaivars *et al.*, 2004; Sigwadi, 2013; Sigwadi, Dhlamini, Mokrani and Nemavhola, 2019)

4.8.4. Graphene Oxide

As a membrane filler, graphene oxide (GO) was used due to its high surface area, which allows for good water uptake and easy proton transport. Various oxygen groups such as hydroxides, epoxies, carboxyl, and carbonyls convert GO into electrically insulating and hydrophilic materials, but with mechanical strength, surface area, gas impermeable, and other properties are preserved (Pumera, 2013). Graphene oxide is compatible with membranes of many types, it can be used as a modifier to increase the selectivity (allowing only specified species to pass through) and performance of these membranes (Choi et al., 2012).

2.9. Proton conduction mechanisms
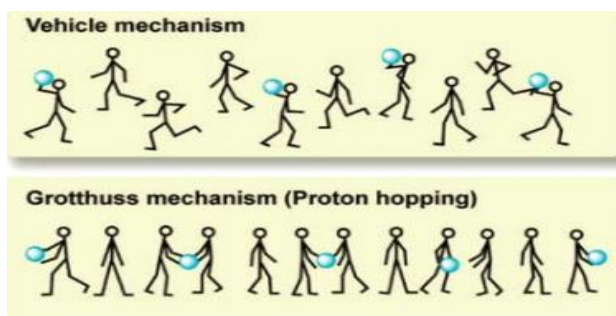
Figure 2.*12*. Vehicle and grottus mechanism (Zuo, Fu and Manthiram, 2012b).

Proton conduction is the most key factor to think about when evaluating the membrane potential use in the fuel cell. There are two primary methods for proton transport, diffusion mechanism, and proton hopping which is a term used to describe Grotthuss' technique. A visual presentation of the above phenomenon is presented in figure 2.16. The diffusion mechanism is also called the vehicular mechanism and it uses water as a vehicle. The transport mechanism of water involves a concentration gradient forced by diffusion and osmotic drag (Zuo, Fu and Manthiram, 2012a; Lin, 2014). Electroosmotic drag carries water molecules through the membrane. This mechanism involves the diffusion of hydrated hydronium ions through aqueous material because of electrochemical reactions difference. The transport of protons by way of the membrane through vehicular mechanism is influenced by the free volume of the polymer chain within the PEM.

Grotthuss mechanism involves protons jumping from one ionic hydrolysed site of the membrane to the other (Suarez *et al.*, 2011; Arntsen *et al.*, 2021).

2.10. Effect of Silica on Membrane Properties

2.10.1. Effect of Silica on Proton Conduction

Pure chitosan structure has no mobile hydrogen ions which contribute to its low conductivity (Pati *et al.*, 2020; Podgorbunskikh *et al.*, 2022). The addition of silica to chitosan increases proton conductivity as silica's large surface area and hydrophilicity retains more water with more proton channels in the membrane (Kusumastuti *et al.*, 2016a). At higher temperatures, inorganic silica with proton conducting groups is anticipated to improve structural/thermal stability as well as proton conductivity (Vijayakumar & Khastgir, 2018; Kusumastuti *et al.*, 2016)).

2.10.2. Effect of Silica on Water Uptake

The addition of hygroscopic inorganic nanoparticles like silica to the polymer matrix improves the properties of composite membranes such as water retention capacity at low to medium temperatures. Many hydrogen bonding sites can be provided by these hydrophilic fillers, allowing membranes to absorb a large amount of water(da Costa Neto *et al.*, 2014; Science, 2021).

2.10.3 Effect of Silica on Methanol Permeability

The advantages of using acid-modified fillers are as follows: The impermeable fillers can impede the methanol transfer channel, lengthening it (Bai *et al.*, 2014). Incorporated silica particles on the chitosan membrane polymer can close pores and absorb most methanol on the surface which will lead to reduced fuel crossover (Handayani et al., 2012) Filler modification grafting with macromolecules or functional groups such as amine and sulfonic acid groups are promising ways to reduce fuel permeability as well as enhancement chitosan structure (Handayani et al., 2012; Bai et al., 2016).

2.11. Methanol in Fuel Cell

Methanol is utilized as a source of energy in direct methanol fuel cells. It is mostly used to supply an output of about 100W (Popovici, 2014). Methanol can be utilized in fuel cells either by Direct methanol fuel cells (DMFC) or by H_2-PEMFC (through methanol steam reforming). A DMFC is a type of PEMFC that generates energy via electrochemical processes using aqueous methanol instead of hydrogen, this enables DMFC to have excellent fuel management, because of its single-carbon structure. Methanol burning produces significantly fewer nitrogen oxides and particulate matter than complex hydrocarbons (Scott *et al.*, 1999; Osifo and Masala, 2010; Tsen, 2020; Purwanto *et al.*, 2021).

Furthermore, during system start, only a small quantity of methanol is used in the combustion chamber, and the anode off-gas created by the reformate mixture is used to sustain the chamber, resulting in significantly lower RMFC emissions than methanol-fed internal combustion engines. Formaldehyde, a by-product molecule in the methanol oxidation path of reaction and a potential health hazard, is another harmful waste that can be produced from methanol-based systems (Garc'ia and Weidner, 2007; Ahmed *et al.*, 2022). Similarly, methanol combustion in internal combustion engines is a bigger problem than in reformed methanol fuel cells. The inadequate conversion of methanol in the reformer and the catalytic burner during the system starting unreacted methanol enters the cathode cell stack, flows through the arrangement of membrane electrodes (MEA), and interacts with oxygen. As a result, while using green methanol, during normal operation, the fuel cell system and reformer emit no hazardous pollutants (Weidner, Sethuraman and Zee, no date; Demirbas, 2008; Zhang *et al.*, 2018).

2.12. Challenges in Direct Methanol Fuel Cell

2.12.1 Methanol Permeability

.

Methanol crossover occurs when methanol from the anode compartment diffuses into the cathode compartment through the separating membrane, which is a serious problem that limits the

performance of DMFCs. Methanol crossover is the major concern of DMFCs and needs to be addressed. High Methanol crossover lowers the capability of the cell to generate optimum power generation (Ren, 1995; Gurau and Smotkin, 2002; Halim *et al.*, 2022). Methanol crossovers occur by electro-osmotic drag, hydraulic permeation, and by diffusion. The drawback associated with direct methanol fuel cells is permeability. Methanol permeability by osmotic drag happens when methanol molecules are dragged by protons from the anode to the cathode side. Methanol hydrates because of a differential in pressure across the membrane Diffusion happens due to a variation in methanol content across the membrane (M. Ahmed & Dincer, 2011).
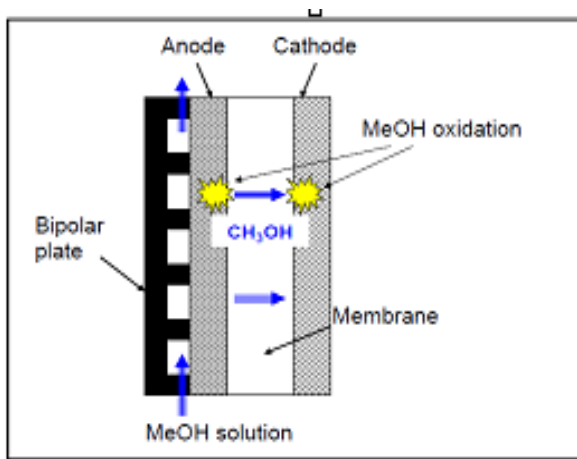
Figure 2.13. Methanol permeability (M. Ahmed & Dincer, 2011).

Figure 2.13. is a representation of how methanol permeability occurs in a fuel cell. Studies have shown that methanol crossover is dependent on methanol concentration, Pressure, operating temperature, catalyst morphology, and membrane thickness. A fuel cell that contains a thin membrane is prone to high fuel permeation compared to one with a thick membrane, because of a high concentration gradient across the membrane which led to the increment in diffusion. Good methanol crossover must be less than 10^{-6} moles/min.cm^{-2} (Q. Xu et al., 2018).Fuel cell crossover causes the production of mixed potential due to the direct reaction of oxygen and hydrogen at the cathode of the cell, which tends to reduce the open circuit voltage of the cell (Mench, 2006; Simari *et al.*, 2021). Additionally, severe fuel crossover autocatalytically speeds up membrane

degradation and pinhole development caused by locally generated heat, which causes proximate membrane thinning, speeding up the crossing process. Crossover in the cell also causes internal short circuits, this causes electrons not to reach the external circuit of the cell (Mench, 2006; Simari *et al.*, 2021).

2.12.2. Durability and Stability

Durability is the most significant challenge impeding the successful commercialization of polymer electrolyte membrane fuel cells in transport and stationary use. The durability of the cell is affected by the degradation of different components of the cell (catalyst layer, degradation phenomena, mechanisms, catalyst degradation), (H. L. Nguyen et al., 2021a) Durability of the cell is affected by the degradation of components of the cell such as catalyst layer, membrane, and bipolar plate sealing caskets, and it is also affected by operating conditions (H. L. Nguyen et al., 2021a).

(i)   Membrane Degradation

The cell membrane is the most important component. Its degradation affects the functionality of the cell badly. Membrane degradation causes fuel crossover and failure of the fuel cell (Osifo & Masala, 2012). Degradation of the membrane happens first at the anode. Degradation on the cathode is increased by fuel crossover through the membrane (Aricò et al., 2015b). Membrane degeneration can happen chemically or mechanically (Junoh et al., 2020) Mechanical degradation is the leading cause of early failure of the cell. Membrane mechanical degradation usually occurs as tearing or cracks on the membrane (Qiu *et al.*, 2018). Chemical degradation occurs when there is complex production of peroxyl and hydroperoxyl radicals. The produced radicals reduce the proton conductivity of the membrane because of the attack on the backbone side chain. Chemical degradation of the membrane causes severe thinning and fluoride release (Prabhakaran, Arges and Ramani, 2012; Zatoń, Rozière and Jones, 2017).

(ii)   catalyst Degradation and Carbon Support

Fuel cells commonly use platinum catalysts at both the cathode and anode compartments of the cell. The degradation of the catalyst and corrosion of the carbon support material of the cell causes a loss in the performance of the electrode (Sandeep et al., 2013). The pt-based catalyst causes catalysation of carbon corrosion, resulting in the reduction of the pt-based particles anchoring site on the corrosion. This leads to sintering and catalyst redistribution, hence, degradation of the catalyst (Yu and Ye, 2007; Padgett *et al.*, 2019). (Tan *et al.*, 2019) reported that most catalyst degradation occurs at the cathode side. Catalyst degradation occurs when there is a loss of pt particles on the carbon support structure and changes in structure and redistribution. Carbon support corrosion occurs when there is a loss of catalyst concentration and active catalyst surface area. Additionally, it reduces the porosity and hydrophobicity of the catalyst layer, lowering total cell performance. Water dissolves pt particles, which then diffusion into the ionomer phase, followed by membrane precipitation. The dissolution of the particles is influenced by voltage cycling (Tan *et al.*, 2019; Yu *et al.*, 2021; Liu, Tu and Chan, 2022).

(iii)   Gas Diffusion Layer

Gas diffusion layer degradation is mainly commonly caused by corrosion due to water droplets formation during harsh operating conditions, for example, fuel starvation, start-up, and shutdown (Kalogirou, n.d.). Degradation of the GDLs occurs as physiochemical degradation or mechanical degradation. Degradation by mechanical and physical damage is caused by freezing. Clamping friction and erosion are caused by the high velocity of gas flow. Carbon oxidation by water cannot be overlooked as a decisive element in GDL hydrophobicity loss and porosity reduction. As a result of the increasing water content in the GDL, gas diffusion is hampered, and the fuel cell's efficiency is reduced (Zhang *et al.*, 2007; Xue, Zhang and Liu, 2017).

(iv) Bipolar Plates

Bipolar plates have a huge impact on fuel cell durability and performance. The use of incorrect plate material causes a rapid increase in MEA degradation. Bipolar plate deterioration results in higher ohmic cell resistance and higher oxygen reduction overpotentials (kinetic losses) due to acid leakage from the CL and a decrease in the electrochemically active surface of the catalyst (Tang *et al.*, 2021; Hala *et al.*, 2022).

2.12.3. Slow Kinetic Reactions and MOR

The kinetic reaction of the cell is influenced by the pressure, concentration, temperature, and physical and chemical characteristics of the reactants. According to (Nguyen *et al.*, 2021) the voltage of the cell will drop due to sluggish current densities and slow methanol electro-oxidation kinetics. Indirect carbon dioxide production involves complex processes in which numerous intermediates are produced via various paths. CO is generated as an intermediary species, and its substantially higher stability prevents methanol oxidation at the anode (Wala and Simka, 2021). Carbon monoxide is generated after a succession of the anode catalyst's adsorption and deprotonation, which limits the active sites of the catalyst. Carbon monoxide is formed because of an indirect method in which CHO or COH is dehydrogenated directly (Wala and Simka, 2021; Nguyen *et al.*, 2022).

2.12.4. Heat Management

When dealing with DMFC, one of the most crucial aspects to consider is heat management. Increasing the operating temperature and current of the direct methanol membrane fuel cell will result in great methanol conversion. Heat management is critical in direct methanol electric cells because products including acetaldehydes, carboxylic acid, and CO_2 are discharged. Under constant current operation, the increased operational temperature can improve aldehyde properties while decreasing carboxylic acid selectivity (M *et al.*, 2019; Baroutaji, Arjunan, Ramadan, *et al.*, 2021; Chen *et al.*, 2021).

2.12.5. Water Management Start

For passive DMFC systems, water crossing the membrane might cause two concerns. First, it causes anode water loss, needing water make-up. Second, a high-water crossover rate increases the chances of cathode flooding which reduces fuel cell performance (Friess, Shahraeeni and Hoorfar, 2008; Yadav *et al.*, 2022). The membrane's ability to handle water is crucial to its efficiency. The fuel cell must function in settings where the membrane must be hydrated so that the by-product water does not evaporate quickly as it is produced (Ji and Wei, 2009). In a direct methanol fuel cell, water is provided through a redox process at the anode. Water molecules are delivered to the negative compartment of a direct methanol fuel cell, while water molecules are created in the cathode compartment. The fuel cell's function will be disrupted if water is not properly handled in the cell, leading to cell resistance (Ji and Wei, 2009; Bhattacharya, 2015)

Flooding at the cathode will come from water loss in the negative compartment of the cell, resulting in short-circuiting within devices. Membranes cannot function without water. Hydration is utilized to maintain optimum membrane efficiency. Second, a high-water crossover rate raises the risk of cathode flooding, which reduces the performance of the fuel cell. To minimize severe flooding, the cathode's water should ideally be evacuated, and water should then be given to the anode to compensate for water loss due to water crossover over the membrane (Bhattacharya, 2015; Vincent, Lee and Kim, 2020). Water is separated and transferred to the anode through the cathode by diffusion. Another water management concern could be membrane water absorption(Bhattacharya, 2015). Temperature, stiffness of polymer matrix, the quantity of conducting groups, the equilibrium constant and types of counter ions membrane preparation, and polymer surface hydrophobicity are all factors that influence water absorption through the chemical compound membrane. Membrane swelling will occur if water absorption exceeds a set threshold. Water uptake and membrane expansion must be avoided, especially in High-temperature fuel cells, and this necessitates changes (Jiao and Li, 2011; Kadirkhan *et al.*, 2022; Trinh *et al.*, 2022).

One of the water management strategies utilized in direct methanol alcohol fuel cells is continuous flow field design. Water control within the internal wicking of electric cells connected to the

membrane has been attempted in several ways by using surface tension to either drain or feed water (Jiao and Li, 2011; Meng and Tian, 2018). Serpentine has been proved to eliminate water and greenhouse gas emissions, as well as to have intelligent stability and a high drop benefit to ensure that the product does not cause the system to become unstable (Masdar, Tsujiguchi and Nakagawa, 2010). Applying a hydrophobic air filter to the cathode of a liquid-fed DMFC device improved water recovery from the cathode to the anode (Masdar, Tsujiguchi and Nakagawa, 2010).

2.13. Application of Fuel Cell

2.13.1. Stationary Application

Fuel cell systems are utilized in stationary applications for a variety of reasons, including backup power supplies, remote power generation, stand-alone power stations for one or more users, distributed generation for buildings, and cogeneration (Masdar, Tsujiguchi and Nakagawa, 2010). Fuel cells due to their superior efficiency have found widespread use in power generation. Both the low and high-temperature fuel cells have considerable potential to be used in this application. Fuel cells such as PEM, SOFC, and PAFC are commonly used. Low-temperature fuel cells, in general, offer the advantage of providing speedier results (De Bruijn, 2005; Masdar, Tsujiguchi and Nakagawa, 2010).

Figure 2.14. CHP building (U.S. Department of Energy, 2016a).

CHP for industrial facilities, buildings, and stand-by generators is the most common stationary application of fuel cell technology. Figure 2.14. is a representation of the CHP unit that is used in the US as a source of power. The plants use natural gas as their primary fuel, and FC technology has been used to show the operation of fully self-contained stationary plants. The initial development of stationary plants has been concentrated on plants with capacities ranging from a few hundred kW to a few MW. (Abdel-aal *et al.*, 2016; U.S. Department of Energy, 2016b)

2.13.2. Portable Application

Small fuel cells are appealing for portable power applications, such as battery replacements in a variety of gadgets and electronic devices or portable power generators. Figure 2.15. demonstrate an example of portable device that uses fuel cell. Fuel cells' high density and flexibility make them attractive contenders for future portable personal devices. Fuel cell portable applications are mostly concentrated in two markets.

Figure 2.15. Portable application (Abdel-aal et al., 2016).

The first is the market of portable power generators designed for light out-door personal uses camping and climbing), light commercial applications such as portable signage and surveillance, and power required for emergency relief efforts battery. The second market is for consumer technological gadgets such as cell phones, computers, cell phones, radios, and virtually any electronic device that uses a battery (Abdel-aal *et al.*, 2016). They can also be utilized as a primary or backup power source for telecommunications transmission towers, switching nodes, and

additional electronic gadgets that benefit from a fuel cell's DC power (De Bruijn, 2005; Wilberforce *et al.*, 2016).

2.13.3. Backup Power Applications

Fuel cells, particularly in the telecommunications industry, could be a feasible backup power source (Olabi *et al.*, 2022; US Department of Energy, 2012).Figure 2.16. represent back up power source that is used in generation of power from fuel cells. In traditional backup power systems, batteries and generators run on diesel, propane, or gasoline. Most backup-power communication and control systems utilize generators and batteries to provide redundancy and avoid service interruptions. Fuel cells have a longer continuous runtime and are more resistant to extreme weather than batteries (US Department of Energy, 2012).

Figure 2.*16*. Backup power source (Olabi *et al.*, 2022).

2.13.4. Transport

Fuel cells has been used in transportation such as buses and this is illustrated in Figure 2.17. The bus uses fuel cell as source of energy. FCs are seen to be a perfect fit in the transportation sector because of these qualities mentioned problems associated with current internal. The Sub-program on Fuel Cells of the Fuel Cell Technologies office has been working to address critical market obstacles. Fuel cells as substitutes for light-duty internal combustion engine cars are being pursued

by the Fuel Cells sub-program to boost the efficiency of vehicles and assist the aims of lowering transportation-related oil consumption and emissions (Þiliukas, 2004; Yan *et al.*, 2022a; Kampker *et al.*, 2023a).In comparison to combustion engines, fuel cells provide several advantages. They are, for example, more efficient, silent, significantly smaller in size, have no or minimal environmental impacts, and can handle a wide range of applications from a few watts to several hundred megawatts (Yan *et al.*, 2022a; Kampker *et al.*, 2023b).

Figure 2.17.Fuel cell bus (Yan *et al.*, 2022b)

2.14. References

Abd El-Rehim, H.A., Zahran, D.A., El-Sawy, N.M., Hegazy, E.-S.A. and Elbarbary, A.M. (2015). Gamma irradiated chitosan and its derivatives as antioxidants for minced chicken. Bioscience, Biotechnology, and Biochemistry, 79(6), pp.997–1004.

Editorial Board. (2016). International Journal of Hydrogen Energy, 41(37), pp. iii–iv.

Adiyar, S.R., Satriyatama, A., Azjuba, A.N. and Sari, N.K.A.K. (2021). An overview of synthetic polymer-based membrane modified with chitosan for direct methanol fuel cell application. IOP Conference Series: Materials Science and Engineering, 1143(1).

Ahmad, H., Kamarudin, S.K., Hasran, U.A. and Daud, W.R.W. (2010). Overview of hybrid membranes for direct-methanol fuel-cell applications. International Journal,35(5), pp.2160–2175.

Ahmed, A.A., Al Labadidi, M., Hamada, A.T. and Orhan, M.F. (2022). Design and Utilization of a Direct Methanol Fuel Cell. Membranes, [online] 12(12), pp. undefined-1266.

Ahmed, S., Arshad, T., Zada, A., Afzal, A., Khan, M., Hussain, A., Hassan, M., Ali, M. and Xu, S. (2021). Preparation and characterization of a novel sulfonated titanium oxide incorporated chitosan nanocomposite membranes for fuel cell application. Membranes, [online] 11(6), pp. undefined–undefined

Amiinu, I.S. et al. (2013) 'Metal oxides as water retention materials for low humidity proton exchange membrane applications', New Developments in Metal Oxides Research, (October), pp. 81–108.

Aranaz, I., Alcántara, A.R., Civera, M.C., Arias, C., Elorza, B., Heras Caballero, A. and Acosta, N. (2021). Chitosan: An Overview of Its Properties and Applications. Polymers, [online] 13(19), pp.3256.

Argüelles-Monal, W., Lizardi-Mendoza, J., Fernández-Quiroz, D., Recillas-Mota, M. and Montiel-Herrera, M. (2018). Chitosan Derivatives: Introducing New Functionalities with a Controlled Molecular Architecture for Innovative Materials. Polymers, 10(3).

Arntsen, C., Chen, C., Calio, P.B., Li, C. and Voth, G.A. (2021). The hopping mechanism of the hydrated excess proton and its contribution to proton diffusion in water. The Journal of Chemical Physics, 154(19).

Arunkumar, P., Meena, M. and Babu, K.S. (2012). A review on cerium oxide-based electrolytes for ITSOFC. Nanomaterials and Energy, 1(5), pp.288–305.

Awang, N., Ismail, A.F., Jaafar, J., Matsuura, T., Junoh, H., Othman, M.H.D. and Rahman, M.A. (2015). Functionalization of polymeric materials as a high-performance membrane for direct methanol fuel cell: A review. Reactive and Functional Polymers,86, pp.248–258.

 Awang, N., Ismail, A.F., Jaafar, J., Matsuura, T., Junoh, H., Othman, M.H.D. and Rahman, M.A. (2015). Functionalization of polymeric materials as a high-performance membrane for direct methanol fuel cell: A review. Reactive and Functional Polymers,86. pp.248–258.

Baglio, V. and Blasi, A.D. (2004) 'Influence of TiO_2 nanometric filler on the behaviour of a composite membrane for applications in direct methanol fuel cells', Journal of New Materials for Electrochemical Systems, 7(4), pp. 275–280.

Bai, H., Zhang, H., He, Y., Liu, J., Zhang, B. and Wang, J. (2014). Enhanced proton conduction of chitosan membrane enabled by halloysite nanotubes bearing sulfonate polyelectrolyte brushes. Journal of Membrane Science, 454, pp.220–232.

Balasubramanian, A. and Vijayakumar, R. (2017) 'A passive DMFC with membrane for diffusion-controlled methanol feed', International Research Journal of Engineering and Technology (IRJET),4(7), pp.605–608.

Banerjee, A., Calay, R.K. and Eregno, F.E. (2022) 'Role and Important Properties of a Membrane with Its Recent Advancement in a Microbial Fuel Cell', Energies, 15(2), pp 1-15.

Baroutaji, A., Arjunan, A., Ramadan, M. (2021) 'Advancements and prospects of thermal management and waste heat recovery of PEMFC', International Journal of Thermofluids, 9, pp.100064.

Baroutaji, A., Arjunan, A., Alaswad, A., Praveen, A.S., Wilberforce, T., Abdelkareem, M.A. and Olabi, A.-G. (2022). Materials for Fuel Cell Membranes. Encyclopedia of Smart Materials, pp.267–272.

Baruah, B. and Deb, P. (2021). Performance and application of carbon-based electrocatalysts in direct methanol fuel cell. Materials Advances, 2(16), pp.5344–5364.

Behling, N.H. (2013) History of Phosphoric Acid Fuel Cells, Fuel Cells, pp 53-135.

Bhattacharya, P.K. (2015) 'Water flooding in the proton exchange membrane fuel cell',: Space Science and Technology, IIT Kanpur publications, 15(01).

Bhosale, A.C., Suseendiran, S.R., Ramya, R., Choudhury, S.R. and Rengaswamy, R. (2022). Phosphoric Acid Fuel Cells. Comprehensive Renewable Energy, pp.437–458.

Boldrin, P., Ruiz-Trejo, E., Mermelstein, J., Bermúdez Menéndez, J.M., Ramírez ReinaT. and Brandon, N.P. (2016). Strategies for Carbon and Sulfur Tolerant Solid Oxide Fuel Cell Materials, Incorporating Lessons from Heterogeneous Catalysis. Chemical Reviews, 116(22), pp.13633–13684.

De Bruijn, F. (2005). The current status of fuel cell technology for mobile and stationary applications. Green Chemistry, 7(3).

Campanari, S., Chiesa, P. and Manzolini, G. (2010) 'CO_2 capture from combined cycles integrated with Molten Carbonate Fuel Cells', International Journal of Greenhouse Gas Control, 4(3), pp. 441–451.

Casadidio, C., Peregrina, D.V., Gigliobianco, M.R., Deng, S., Censi, R. and Di Martino, P. (2019). Chitin and Chitosans: Characteristics, Eco-Friendly Processes, and Applications in Cosmetic Science. Marine Drugs, 17(6), pp. undefined-369.

Chen, Q., Zhang, G., Zhang, X., Sun, C., Jiao, K. and Wang, Y. (2021). Thermal management of polymer electrolyte membrane fuel cells: A review of cooling methods, material properties, and durability. Applied Energy, 286, pp. undefined-14.

Chen, Q., Qi, Y., Jiang, Y., Quan, W., Luo, H., Wu, K., Li, S. and Ouyang, Q. (2022). Progress in Research of Chitosan Chemical Modification Technologies and Their Applications. Marine Drugs, 20(8), pp. undefined-536.

Chiesa, P., Campanari, S. and Manzolini, G. (2011) 'CO_2 cryogenic separation from combined cycles integrated with molten carbonate fuel cells', International Journal of Hydrogen Energy, 36(16), pp. undefined-10355.

CHO, C., KIM, Y. and CHANG, Y.-S. (2009) 'Performance Analysis of Direct Methanol Fuel Cell for Optimal Operation', Journal of Thermal Science and Technology, 4(3), pp. 414–423.

Contreras, R.R., Almarza, J. and Rincón, L. (2021) 'Molten carbonate fuel cells: a technological perspective and review', Energy Sources, Part A: Recovery, Utilization and EnvironmentalEffects.00(00), pp.1–15.

Corigliano, O., Pagnotta, L. and Fragiacomo, P. (2022) 'On the Technology of Solid Oxide Fuel Cell (SOFC) Energy Systems for Stationary Power Generation: A Review', Sustainability (Switzerland), 14(22).

Da Costa Neto, B.P., da Mata, A.L.M.L., Lopes, M.V., Rossi-Bergmann, B. and Ré, M.I. (2014). Preparation and evaluation of chitosan–hydrophobic silica composite microspheres: Role of hydrophobic silica in modifying their properties. Powder Technology, 255, pp.109–119.

Das, G., Choi, J.-H., Nguyen, P.K.T., Kim, D.-J. and Yoon, Y.S. (2022). Anion Exchange Membranes for Fuel Cell Application: A Review. Polymers, [online] 14(6), pp. undefined-1197.

Demirbas, A. (2008) 'Direct use of methanol in fuel cells', Energy Sources, Part A: Recovery, Utilization and Environmental Effects, 30(6), pp. 529–535.

Devrim, Y., Erkan, S., Baç, N. and Eroglu, I. (2012). Nafion/titanium silicon oxide nanocomposite membranes for PEM fuel cells. International Journal of Energy Research, 37(5), pp.435–442.

Du, Z. and Zhan, H. (2021) 'Analysis of Related Technologies Used in Fuel Cell Vehicles', Journal Physics: Conference Series, 2125(1).pp. undefined-012011 .

Feng, S., Yang, G., Zheng, D., Rauf, A., Khan, U., Cheng, R., Wang, L., Wang, W. and Liu, F. (2022). Completely eliminating the metal barrier cracks on Nafion for suppressing methanol crossover with anodic aluminum oxide substrates,47(42), pp.18496–18503.

Feng, Y., Liu, H. and Yang, J. (2017) 'A selective electrocatalyst–based direct methanol fuel cell operated at high concentrations of methanol', Science Advances, 3(6).

Ferguson, S. and Tarrant, A. (2021) 'Molten Carbonate Fuel Cells for 90% Post Combustion CO_2 Capture from a New Build CCGT', Frontiers in Energy Research, 9(July), pp. 1–6.

Ferriday, T.B. and Middleton, P.H. (2021) 'Alkaline fuel cell technology - A review', International Journal of Hydrogen Energy. Elsevier Ltd, pp. 18489–18510.

Friess, B.R., Shahraeeni, M. and Hoorfar, M. (2008) 'Water management in PEM fuel cells', AIChE Annual Meeting, Conference Proceedings [Preprint], (May 2014).

Garc'ia, B.L. and Weidner, J.W. (2007) Review of Direct Methanol Fuel Cells.pp.229-285.

García, M.A., de la Paz, N., Castro, C., Rodríguez, J.L., Rapado, M., Zuluaga, R., Gañán, P. and Casariego, A. (2015). Effect of molecular weight reduction by gamma irradiation on the antioxidant capacity of chitosan from lobster shells. Journal of Radiation Research and Applied Sciences, 8(2), pp.190–200.

Ghassemi, Z. and Slaughter, G. (2017) 'Biological fuel cells and membranes', Membranes,7(1).

Giorgi, L. (2013a) 'Fuel Cells: Technologies and Applications', The Open Fuel Cells Journal, 6(1), pp. 1–20.

Giorgi, L. and Leccese, F. (no date) Send Orders of Reprints at reprints@benthamscience.net Fuel Cells: Technologies and Applications.

Gloukhovski, R., Freger, V. and Tsur, Y. (2018) 'Understanding methods of preparation and characterization of pore-filling polymer composites for proton exchange membranes: A beginner's guide', Reviews in Chemical Engineering, 34(4), pp. 455–479.

Goh, J.T.E., Abdul Rahim, A.R., Masdar, M.S. and Shyuan, L.K. (2021). Enhanced Performance of Polymer Electrolyte Membranes via Modification with Ionic Liquids for FC. Membranes,11(6).

Gorji, B. Fazaeli, R. and Niksarat. N. (2021) 'Synthesis and Characterizations of Silica Nanoparticles by a New Sol-Gel Method', Journal of Applied Chemical Research, 6(3), pp. 22–25.

Guangul, F.M. and Chala, G.T. (2020) 'A comparative study between the seven types of fuel cells', Applied Science and Engineering Progress, 13(3), pp. 185–194.

Gurau, B. and Smotkin, E.S. (2002) 'Methanol crossover in direct methanol fuel cells: A link between power and energy density', Journal of Power Sources, 112(2), pp. 339–352.

Hacquard, A. (no date) Improving and Understanding Direct Methanol Fuel Cell (DMFC) Performance.

Haile, S.M. (2003) 'Fuel cell materials and components', Acta Materialia, 51(19), pp. 5981–6000.

Hala, M., Mališ, J., Paidar, M. and Bouzek, K. (2022). Characterization of Commercial Polymer–Carbon Composite Bipolar Plates Used in PEM Fuel Cells. Membranes, 12(11).

Halim, E.M., Chemchoub, S., El Attar, A., Salih, F.E., Oularbi, L. and EL RHAZI, M. (2022). Recent Advances in Anode Metallic Catalysts Supported on Conducting Polymer-Based Materials for Direct Alcohol Fuel Cells. Frontiers in Energy Research, 10.

Halim, F.A., Hasran, U.A., Masdar, M.S., Kamarudin, S.K. and Daud, W.R.W. (2012). Overview on Vapor Feed Direct Methanol Fuel Cell. APCBEE Procedia, 3, pp.40–45.

Rosli, N.A.H., Loh, K.S., Wong, W.Y., Yunus, R.M., Lee, T.K., Ahmad, A. and Chong, S.T. (2020). Review of Chitosan-Based Polymers as Proton Exchange Membranes and Roles of Chitosan-Supported Ionic Liquids. International Journal of Molecular Sciences, 21(2)

Hertel, P. (2005) 'Membranes for fuel cells', ATZ worldwide, 107(6), pp. 22–25.

Hilmi, A., Yuh, C. and Farooque, M. (2009) 'Fuel Cells - Molten Carbonate Fuel Cells | Anodes', in Encyclopedia of Electrochemical Power Sources. Elsevier, pp. 454–461.

Hlavatá, L., Vyskočil, V., Beníková, K., Borbélyová, M. and Labuda, J. (2014). DNA-based biosensors with external Nafion and chitosan membranes for the evaluation of the antioxidant activity of beer, coffee, and tea. Open Chemistry, 12(5), pp.604–611.

Hosseini, S.E. and Butler, B. (2020) 'An overview of development and challenges in hydrogen powered vehicles', International Journal of Green Energy, 17(1), pp. 13–37.

Hou, J., Aydemir, B.E. and Dumanli, A.G. (2021) 'Understanding the structural diversity of chitins as a versatile biomaterial', Philosophical Transactions of the Royal Society A: Mathematical, Physical and Engineering Sciences, 379(2206).

Hren, M., Božič, M., Fakin, D., Kleinschek, K.S. and Gorgieva, S. (2021). Alkaline membrane fuel cells: anion exchange membranes and fuels. Sustainable Energy & Fuels, [online] 5(3), pp.604–637.

Hu, L. (no date) Molten Carbonate Fuel Cells for Electrolysis.pp.1-31.

Hussain, S. and Yangping, L. (2020) 'Review of solid oxide fuel cell materials: cathode, anode, and electrolyte', Energy Transitions, 4(2), pp. 113–126.

I Ibrahim, I., Ebeid, H., Kishk, Y., Abdel Fattah, A.F., Mahmoud, K., Ibrahim, A., Ebeid, H., Kishk, Y., Abdel Fattah, A. and Mahmoud, K. (2019). Effect of grinding and particle size on some

physical and rheological properties of Chitosan. Arab Universities Journal of Agricultural Sciences, 27(2), pp.1513–1527.

Jain, Ankit. (2013) 'A new horizon in modifications of chitosan: Syntheses and applications', Critical Reviews in Therapeutic Drug Carrier Systems, 30(2), pp. 91–181.

Jawad, N.H., Yahya, A.A., Al-Shathr, A.R., Salih, H.G., Rashid, K.T., Al-Saadi, S., AbdulRazak, A.A., Salih, I.K., Zrelli, A. and Alsalhy, Q.F. (2022). Fuel Cell Types, Properties of Membrane, and Operating Conditions: A Review. Sustainability, [online] 14(21), pp. undefined-14653.

Ji, M. and Wei, Z. (2009) 'A review of water management in polymer electrolyte membrane fuel cells', Energies, 2(4), pp. 1057–1106.

Jiao, K. and Li, X. (2011) 'Water transport in polymer electrolyte membrane fuel cells', Progress in Energy and Combustion Science, pp. 221–291.

Junoh, H., Jaafar, J., Mohd Norddin, M.N.A., Ismail, A.F., Othman, M.H.D., Rahman, M.A., Yusof, N., Wan Salleh, W.N. and Ilbeygi, H. (2015). A Review on the Fabrication of Electrospun Polymer Electrolyte Membrane for Direct Methanol Fuel Cell. Journal of Nanomaterials, 2015, pp.1–16.

Junoh, H., Jaafar, J., Nordin, N., Ismail, A., Othman, M., Rahman, M., Aziz, F. and Yusof, N. (2020). Performance of Polymer Electrolyte Membrane for Direct Methanol Fuel Cell Application: Perspective on Morphological Structure. Membranes, 10(3), pp.34.

Kadirkhan, F., Goh, P.S., Ismail, A.F., Wan Mustapa, W.N.F., Halim, M.H.M., Soh, W.K. and Yeo, S.Y. (2022). Recent Advances of Polymeric Membranes in Tackling Plasticization and Aging for Practical Industrial CO_2/CH_4 Applications—A Review. Membranes,12(1), pp.71.

Kalamaras, C.M. and Efstathiou, A.M. (2013) 'Hydrogen Production Technologies: Current State and Future Developments', Conference Papers in Energy, 2013, pp. 1–9.

Kampker, A., Heimes, H., Kehrer, M., Hagedorn, S., Reims, P. and Kaul, O. (2023). Fuel cell system production cost Modeling and analysis. Energy Reports, 9, pp.248–255.

Kang, M.-S. (2013) 'Development of Pore-filled Ion-exchange Membranes for Efficient All Vanadium Redox Flow Batteries', Journal of the Korean Electrochemical Society, 16(4), pp. 204–210.

Kannan, A., Aili, D., Cleemann, L.N., Li, Q. and Jensen, J.O. (2020). Three-layered electrolyte membranes with acid reservoir for prolonged lifetime of high-temperature polymer electrolyte membrane fuel cells. International Journal of Hydrogen Energy, 45(1), pp.1008–1017.

Karan, K. (2019) 'Interesting Facets of Surface, Interfacial, and Bulk Characteristics of Perfluorinated Ionomer Films', Langmuir. American Chemical Society, pp.13489–13520.

Kargupta, K., Saha, S., Banerjee, D., Seal, M. and Ganguly, S. (2012). Performance enhancement of phosphoric acid fuel cell by using phosphosilicate gel-based electrolyte. Journal of Fuel Chemistry and Technology, 40(6), pp.707–713.

Karim, M. (2021) 'Titanium dioxide nanoparticle incorporated PVDF-HFP based composite membrane for direct methanol fuel cells application', Bangladesh Journal of Scientific and Industrial Research, 56(2), pp. 125–132.

Kasaai, M.R., Arul, J. and Charlet, G. (2008) 'Fragmentation of chitosan by ultrasonic irradiation', Ultrasonics Sonochemistry, 15(6), pp. 1001–1008.

Kasyanova, A.V., Zvonareva, I.A., Tarasova, N.A., Bi, L., Medvedev, D.A. and Shao, Z. (2022). Electrolyte materials for protonic ceramic electrochemical cells: Main limitations and potential solutions. Materials Reports: Energy, 2(4), pp. undefined-100158.

Kee, R.J., Zhu, H., Sukeshini, A.M. and Jackson, G.S. (2008). Solid Oxide Fuel Cells: Operating Principles, Current Challenges, and the Role of Syngas. Combustion Science,180(6), pp.1207–1244.Kim, K., Kim, S.-K., Park, J.O., Choi, S.-W., Kim, K.-H., Ko, T., Pak, C. and Lee, J.-C. (2017). Highly reinforced pore-filling membranes based on sulfonated poly (arylene ether sulfone)s for high-temperature/low-humidity polymer electrolyte membrane. Membrane Science, 537, pp 11-21.

Kim, Y.S., Welch, C.F., Hjelm, R.P., Mack, N.H., Labouriau, A. and Orler, E.B. (2015). Origin of Toughness in Dispersion-Cast Nafion Membranes. Macromolecules,48(7), pp.2161–2172.

Kong, W.L., Masdar, M.S. and Zainoodin, A.M. (2015) 'Performances on Direct Liquid Fuel Cell in Semi-Passive and Passive Modes', 5, pp. 35–39.

Kordesch, K., Hacker, V., Reichmann, K., Cifrain, M., Hejze, T. and Aronsson, R.R. (2008). The Safe and Economic Revival of Alkaline Hydrogen/Air Fuel Cells with Circulating Electrolytes,

Recommended for Vehicles Using Battery Hybrid Systems and H2 from Ammonia Crackers. ECS Transactions, 11(32), pp.167–185.

Kozma, M., Acharya, B. and Bissessur, R. (2022) 'Chitin, Chitosan, and Nanochitin: Extraction, Synthesis, and Applications', pp. 1–28.

Kumuk, B. (2019) 'A Review of Fuel Cell Types and Applications', Turkish Journal of Energy Policy, 4(9).

Kusoglu, A. and Weber, A.Z. (2017) 'New Insights into Perfluorinated Sulfonic-Acid Ionomers', Reviews,117(3), pp.987–1104.

Kusumastuti, E., Siniwi, W.T., Mahatmanti, F.W., Jumaeri, Atmaja, L. and Widiastuti, N. (2016). Modification of chitosan membranes with nano-silica particles as polymer electrolyte membranes.

Kyzas, G.Z. and Bikiaris, D.N. (2015) 'Recent modifications of chitosan for adsorption applications: A critical and systematic review', Marine Drugs. MDPI AG, pp. 312–337.

Li, H. et al. (2020) 'Molten Carbonate Fuel Cell Power Generation Technology and its Challenges', pp. 1–12.

Li, Q., Dunn, E.T., Grandmaison, E.W. and Goosen, M.F.A. (1992). Applications and Properties of Chitosan. Journal of Bioactive and Compatible Polymers, 7(4), pp.370–397.

Mack, F. (2015) 'Novel phosphoric acid-doped PBI-blends as membranes for high-temperature PEM fuel cells', Journal of Materials Chemistry A, 3(20), pp. 10864–10874.

Mahmud, M., Naziri, M.I., Yacob, N., Talip, N. and Abdullah, Z. (2014). Degradation of chitosan by gamma-ray with the presence of hydrogen peroxide. AIP Conference Proceedings.

Maiyalagan, T. and Pasupathi, S. (2010) Components for PEM fuel cells: An overview, Materials Science Forum.pp.143-189.

Mallick, R.K., Moharana, H.S. and Mohapatra, K. (2018) 'Performance Simulation of Passive Direct Methanol Fuel Cell', 8(1), pp. 205–212.

Mansor, M., Timmiati, S.N., Lim, K.L., Wong, W.Y., Kamarudin, S.K. and Nazirah Kamarudin, N.H. (2019). Recent progress of anode catalysts and their support materials for methanol electrooxidation reaction. International Journal of Hydrogen Energy, 44(29), pp.14744–14769.

Masdar, M.S., Dedikarni, Zainoodin, A.M., Rosli, M.I., Kamarudin, S.K. and Daud, W.R.W. (2017). Performance and stability of single and 6-cell stack passive direct methanol fuel cell (DMFC) for long-term operation. International Journal of Hydrogen Energy, [online] 42(14), pp.9230–9242.

Masdar, M.S., Tsujiguchi, T. and Nakagawa, N. (2010) 'Improvement of water management in a vapor feed direct methanol fuel cell', Journal of Power Sources, 195(24), pp. 8028–8035.

Mayadevi, T.S., Goo, B.-H., Paek, S.Y., Choi, O., Kim, Y., Kwon, O.J., Lee, S.Y., Kim, H.-J. and Kim, T.-H. (2022). Nafion Composite Membranes Impregnated with Polydopamine and Poly (Sulfonated Dopamine) for High-Performance Proton Exchange Membranes. ACS Omega, 7(15), pp.12956–12970.

Mekhilef, S., Saidur, R. and Safari, A. (2012) 'Comparative study of different fuel cell technologies', Renewable and Sustainable Energy Reviews. Elsevier Ltd, pp. 981–989.

Mench, M.M. (2006) 'Fuel Cells', Mechanical Engineers' Handbook: Energy and Power: Third Edition, 4, pp. 922–957.

Meng, Q. and Tian, A. (2018) 'INfluence of flow field path design of direct methanol fuel cell on "water flooding phenomenon" of cathode', in. ZIbeline International Publishing, pp. 459–462.

Merle, G., Wessling, M. and Nijmeijer, K. (2011) 'Anion exchange membranes for alkaline fuel cells: A review', Journal of Membrane Science, pp. 1–35.

Mohammed Hello, K. and Kadhim Hlial, E. (2019) 'Modification of silica with sulfuric acid and phosphoric acid for cellulose hydrolysis', Journal of Physics: Conference Series, 1294(5).

Mohsenpour, S., Kamgar, A. and Esmaeilzadeh, F. (2018) 'Investigation the Effect of TiO_2 Nanoparticles on Proton Exchange Membrane of sPEEK Used as a Fuel Cell Electrolyte Based on Phase Diagram', Journal of Inorganic and Organometallic Polymers and Materials, 28(1), pp. 63–72.

Mukoma, P., Jooste, B.R. and Vosloo, H.C.M. (2004) 'A comparison of methanol permeability in Chitosan and Nafion 117 membranes at high to medium methanol concentrations', Journal of Membrane Science, 243(1–2), pp. 293–299.

Myndrul, V., Iatsunskyi, I., Babayevska, N., Jarek, M. and Jesionowski, T. (2022). Effect of Electrode Modification with Chitosan and Nafion® on the Efficiency of Real-Time Enzyme Glucose Biosensors Based on ZnO Tetrapods. Materials, 15(13), pp.4651-4672.

Neburchilov, V., Martin, J., Wang, H. and Zhang, J. (2007). A review of polymer electrolyte membranes for direct methanol fuel cells. Journal of Power Sources, 169(2), pp.221–238.

Ng, W.W., Thiam, H.S., Pang, Y.L., Chong, K.C. and Lai, S.O. (2022). A State-of-Art on the Development of Nafion-Based Membrane for Performance Improvement in Direct Methanol Fuel Cells. Membranes, 12(5), pp. 506.

Nguyen, H.L., Han, J., Nguyen, X.L., Yu, S., Goo, Y.-M. and Le, D.D. (2021). Review of the Durability of Polymer Electrolyte Membrane Fuel Cell in Long-Term Operation: Main Influencing Parameters and Testing Protocols. Energies, 14(13),

Nguyen, H.L., Han, J., Vu, H.N. and Yu, S. (2022). Investigation of Multiple Degradation Mechanisms of a Proton Exchange Membrane Fuel Cell under Dynamic Operation. Energies, 15(24), pp. 1-21.

Niakolas, D.K. Daliteu, M., Neophytides, S.G. and Vayenas, C.G. (2016) 'Fuel cells are a commercially viable alternative for the production of "clean" energy', Ambio, 45(1), pp. 32–37.

Ogungbemi, E., Ijaodola, O., Khatib, F.N., Wilberforce, T., El Hassan, Z., Thompson, J., Ramadan, M. and Olabi, A.G. (2019). Fuel cell membranes – Pros and cons. Energy, 172, pp.155–172.

Olabi, A.G., Wilberforce, T., Alanazi, A., Vichare, P., Sayed, E.T., Maghrabie, H.M., Elsaid, K. and Abdelkareem, M.A. (2022). Novel Trends in Proton Exchange Membrane Fuel Cells. Energies, 15(14), pp.4939-4949.

Osifo, P.O. and Masala, A. (2010) 'Characterization of direct methanol fuel cell (DMFC) applications with H2SO4 modified chitosan membrane', Journal of Power Sources, 195(15), pp. 4915–4922.

Padgett, E., Yarlagadda, V., Holtz, M.E., Ko, M., Levin, B.D.A., Kukreja, R.S., Ziegelbauer, J.M., Andrews, R.N., Ilavsky, J., Kongkanand, A. and Muller, D.A. (2019). Mitigation of PEM Fuel Cell Catalyst Degradation with Porous Carbon Supports. Journal of The Electrochemical Society, 166(4), pp. F198–F207.

Pal, J. (2014) 'Biological method of chitin extraction from shrimp waste an eco-friendly low cost technology and its advanced application', International Journal of Fisheries and Aquatic Studies IJFAS, 1(6), pp. 104–107.

Pati, S., Chatterji, A., Dash, B.P., Raveen Nelson, B., Sarkar, T., Shahimi, S., Atan Edinur, H., Binti Abd Manan, T.S., Jena, P., Mohanta, Y.K. and Acharya, D. (2020). Structural Characterization and Antioxidant Potential of Chitosan by γ-Irradiation from the Carapace of Horseshoe Crab. Polymers, [online] 12(10), pp. 2361.

Peighambardoust, S.J., Rowshanzamir, S. and Amjadi, M. (2010) Review of the proton exchange membranes for fuel cell applications, International Journal of Hydrogen Energy Elsevier Ltd.

Permana, D., Ahmad, L.Od. and Ramadhan, L.O.A.N.N. (2016) 'Enhanced Conductivity and Ion Exchange Capacity of Chitosan Membranes through Modification with Lithium for Lithium Polymer Battery Application | Request PDF', WSEAS Transactions on Power Systems, 11, pp. 183–189.

Pica, M. (2014) 'Non-fluorinated Membranes: Fuel Cell Applications', in Encyclopedia of Membranes. Springer Berlin Heidelberg, pp. 1–2.

Pighinelli, L. (2019) 'Methods of Chitin Production a Short Review', American Journal of Biomedical Science & Research, 3(4), pp. 307–314.

Pihlatie, M. (2010) Stability of Ni-YSZ composites for solid oxide fuel cells during reduction and re-oxidation, VTT Publications.

Podgorbunskikh, E., Kuskov, T., Rychkov, D., Lomovskii, O. and Bychkov, A. (2022). Mechanical Amorphization of Chitosan with Different Molecular Weights. Polymers, 14(20), pp.4422-4438.

Popovici, O. (2014) 'The study of the efficiency of a direct methanol fuel cell', Journal of Electrical and Electronics Engineering, 7(2), pp. 31–34.

Prabhakaran, V., Arges, C.G. and Ramani, V. (2012) 'Investigation of polymer electrolyte membrane chemical degradation and degradation mitigation using in situ fluorescence spectroscopy', Proceedings of the National Academy of Sciences of the United States of America, 109(4), pp. 1029–1034.

Purwanto, M., Widiastuti, N., Saga, B.H. and Gusmawan, H. (2021). Synthesis of Composite Membrane Based Biopolymer Chitosan with Silica from Rice Husk Ash for Direct Methanol Fuel Cell Application. IOP Conference Series: Earth and Environmental Science, 830(1), pp.012011-012021.

Qiu, D., Peng, L., Liang, P., Yi, P. and Lai, X. (2018). Mechanical degradation of proton exchange membrane along the MEA frame in proton exchange membrane fuel cells. Energy, 165, pp.210–222.

Ramkrishna Joshi, M.N. (2014) 'Development in Direct Methanol – Oxygen Fuel Cell (DMFC)', IOSR Journal of Applied Chemistry, 7(9), pp. 24–26.

Ren, X. (1995) 'Methanol Cross-over in Direct Methanol Fuel Cells', ECS Proceedings Volumes, 1995–23(1), pp. 284–298.

Rinaudo, M. (2006) 'Chitin and chitosan: Properties and applications', Progress in Polymer Science (Oxford), pp. 603–632.

Robertson, J. (2004) '11119', The American Mathematical Monthly, 111(10), pp.891- 915.

Romanazzi, G., Gabler, F.M., Margosan, D., Mackey, B.E. and Smilanick, J.L. (2009). Effect of Chitosan Dissolved in Different Acids on Its Ability to Control Postharvest Gray Mold of Table Grape. Phytopathology®, 99(9), pp.1028–1036.

Roziére, J. and Jones, D.J. (2003) 'Non-fluorinated polymer materials for proton exchange membrane fuel cells', Annual Review of Materials Research, 33, pp. 503–555.

Anon, (n.d.). International Journal of Current Engineering and Technology - Inpressco.

Salarizadeh, P., Javanbakht, M., Pourmahdian, S., Hazer, M.S.A., Hooshyari, K. and Askari, M.B. (2019). Novel proton exchange membranes based on proton conductive sulfonated PAMPS/PSSA-TiO$_2$ hybrid nanoparticles and sulfonated poly (ether ether ketone) for PEMFC. International Journal of Hydrogen Energy, 44(5), pp.3099–3114.

Schröder, A., Wippermann, K., Lehnert, W., Stolten, D., Sanders, T., Baumhöfer, T., Kardjilov, N., Hilger, A., Banhart, J. and Manke, I. (2010). The influence of gas diffusion layer wettability on direct methanol fuel cell performance: A combined local current distribution and high-resolution neutron radiography study. Journal of Power Sources, 195(15), pp.4765–4771.

Science, E. (2021) 'Synthesis of Composite Membrane Based Biopolymer Chitosan with Silica from Rice Husk Ash For Direct Methanol Fuel Cell Application Synthesis of Composite Membrane Based Biopolymer Chitosan With Silica From Rice Husk Ash For Direct Methanol Fuel Cell Application'.

Scott, K., Taama, W.M., Argyropoulos, P. and Sundmacher, K. (1999). The impact of mass transport and methanol crossover on the direct methanol fuel cell. Journal of Power Sources, 83(1-2), pp.204–216.

Scott, K. and Xing, L. (2012) 'Direct Methanol Fuel Cells', in Advances in Chemical Engineering, pp. 145–196.

Shaari, N. and Kamarudin, S.K. (2015) 'Chitosan and alginate types of bio-membrane in fuel cell application: An overview', Journal of Power Sources, 289, pp. 71–80.

Shafer, W., Gnanamani, M., Graham, U., Yang, J., Masuku, C., Jacobs, G. and Davis, B. (2019). Fischer–Tropsch: Product Selectivity–The Fingerprint of Synthetic Fuels. Catalysts, 9(3), pp. 1-57.

Shi, N., Xie, Y., Yang, Y., Xue, S., Li, X., Zhu, K., Huan, D., Peng, R., Xia, C. and Lu, Y. (2020). Review of anodic reactions in hydrocarbon fueled solid oxide fuel cells and strategies to improve anode performance and stability. Materials for Renewable and Sustainable Energy, 9(1).

Shimpalee, S., Lilavivat, V., Xu, H., Rowlett, J.R., Mittelsteadt, C. and Van Zee, J. W. (2018). The Effect of Membrane Properties on Performance and Transports inside Polymer Electrolyte Membrane Fuel Cells. Journal of The Electrochemical Society, 165(11), pp. F1019–F1026.

Shrivastava, N.K., Thombre, S.B. and Chadge, R.B. (2016) 'Liquid feed passive direct methanol fuel cell : challenges and recent advances', pp. 1–23.

Shukla, A.K., Ramesh, K. V. and Kannan, A.M. (1986) 'Fuel cells: Problems and prospects', Proceedings of the Indian Academy of Sciences - Chemical Sciences, 97(3–4), pp. 513–527.

Sigwadi, R. (2013) Zirconia based /Nafion composite membranes for fuel cell applications.

Sigwadi, R., Dhlamini, M.S., Mokrani, T. and Nemavhola, F. (2019). Enhancing the mechanical properties of zirconia/Nafion® nanocomposite membrane through carbon nanotubes for fuel cell application. Heliyon, 5(7), p.e02112.

Simari, C., Lufrano, E., Godbert, N., Gournis, D., Coppola, L. and Nicotera, I. (2020). Titanium Dioxide Grafted on Graphene Oxide: Hybrid Nanofiller for Effective and Low-Cost Proton Exchange Membranes. Nanomaterials, 10(8), pp.1572.

Simari, C., Nicotera, I., Aricò, A.S., Baglio, V. and Lufrano, F. (2021). New Insights into Properties of Methanol Transport in Sulfonated Polysulfone Composite Membranes for Direct Methanol Fuel Cells. Polymers, 13(9).

Singh, M., Zappa, D. and Comini, E. (2021) 'Solid oxide fuel cell: Decade of progress, future perspectives and challenges', International Journal of Hydrogen Energy, 46(54), pp. 27643–27674.

Sugino, Y. and Kawaguchi, M. (2017) 'Fumed and precipitated hydrophilic silica suspension gels in mineral oil: Stability and rheological properties', Gels, 3(3). pp. 32.

Sun, X., Simonsen, S., Norby, T. and Chatzitakis, A. (2019). Composite Membranes for High-Temperature PEM Fuel Cells and Electrolysers: A Critical Review. Membranes, 9(7), pp.83.

Suraparaju, S.K., Natarajan, S.K. and Karthikeyan, P. (2019) 'A succinct review on fuel cells', IOP Conference Series: Earth and Environmental Science, 312(1). pp 012012.

Szliszka, E., Kumar, Y., Joly, N. and Martin. P. (2009) 'Ionotropic Gerlation of Chitosan Flat Structures and Potential Applications', Molecules, 14(2), pp. 738–754.

Szymańska, E. and Winnicka, K. (2015) 'Stability of chitosan - A challenge for pharmaceutical and biomedical applications', Marine Drugs. MDPI AG, pp. 1819–1846.

Tafaoli-Masoule, M., Bahrami, A. and Mohammadrezaei, D. (2013) 'Optimum conditions for a maximum power of a direct methanol fuel cell', ISRN Mechanical Engineering, 2013(i).pp 1-6.

Tan, Y., Matsui, H., Ishiguro, N., Uruga, T., Nguyen, D.-N., Sekizawa, O., Sakata, T., Maejima, N., Higashi, K., Dam, H.C. and Tada, M. (2019). Pt–Co/C Cathode Catalyst Degradation in a Polymer Electrolyte Fuel Cell Investigated by an Infographic Approach Combining Three-Dimensional Spectroimaging and Unsupervised Learning. The Journal of Physical Chemistry C, 123(31), pp.18844–18853.

Tang, A. (2021) 'An overview of bipolar plates in proton exchange membrane fuel cells', Journal of Renewable and Sustainable Energy, 13(2).pp. 02271.

Thmaini, N., Charradi, K., Ahmed, Z., Aranda, P. and Chtourou, R. (2022). Nafion/ SiO 2 @ TiO$_2$ -palygorskite membranes with improved proton conductivity. Journal of Applied Polymer Science, 139(21), pp.52201-52208.

Tjiptowidjojo, K., Park, J., Mauger, S.A., Ulsh, M. and Schunk, P.R. (2021). Process model for multilayer slide coating of polymer electrolyte membrane fuel cells. Journal of Coatings Technology and Research, 19(1), pp.73–81.

Tran, T.N., Anh Pham, T.V., Phung Le, M.L., Thoa Nguyen, T.P. and Tran, V.M. (2013). Synthesis of amorphous silica and sulfonic acid functionalized silica used as reinforced phase for polymer electrolyte membrane. Advances in Natural Sciences: Nanoscience and Nanotechnology, 4(4), pp.04500-045007.

Trinh, N.V., Nguyen, X.L., Kim, Y. and Yu, S. (2022). Characteristics of Water Transport of Membrane Electrolyte over Selected Temperature for Proton Exchange Membrane Fuel Cell. Polymers, 14(15).

Tsen, W.C. (2020) 'Composite proton exchange membranes based on chitosan and phosphotungstic acid immobilized one-dimensional attapulgite for direct methanol fuel cells', Nanomaterials, 10(9), pp. 1–15.

U.S. Department of Energy (2016) 'Combined heat and power technology fact sheet series - Fuel Cells', Combined Heat and Power Technology Fact Sheet Series.

Università,(2013) FuelCells: Technologies and Applications Fuel Cells: Technologies and Applications, The Open Journal.

US Department of Energy (2012) 'Fuel cell technologies office Early Markets : Fuel Cells for Backup Power The Case for Fuel Cells'.

Vaghari, H., Jafarizadeh-Malmiri, H., Berenjian, A. and Anarjan, N. (2013). Recent advances in application of chitosan in fuel cells. Sustainable Chemical Processes, 1(1).

Vaivars, (2004) 'Zirconium Phosphate Based Inorganic Direct Methanol Fuel Cell', materials Science, 10(2), pp. 162–165.

Vallejo-Domínguez, D., Rubio-Rosas, E., Aguila-Almanza, E., Hernández-Cocoletzi, H., Ramos-Cassellis, M.E., Luna-Guevara, M.L., Rambabu, K., Manickam, S., Siti Halimatul Munawaroh, H.

and Loke Show, P. (2021). Ultrasound in the deproteinization process for chitin and chitosan production. Ultrasonics Sonochemistry, 72, pp.105410-105417.

Vincent, I., Lee, E.C. and Kim, H.M. (2020) 'Solutions to the water flooding problem for unitized regenerative fuel cells: status and perspectives', RSC Advances, 10(29), pp. 16844–16860.

Vostakola, M.F. and Horri, B.A. (2021) 'Progress in material development for low-temperature solid oxide fuel cells: A review', Energies, 14(5).pp.1-53.

Wala, M. and Simka, W. (2021) 'Effect of anode material on electrochemical oxidation of low molecular weight alcohols—a review', Molecules, 26(8).

Walkowiak-Kulikowska, J., Wolska, J. and Koroniak, H. (2017) 'Polymers application in proton exchange membranes for fuel cells (PEMFCs)', Physical Sciences Reviews. pp.61-614.

Wang, C. (2013) 'Structure and Morphology of Sulfonated Polysulfone and Perfluorosulfonic Acid Ionomers'.pp. 1-176.

Wang, C., He, Q., Li, Z., Xu, Q., Han, M. and Ni, M. (2022). Modeling of solid oxide fuel cells with internal glycerol steam reforming. International Journal of Hydrogen Energy. pp. 15012-15023.

Wang, C. et al. (2022b) 'Modelling of solid oxide fuel cells with internal glycerol steam reforming', International Journal of Hydrogen Energy, 47(33), pp. 15012–15023.

Wang, Y., Moura, S.J., Advani, S.G. and Prasad, A.K. (2019). Power management system for a fuel cell/battery hybrid vehicle incorporating fuel cell and battery degradation. International Journal of Hydrogen Energy, 44(16), pp.8479–8492.

Weber, A.Z., Balasubramanian, S. and Das, P.K. (2012) 'Proton Exchange Membrane Fuel Cells', in Advances in Chemical Engineering, pp. 65–144.

Wee, J.H. (2014) 'Carbon dioxide emission reduction using molten carbonate fuel cell systems', Renewable and Sustainable Energy Reviews, 32, pp. 178–191.

Weidner, J.W., Sethuraman, V. and Zee, J.W. Van (no date) Membrane Electrode Assembly Direct Methanol Fuel Cell Modeling View project Graduate Work View project.pp.40-43.

Wilberforce, T., Alaswad, A., Palumbo, A., Dassisti, M. and Olabi, A.G. (2016). Advances in stationary and portable fuel cell applications. International Journal of Hydrogen Energy, 41(37), pp.16509–16522.

Williams, M.C. (2011) 'Fuel Cells', in Fuel Cells: Technologies for Fuel Processing. Elsevier, pp. 11–27.

Winter, M. and Brodd, R.J. (2004) 'What are batteries, fuel cells, and supercapacitors?', Chemical Reviews, 104(10), pp. 4245–4269.

Wisniak, J. (2015) 'Historical Notes: Electrochemistry and Fuel Cells: The Contribution of William Robert Grove', Indian Journal of History of Science, 50(4).pp. 476-490.

Xia, Z., Zhang, X., Sun, H., Wang, S. and Sun, G. (2019). Recent advances in multi-scale design and construction of materials for direct methanol fuel cells. Nano Energy, 65.

Xue, R., Zhang, Y. and Liu, X. (2017) 'A novel cathode gas diffusion layer for water management of passive M-DMFC', Energy, 139, pp. 535–541.

Yadav, R., Kalyan, B., Vig, S. and Sharma, H.G. (2022). Modeling of Proton Exchange Membrane Fuel Cell. Cognitive Informatics and Soft Computing, pp.163–172.

Yamaguchi, T., Miyata, F. and Nakao, S.I. (2003) 'Pore-filling type polymer electrolyte membranes for a direct methanol fuel cell', Journal of Membrane Science, 214(2), pp. 283–292.

Yan, M., Li, G., Li, M., He, H., Xu, H. and Liu, H. (2022). Hierarchical predictive energy management of fuel cell buses with launch control integrating traffic information. Energy Conversion and Management, 256, pp.115397.

Younes, I. and Rinaudo, M. (2015) 'Chitin and chitosan preparation from marine sources. Structure, properties and applications', Marine Drugs, 13(3), pp. 1133–1174.

Yu, E.H., Wang, X., Krewer, U., Li, L. and Scott, K. (2012). Direct oxidation alkaline fuel cells: from materials to systems. Energy Environ. Sci., 5(2), pp.5668–5680.

Yu, H., Zachman, M.J., Li, C., Hu, L., Kariuki, N.N., Mukundan, R., Xie, J., Neyerlin, K.C., Myers, D.J. and Cullen, D.A. (2022). Recreating Fuel Cell Catalyst Degradation in Aqueous Environments for Identical-Location Scanning Transmission Electron Microscopy Studies. ACS Applied Materials & Interfaces, 14(18), pp.20418–20429.

Yu, X. and Ye, S. (2007) 'Recent advances in activity and durability enhancement of Pt/C catalytic cathode in PEMFC. Part II: Degradation mechanism and durability enhancement of carbon-supported platinum catalyst', Journal of Power Sources, 172(1), pp. 145–154.

Yuda, A., Ashok, A. and Kumar, A. (2022) 'A comprehensive and critical review on recent progress in anode catalyst for methanol oxidation reaction', Catalysis Reviews - Science and Engineering, 64(1), pp. 126–228.

Zarabi Golkhatmi, S., Asghar, M.I. and Lund, P.D. (2022) 'A review on solid oxide fuel cell durability: Latest progress, mechanisms, and study tools', Renewable and Sustainable Energy Reviews, 161, pp. 112339.

Zatoń, M., Rozière, J. and Jones, D.J. (2017) 'Current understanding of chemical degradation mechanisms of perfluorosulfonic acid membranes and their mitigation strategies: A review', Sustainable Energy and Fuels, 1(3), pp. 409–438

Zhang, J., Yin, G.-P., Lai, Q.-Z., Wang, Z.-B., Cai, K.-D. and Liu, P. (2007). The influence of anode gas diffusion layer on the performance of low-temperature DMFC. Journal of Power Sources, [online] 168(2), pp.453–458.

Zhang, J. (2020). Thermodynamic Analyses of a Phosphoric Acid Fuel Cell / Thermoelectric Generator Hybrid System with the Thomson Effect. International Journal of Electrochemical Science, pp.3068–3088.

Zhang, S., Zhang, Y., Chen, J., Yin, C. and Liu, X. (2018). Design, fabrication, and performance evaluation of an integrated reformed methanol fuel cell for portable use. Journal of Power Sources, 389, pp.37–49.

Zhang, X.-W. and Pandalai, S.G. (2005) Advances in fuel cells. Research signpost.pp.1-143.

Zhu, L.-Y., Li, Y.-C., Liu, J., He, J., Wang, L.-Y. and Lei, J.-D. (2022). Recent developments in high-performance Nafion® membranes for hydrogen fuel cell applications. Petroleum Science, 19(3), pp.1371–1381.

Zuo, Z., Fu, Y. and Manthiram, A. (2012a) 'Novel blend membranes based on acid-base interactions for fuel cells', Polymers. MDPI AG, pp. 1627–1644.

Zuo, Z., Fu, Y. and Manthiram, A. (2012b) 'Novel blend membranes based on acid-base interactions for fuel cells', Polymers, 4(4), pp. 1627–1644.

Chapter 3 Methodology

3.1. Chemicals

Chitosan flakes, Medium molecular weight, (Merck)

Tetraethyl orthosilicate, $Si(OC_2H_5)_4$, 98%, (Merck)

Ammonia, NH_3, 25%, (Merck)

Acetic acid, CH_3COOH, 99%, (Merck)

Sodium hydroxide, NaOH, (Merck)

Ethanol, C_2H_5OH, 99.9%, (Merck)

Methanol, CH_3OH, 99.9% (Merck)

Sodium chloride, NaCl, (Merck)

Hydrochloric acid, HCl, 37%, (Merck)

Sulfuric acid, H_2SO_4, 99%, (Merck)

Taurine, $C_2H_7NO_3S$, 99%, (Merck)

3.2. Nanoparticle synthesis and Membrane fabrication

3.2.1. Synthesis of Silica Nanoparticles

3.2.1.1. Synthesis of Unmodified Silica Nanoparticles by **Sol-Gel Method**

Tetraethyl orthosilicate was used to make pure silica particles. This process includes hydrolysis and condensation of TEOS. Silica particles were prepared according to the method used by (Verma, 2018). 80 ml of TEOS and 200 ml of ethanol were stirred at room temperature for 30 minutes. A solution of ammonia was introduced dropwise and was stirred for an hour at 70 ℃. A sol-gel-like substance was dried at 100 ℃ for a day. Obtained silica particles were calcinated at 600 ℃ for 2 h and 24 h respectively to remove impurities from the particles.

3.2.1.2. Synthesis of Unmodified Silica Nanoparticles by the **Stober Method**

TEOS was used as the precursor for silica during the stober process. The nanoparticles were synthesized according to (Sivolapov, Myronyuk and Baklan, 2022). 80 ml of TEOS and ethanol were stirred at room temperature. A solution of ammonia, ethanol, and water was added and stirred for another hour at room temperature. The obtained mixture was centrifuged for 31 minutes 44 seconds at 3700 rpm. The white solid substances were dried at 100 °C for 24 h and purified by a furnace at different periods which are 2 h and 24 h.

3.2.1.3. Sulfonation of Silica Nanoparticles

Prepared silica nanoparticles were sulfonated using sulfuric acid. This was done to improve the proton conductivity of the nanoparticles. The sulfonation process for both particles produced by the sol-gel and stober process was the same. Sulfonation was done according to (Joseph Helen Therese *et al.*, 2019). 10 g of silica nanoparticles was mixed with 5ml of sulfuric acid and 200 ml methanol at room temperature, the mixture was stirred vigorously at 1500 rpm for 4 h. Sulfonated silica particles were then centrifuged for 31 minutes 44 seconds at 3700 rpm. Excess acid was removed by washing with deionized water and then dried at 100 °C for 24 h.
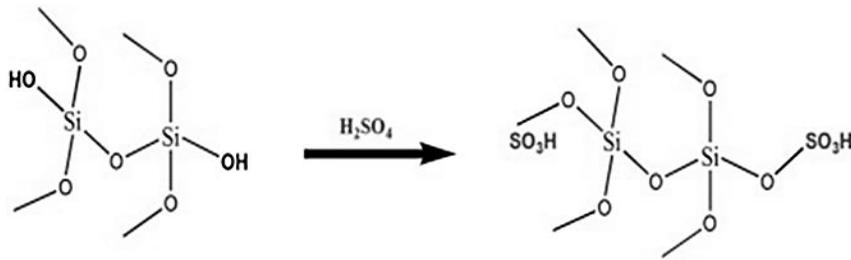

Figure 3.1. Sulfonation of silica

3.2.2. Membrane Fabrication

Chitosan membranes were fabricated using chitosan flakes as the main raw material. Membranes were fabricated according to (Mukoma, Jooste and Vosloo, 2004b) method. The membranes were synthesized by casting method. 2g of chitosan flakes were added to 2% v/v of acetic acid solution and stirred for an hour. Silica nanoparticles were added after an hour at the different weights (0%, 2%, and 4%) of silica nanoparticles. The gel solution was cast and dried at 60 ℃ for 4 h and then at room temperature. This procedure was also used for chitosan-sulfonated membranes.

3.3. Characterization Techniques

3.3.1. Fourier Transform Infrared Spectroscopy (FTIR)

Figure 3.2. Fourier Transform Infrared.

The functional groups present in the nanoparticles and membranes were investigated using infrared spectroscopy. A PerkinElmer paragon 1000 FTIR instrument was used to obtain the FTIR spectra, which had a resolution of 4 cm^{-1} and a range of 4000-600 cm^{-1}. The ideal technique for infrared spectroscopy is known as Fourier Transform Infrared (FT-IR). IR photons through a sample. A part of the infrared light is absorbed while another portion is passed through the sample. The resulting spectrum depicts the molecule absorption and transmission of the sample, yielding a molecular fingerprint. Functional groups have distinct absorption bands that correspond to the

functional groups' fundamental vibrations (Berthomieu and Hienerwadel, 2009; Sharma *et al.*, 2018).

3.3.2. Brunauer-Emmett-Teller (BET) measurements

Brunauer-Emmett-Teller theory BET is used to identify the surface area of particles, and it usually employs as adsorbate probing gases that do not react chemically with the material surfaces. The chemical or physical forces of contact cause gas adsorption on solid surfaces. The first is non-specific physical adsorption, whereas the second is highly specific chemisorption (Ambroz *et al.*, 2018; Raja and Barron, 2019). Although there are some classical differences between these two in terms of the interactions embroiled, many processes in nature are intermediate. Physical adsorption mechanisms can occur independently, while chemisorption requires non-specific adsorption. The theory attempts to describe the adsorption process of gas particles on a hard object and serves as the basis for a crucial analytical technique for determining the material's specific area. Nitrogen is the most utilized gaseous adsorbate for surface probing using BET techniques. As a result, standard BET analysis is typically carried out at the boiling temperature of N_2 (Brame and Griggs, 2016; Maponya *et al.*, 2022).
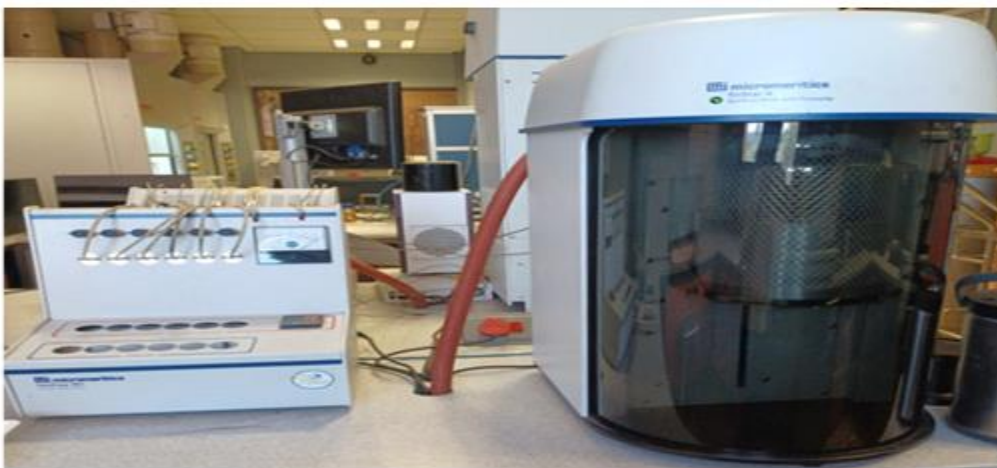

Figure 3.3. Brunauer Emmett Teller

The Micrometric 3-Flex equipment was used to conduct the BET analysis. Liquid nitrogen was used to cool a dry sample to 77 K after it was purged of all gas. A thin film of inert gas adheres to the sample's surface and lowers the pressure in the analysis chamber (' Walton and Snurr, 2007; Peyrovi and Parizi, 2022). The experiment's measured absorption isotherm was used to compute the surface area. All samples were de-gassed for 2 hours at 200-300 ℃ under vacuum before analysis. Before adsorption tests, test materials were degassed for 2 hours at 470 K at a pressure of 3×10^{-5} mbar. The measurements were performed on the powders that have been synthesized. The size of the particles was determined using the equation:

$$S= \frac{6}{\rho D_{BET}} \times 10^3$$

ρ-denote the theoretical density of the material which is estimated to be 6.27 g/cm^3 and $D_{BET} -$ denote the size of the particle in nm

3.3.3. X-ray Powder Diffraction Analysis (XRD)

The X-ray automated diffracto-meter from Philips (Model: PW 1830 diffracto-meter, Phillips, Netherlands). Cu KD radiation (O = 1.54 nm) was used in the XRD measurements. At a power of 60 KV and 60 mA, radiation was produced. A nominal step size of 0.033o 2T and a step period of 100 seconds were used to explore the 2T angular areas between 10 and 60º.

Structures, preferred crystal orientations (texture), and other structural factors such as crystallinity, average grain size, crystal defects, and strain are all included. X-ray diffraction peaks are produced by the constructive interference of a monochrome beam of X-rays scattered at exact angles from each pair of a sample's lattice planes. Peak intensities are determined by the arrangement of atoms within the lattice. As a result, the X-ray diffraction peaks identify periodic atomic setups in each material. According to Bragg's law, when incident rays contact a sample, constructive interference (and a diffracted ray) occurs (Bunaciu, Udriştioiu and Aboul-Enein, 2015).

nλ =2dsin

This principle integrates the spectrum of electromagnetic radiation to lattice spacing and diffraction angle in a crystalline sample. The diffracted X-rays are then identified, analyzed, and tallied. Because the powdered material has a non-uniform distribution, scanning the sample at a range of 2θ should produce all potential lattice diffraction directions. Although each material has a distinct set of d-spacings, transitioning the diffraction peaks to d-spacings allows the chemical to be identified. Generally, this is achieved by comparing d-spacings to known reference patterns (Bunaciu, Udriştioiu and Aboul-Enein, 2015.

3.3.4. Scanning Electron Microscopy (SEM)

Electron microscopy is an imaging technique for determining the topology, morphology, and surface structure of solid materials. The Hitachi x650 (FEI, Mode: Quanta 200) equipment was utilized to collect the surface data for the composite membranes and nanoparticles. SEM uses accelerated electromagnetic lenses or electron beams and electrostatic to create images with significantly greater resolution than visible light photons because electrons have shorter wavelengths than visible light photons (Guzzinati *et al.*, 2018; Abdullah and Mohammed, 2019).

3.3.5. Tensile Strength

Figure 3.4. Tensile strength testing.

A uniaxial testing technique was used to capture the uniaxial mechanical properties of membranes. Before testing, the samples' width, length, and thickness were measured with a Vernier caliper. The samples were prepared in such a manner that they can be clamped on all sides while still allowing for a testing area. Digital micrometers were used to measure the membrane thickness. Each thickness was determined by taking an average of 10 readings at various locations on the membrane and repeating the process twice on each membrane to reach the average result. The stress applied to the sample was measured using the thickness of the composite membrane. Membrane tensile strength was evaluated by use of a cell scale-stretch device, which were dried at room temperature 24.6 ℃ at a different speed.

3.4. Membrane Properties

3.4.1. Proton Conductivity

According to Christine et al (2018), Proton conductivity can be evaluated by the AC impedance technique. The polymer film was placed between platinum electrodes. Conductivity was calculated using the below equation:

$$\sigma = \frac{l}{A \times R}$$

Where σ is the conductivity of the membrane, is the distance between the electrodes, A is the effective area and R is the resistance of the membrane.

3.4.2. Methanol Permeability

Methanol permeability is the most crucial aspect in determining the efficiency of the cell. The high crossover will limit fuel cell performance. Membrane permeability to methanol will be determined by a two-compartment diffusion cell having the membrane in-between (Harmoko, Mujiburohman and Purnama, 2019).
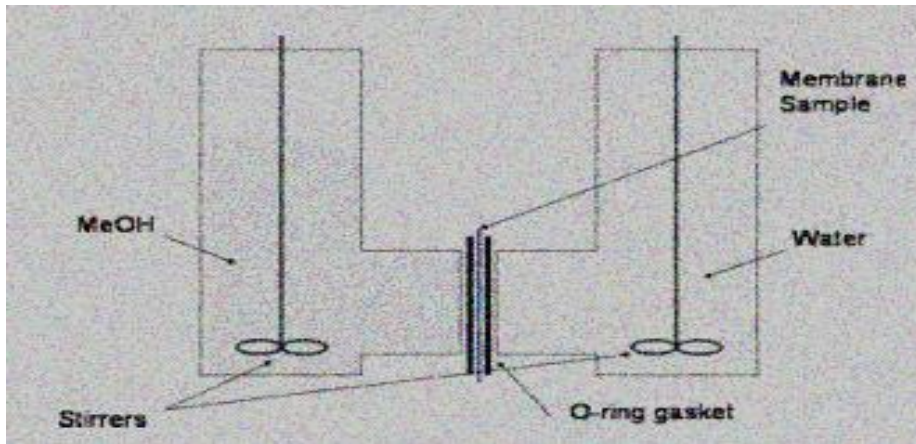
Figure 3.5. Diffusion Cell.

Both A and B cell compartments were loaded with the same amount of Methanol fuel and water respectively. Both sides of the cell will be stirring. Permeability values will be calculated as follows:

$$P = \frac{L}{A} \times \frac{V_b}{C_a} \times \frac{\Delta C}{\Delta t}$$

P-Permeability-Thickness of the membrane, A-Area available for diffusion in the membrane-Volume of receiving compartment, C_a is the Concentration of sample in component A, ΔC is the change in methanol concentration, Δt is the permeation time.

3.4.3. Water Uptake

Water uptake is defined as how much water can a membrane absorb, this factor contributes to the swelling ratio of a membrane. The membrane's water uptake is a very crucial aspect of the use of a membrane in fuel cell technology (Mukoma, Jooste and Vosloo, 2004b). The difference in mass between the hydrated and dehydrated membranes is utilized to calculate the proportion of water taken up. The mass of a wet membrane was obtained by soaking it for 24 hours and that of a dry membrane will be measured before the membrane is soaked in water (Lupatini *et al.*, 2016). Water uptake is calculated as follows:

Water (%) = $(\frac{Gw-GD}{GD}) \times 100\%$

Where G_W is described as the weight of wet membranes and G_D is the Dry membrane's weight.

3.4.5. Ion Exchange Capacity (IEC)

The ion exchange capacity was measured using the method used by Sigwadi et al., (2009). Membranes that will be in the acidic form will be put in NaCl solution for 2 days for Na^+ to interchange H^+ ions. The H^+ ion that will be released will be titrated with a solution of sodium hydroxide using a phenolphthalein indicator. The membrane film was then dipped in a 20 ml aqueous solution of 2M sodium chloride to allow the substitution of protons with Na^+ ions. The protons that were ejected were titrated with 0.01 M sodium chloride solution until it reaches a pH balance. Ion exchange capacity will be calculated as follows:

$$IEC = \frac{VNaOH * CNaOH}{Mdry}$$

Where IEC is the ion exchange capacity of the membrane, C_{NaOH} is – Concentration of NaOH in mol/l, $V_{NaOH\ is}$- Volume of NaOH that will be used to neutralize H+ in ml, Mdry is- Mass of dry membrane in g.

3.5. References

Abdullah, A. and Mohammed, A. (2019) 'Scanning Electron Microscopy (SEM): A Review', Proceedings of 2018 International Conference on Hydraulics and Pneumatics - HERVEX, (January), pp. 77–85.

Ambroz, F., Macdonald, T.J., Martis, V. and Parkin, I.P. (2018) 'Evaluation of the BET theory for the characterization of meso and microporous MOFs', Small Methods, 2(11).

Berthomieu, C. and Hienerwadel, R. (2009) 'Fourier transform infrared (FTIR) spectroscopy', Photosynthesis Research, 101(2–3), pp. 157–170.

Brame, J. A. and Griggs, C. (2016) 'Surface Area Analysis Using the Brunauer-Emmett-Teller (BET) Method: Scientific Operation Procedure Series: SOP-C', U.S Army Engineer Research and Development Center, (September), pp. 1–23.

Bunaciu, A. A., Udriştioiu, E. gabriela and Aboul-Enein, H. Y. (2015) 'X-Ray Diffraction: Instrumentation and Applications', Critical Reviews in Analytical Chemistry, 45(4), pp. 289–299.

Guzzinati, G., Antlantiz, T., Batuk, M., Samae, V., Batuk, D., Idrissi, H., Hadermann, J., Van Alert, S., Schryvers, D., Verbeeck, J. and Bals, S. (2018) 'Recent advances in transmission electron microscopy for materials science at the EMAT lab of the university of Antwerp, Materials, 11(8).

Maponya, T. C., Makgoba, K., Somo, T.R. and Modibane, T.R. (2022) 'Highlighting the Importance of Characterization Techniques Employed in Adsorption Using Metal–Organic Frameworks for Water Treatment', Polymers, 14(17).

Peyrovi, M. H. and Parizi, M. A. (2022) 'The Modification of the BET Surface Area by Considering the Excluded Area of Adsorbed Molecules', Physical Chemistry Research, 10(2), pp. 173–177.

Raja, P. M. V. and Barron, A. R. (2019) '2 .3: BET surface area analysis of nanoparticles', Physical Methods in Chemistry and Nano Science, pp. 1–7.

Sharma, S. K. Verma, D.S., Kumar, S. and Khan, S.B. (2018) 'Handbook of Materials Characterization', Handbook of Materials Characterization, (July 2020), pp. 1–613.

Chapter 4 Synthesis of Silica Particles

4.1. Introduction

A variety of types of silicon are found in the environment. In addition to not existing in nascent form, it is always present in coexisting with hydroxides, such as silicic acid, or oxygen, as in silica. Silicon and oxygen compounds make up 78% of the earth's crust (Wazamtu, Sani and Abdulsalam, 2013; Carol Deutsch1 Pengse Po1 Erin Delaney1, 2017; Elliston, 2018). Additionally, silica is present in living things such as sponges, algae, and grasses (Farooq and Dietz, 2015). The dissolved form of silicon, silicic acid, is abundant in the oceans (Crundwell, 2017). Silica can be found in both amorphous and crystalline forms, such as quartz, flint, opal, and silicate. Silica characteristics such as low density, outstanding mechanical and thermal stability, and chemical inertia, makes it to be a better promising material for modifying polymer membranes used in a fuel cell (Farooq and Dietz, 2015; Crundwell, 2017). Their adaptability in terms of structure, size, biocompatibility, large surface area, and variable functionalization makes particles have a vast array of industrial, biotechnological, and biomedical/pharmaceutical uses, as a result, they are frequently used in a variety of contexts (Farooq and Dietz, 2015; Joseph *et al.*, 2023). According to the literature, conventional techniques have been utilized to create silica: flame synthesis, Sol-gel procedures, the Stober process, and Microemulsions (Rahman and Padavettan, 2012).

The parameters that are used to produce synthesized silica, such as the synthesis temperature, the duration of condensation and hydrolysis, solvent concentration, and methods for washing and drying, all have a significant impact on the material's properties (Wan *et al.*, no date). These parameters have an impact on the size and size distribution of SiO_2 particles (Wan *et al.*, no date). When silica particles are incorporated into a polymer matrix, they promote interfacial interaction or reaction. According to (Kusumastuti *et al.*, 2016a) and (Wan et al, no date), silica particles incorporated into the chitosan membrane reduce crystallinity and lower methanol crossover whilst improving tensile strength. Recent research indicated that extra silica functional groups are produced due to two contact mechanisms, which are hydrogen bonding and an interfacial connecting network. The interaction between silica molecules' hydroxyl groups and the main functional groups of chitosan polymer results in hydrogen bonding between silica particles and

chitosan (Wan *et al.*, no date). Silica particles were also sulfated, and this was done to evaluate the effect of sulfonation on the applications of silica particles. Sulfonated silica particles improve the physio-chemical and electrical properties of the membrane. According to (Oh et al,2019) membranes with sulfonated silica shows an improvement in proton conductivity, thermal stability, and tensile strength (Oh *et al.*, 2019).

4.2. Results

4.2.1. Sol-gel and Stober Processes Calcinated for 2h

4.2.1.1 FTIR for Pure and Sulfonated Silica Calcinated at 2h
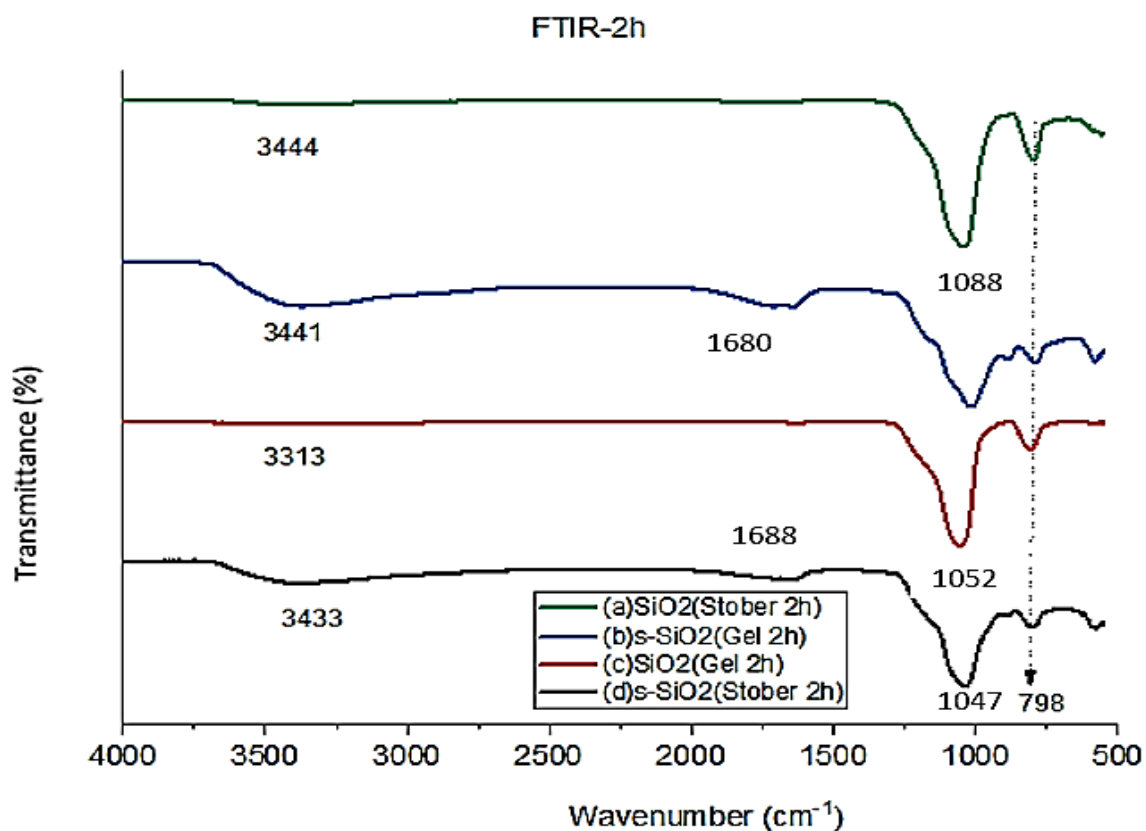
Figure 4.1. FTIR of (a) SiO$_2$ Stober (b) s-SiO$_2$ Sol-gel (c) SiO$_2$ sol-gel (d) s-SiO$_2$ -Stober(2h)

Figure 4.1 demonstrates FTIR of synthesized silica particles by Stober and Sol-gel method, calcinated for 2h. The IR band is between 3000 and 3400 cm^{-1} of figure 4.1. (a, b, c, and d) indicate adsorbed water molecule or OH^{-} stretching vibration of the silanol group, this band is exactly found in figure 4.1. (a) 3444 cm^{-1}, (b) 3441 cm^{-1}, 3313 cm$^{-1,}$ and figure 4.1. (d) 3433 cm^{-1} of 2h calcinated silica particles. However, the intensity of the band in (a) and (c) is not strong compared to that of sulfonated silica by the Stober and sol-gel process. This is due to the addition of sulfate in SiO_2 leading to s-SiO_2 having a strong peak than SiO_2, indicating successful sulfonation (S. Wang *et al.*, 2022). Treated silica's higher and more pronounced wavenumbers were found to correspond to denser silanol groups reported by (S. Wang *et al.*, 2022). Another potential explanation for the treated silica's higher and more dramatic wavenumbers is that more moisture is absorbed due to the denser and more abundant silanol groups on the silica surface. Martin et al,2020; Kalaiselvimary and Prabhu,2018 also reported that the addition of sulfur to silica broadens and increases the intensity of the peaks when TEOS is used as a precursor (Kalaiselvimary, Sundararajan and Prabhu, 2018; Martina *et al.*, 2020).

At 1680,1604 cm^{-1}, and 1688 cm^{-1}, there is a peak of the bending vibration of H_2O molecules trapped in the SiO_2 and s-SiO_2 matrix corresponding to figure 4.1. (b, c, and d) respectively. The strength of this band is reduced by heating, but it could not be entirely eradicated (Adam and Fook, 2009). The siloxane bond (Si-OH) exhibits a stretching vibration, which correlates to the strong band at 798 cm^{-1} of figure 4.1. (a, b, c, and d). The silica matrix's structural support is provided by this band (Rangasamy *et al.*, 2015). This band is reduced in the corresponding SiO_2 (a) and s-siO_2 (b) spectra due elimination of volatile components during the calcination of silica. The peaks located at 1038,1072,1052 and 1047 cm^{-1} in figure 4.1 (a, b, c, and d), are caused by the bending vibrations of Si-O-Si. The FTIR spectra of the silica particles demonstrate successful alteration on the silica surface.

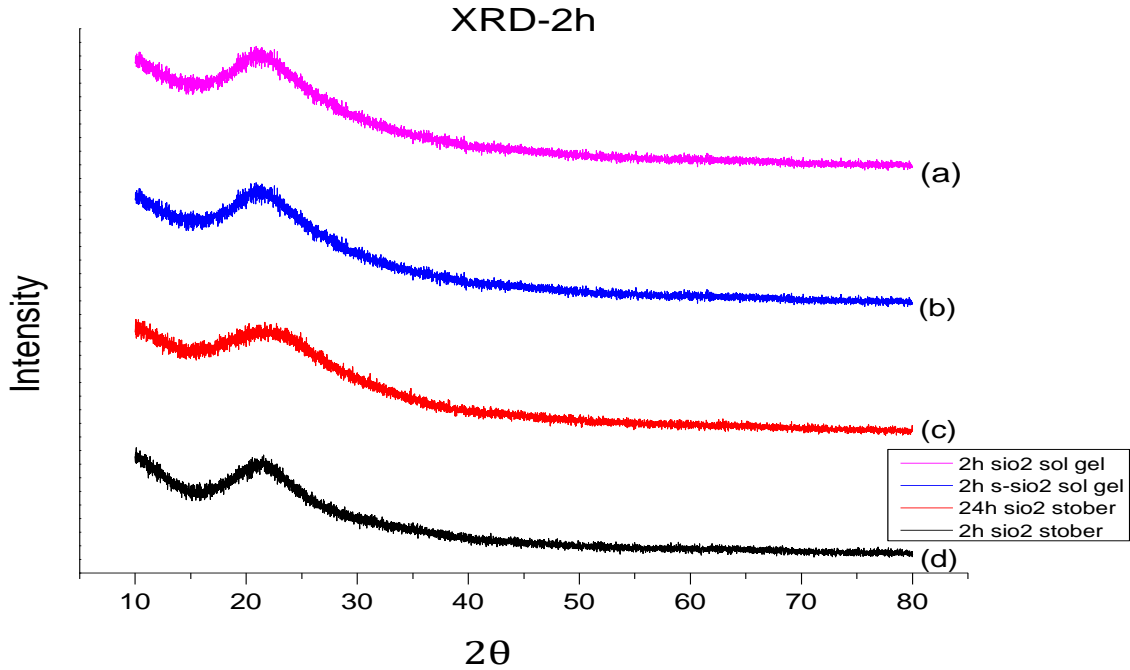4.2.1.2. XRD for Pure and Sulfonated Silica Calcinated at 2h.

Figure 4.2. XRD of (a) s-SiO$_2$ Stober (b) SiO$_2$ Stober (c) s-SiO$_2$ sol-gel (d)SiO$_2$ sol-gel, calcinated for 2h

Figure 4.2. indicate X-ray diffraction (XRD) of silica particles (SiO$_2$ and s-SiO$_2$) synthesized by sol-gel and Stober processes. As seen in Figure 4.2. (a, b, c, and d), the silica particles' XRD patterns display standard diffraction peaks between 21° and 23° that correspond to amorphous nano-silica. The nanoparticles have Bragg's angle (2θ) of (a) 21.37°, (b) 21.8°, (C) 22.06° and (d) 21.06°. The XRD peaks in Figure 4.2 indicate shifting and a decrease in peak after sulfonation of silica. This is due to sulfonated silica containing sulfonic acid groups, which introduces new functional groups into the substance (Palanisamy *et al.*, 2023). These groups can alter the normal atomic arrangement in the pure silica crystal lattice. As a result, the sulfonated silica's interatomic distance between its atoms may widen, which would lower its XRD peak position (Palanisamy *et al.*, 2023). The Silica particles (a, b, c, and d) show a broad humped peak which confirms the short-range ordering of amorphous silica. This implies that the synthetic particles are made of amorphous silica, similar results were reported by (Tshavhungwe, 2010; Sompech, Dasri and Thaomola, 2016;

Trisunaryanti *et al.*, 2020). The XRD graph of figure 4.2. show the greatest average peak at a specific diffraction angle because amorphous materials lack a periodic arrangement and have no organized crystalline structure (Biswas *et al.*, 2018). The two-dimensional structures of the amorphous silica have local short-range ordering regarding the tetrahedral structure of O atoms around the Si atoms (Büchner *et al.*, 2015; Büchner and Heyde, 2017; Shi and Tanaka, 2019).

4.2.1.3. SEM for pure and sulfonated silica calcinated at 2h
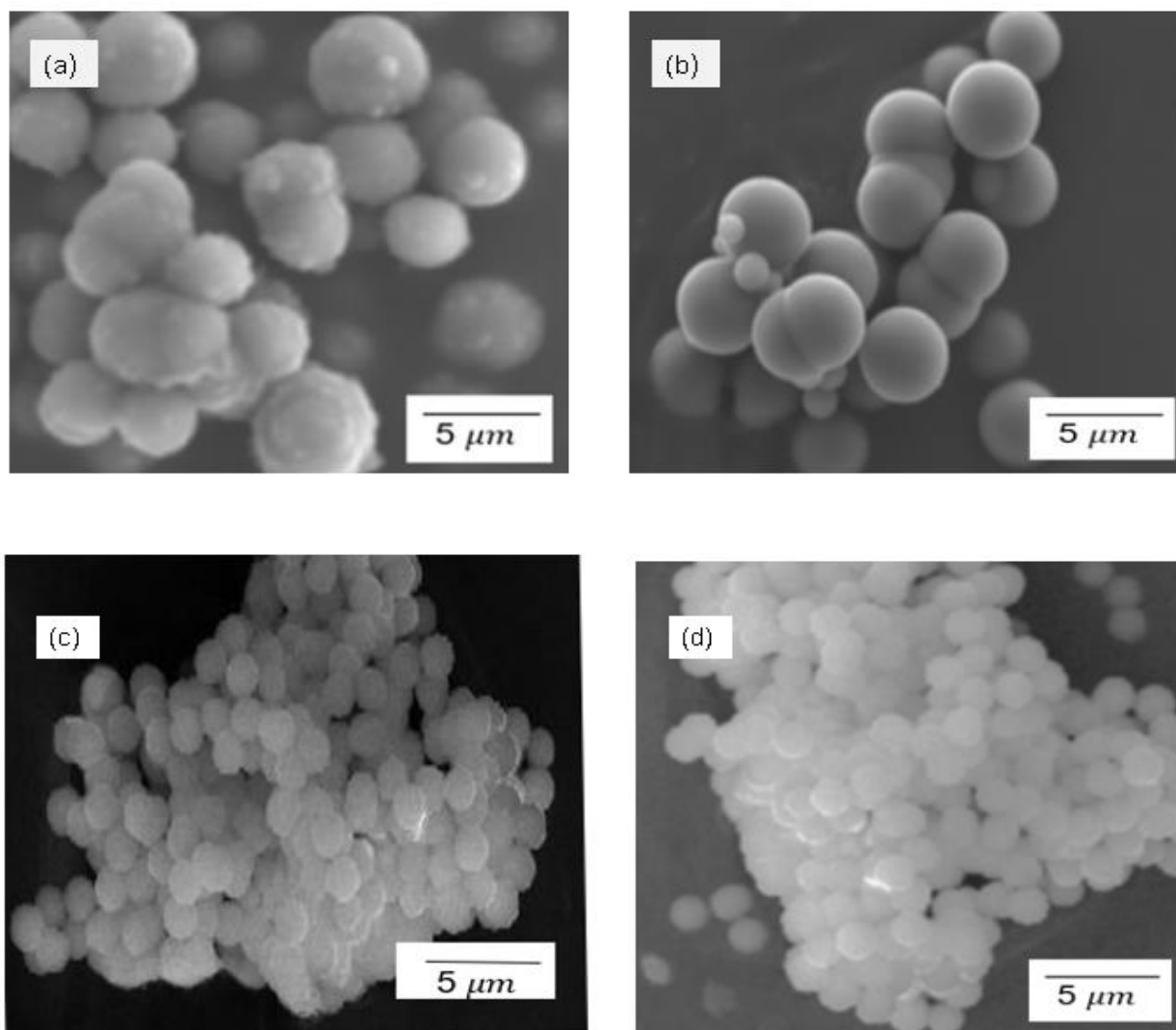
Figure 4.3. SEM for (a)SiO$_2$ sol-gel (2h) (b) s-SiO2 sol-gel(2h) (c) SiO$_2$ Stober (2h) (d) s-SiO$_2$ Stober (2h) **-calcinated for 2h**

Figure 4.3. demonstrate SEM results for silica particles produced by sol-gel and Stober methods, calcinated for 2h. The SEM image for the sol-gel method in Figures 4.2(a) and 4.2 (b) indicates an uneven distribution of the amorphous silica particles. The morphology of pure and sulfonated silica particles synthesized by sol-gel [figure 4.3. (a) and (b)] indicate smaller silica particles attached to silica agglomerates. Particle clusters of Stober silica are in figure 4.2. (c) and 4.2. (d) show a non-uniform size distribution when viewed (Ferreira, Wallau and Urquieta-González, 2003; Deshmukh *et al.*, 2012; Kohns *et al.*, 2021) reported synthesized silica particles of different shapes and sizes when TEOS was used as a precursor.

4.2.1.4 BET for Pure and Sulfonated Silica Calcinated at 2h

Table 4.1. BET for Silica Particles Calcinated for 2h

	Bet surface area (m²/g)	Total pore volume (cm³/g)	Average pore diameter (nm)
s-SiO$_2$(sol-gel)	280	0.76	21.00
SiO$_2$ (sol-gel)	398	0.98	10.67
s-SiO$_2$ (Stober)	271	0.76	20.89
SiO$_2$ (Stober)	487	1.59	12.45

Table 4.1. indicate the surface area, total pore volume, and average pore diameter of sol-gel and Stober silica particles calcinated for 2h. According to table 4.1. The extracted silica has pore diameters that range in size from 10.67 to 21.00 nm. This suggests that silica is a mesoporous substance. A mesoporous material is one whose pores are smaller than 50 nm in diameter, according to the International Union of Pure and Applied Chemistry (Javdani *et al.*, 2020). Sulfonated silica had surface areas and pore volumes that are roughly twice small as those of SiO$_2$

particles, with SiO_2 having a surface area of 4872 m^2/g and the corresponding sulfonated silica 271 m^2/g with pore volumes of 1.56 and 0.76 cm^3/g respectively. The surface area of silica particles in Table 4.1 decreases after sulfonation. This due to introduction of sulfonic groups that blocks the pores in the silica resulting in low BET surface area, also the concentration of sulfuric acid plays a huge role (Petrovic, Gorbounov and Masoudi Soltani, 2021). Results tabulated in 4.1. indicate that particles with a high surface area have high pore volume and small pore diameter, similar results were reported by (Johansson, 2010; Kumar, Malik and Purohit, 2018; Thahir *et al.*, 2019). The high surface area of SiO_2 is likely due to the inductive effect of the preformed silica network in the SiO_2 (Zeng *et al.*, 2017). Silica-based mesoporous particles (MSNs) produced feature a high specific surface area, facile and varied surface chemistry modification, narrow pore size distribution, customizable properties of the pore network, and great biocompatibility with a low incidence of non-specific or negative effects (Rizzi *et al.*, 2021). Due to these qualities, these particles are promising candidates for application in the fuel cell. Silica particles produced can be used as particles blocking agents (Rizzi *et al.*, 2021).

4.2.2. Sol-gel and Stober Processes Calcinated for 24h
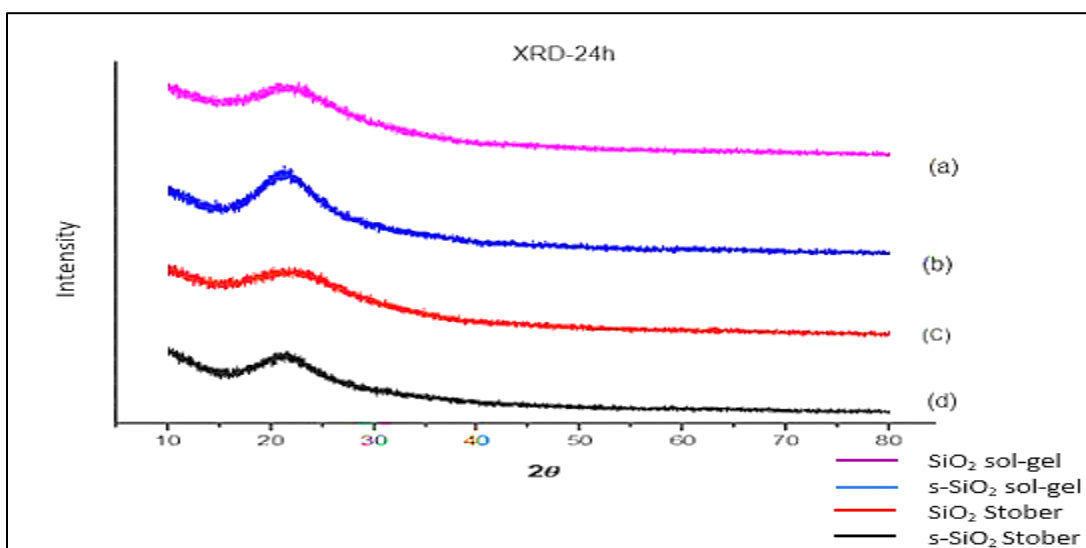
4.2.2.1. FTIR for pure and sulfonated silica calcinated at 24h
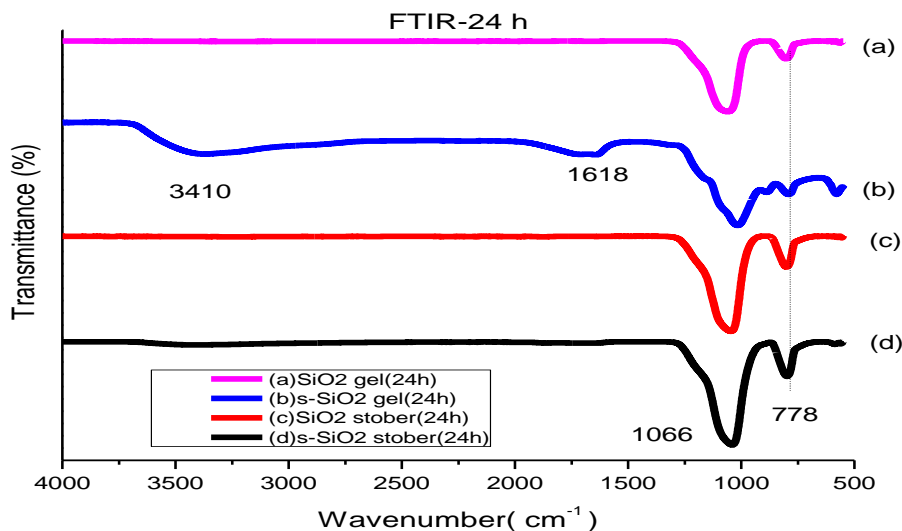
Figure 4.4. FTIR for (a) SiO_2 sol-gel (b) s-SiO_2 sol-gel (c) SiO_2 Stober (d) s-SiO_2 Stober silica particles calcinated for 24h.

FTIR analysis of silica particles calcinated for 24h, synthesized by sol-gel and Stober processes are demonstrated in Figure 4.4. The FTIR spectra of Figure 4.4.(a) does not clearly show absorption band of water molecule around 3400 but Figure 4.4. (b) and 4.4. (d) has this IR band around 3410 cm^{-1} which corresponds to characteristics of water on silica particles. The disappearance in this peak is an indication of reaction between silica and the hydroxyl group. This is due to the hydrolysis of TEOS, which varies with the concentration of H_2O and NH_3 in the solution. As the concentration of NH_3 rises, H_2O dissociates, releasing more OH^- ions, which attack the Si atoms and accelerate hydrolysis (Huber, 2020). The asymmetric Si-O (1001 cm^{-1}), asymmetric Si-OH (996 cm^{-1}), and symmetric Si-O (778 cm^{-1}) vibrations are more visible in the amorphous silica particles in figure 4.4.b while the corresponding spectra (a, c, and d) are not visible except that of symmetric Si-O band of (a, b, c, and d) which is around 778 cm^{-1}. The superimposition of distinct SiO_2 peaks, Si-OH bonding peaks, caused by leftover organic groups ascribed as the origin of the absorption bands between 800 and 1270 cm^{-1} in both Figure 4.4. (a, b, c, and d.)

4.2.2.2. XRD for pure and sulfonated silica calcinated at 24h

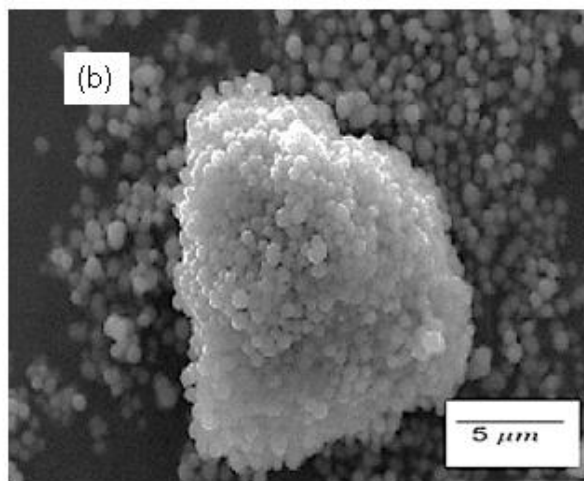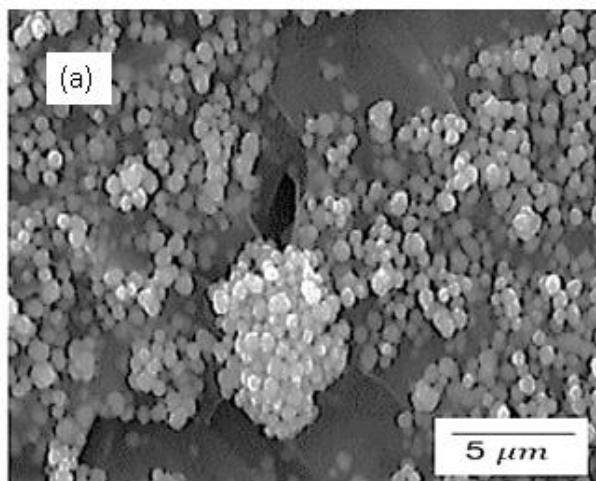Figure 4.5. XRD for (a) SiO_2 sol-gel (b) s-SiO_2 sol-gel (c) SiO_2 Stober (d) s-SiO_2 Stober silica particles calcinated for 24h

Surface morphology for sol-gel and Stober silica particles calcinated for 24 h is demonstrated in the XRD graph of Figure 4.5. Pure and sulfonated silica particles are in Figure 4.5. bear amorphous structure. The amorphous peak of these particles is situated at $2\theta=20°$. This is in line with what is reported by Beganskiene et al,2014 (BeganskienE *et al.*, 2004) who found amorphous silica has 2θ hump between 15° and 35°. Also, the outcome is consistent with the silica standard pattern established by the Joint Committee on Powder Diffraction (JCPDS) for Standards (Tiwary and Rana, 2010). Both silica particles have no sharp peaks as they have no long-range order so there are no well-defined scattering planes and therefore no sharp peaks. Amorphous nano-silica particles can function as a nucleus for silicic acid when the right amount of H_2O is added to NH_3 at the right temperature, resulting in microspheres with rounded and smooth surfaces. When nano-silica is formed, silicic acid acts as a nucleating agent, creating a substrate on which symmetric particles can grow (Zulfiqar, Subhani and Husain, 2018).

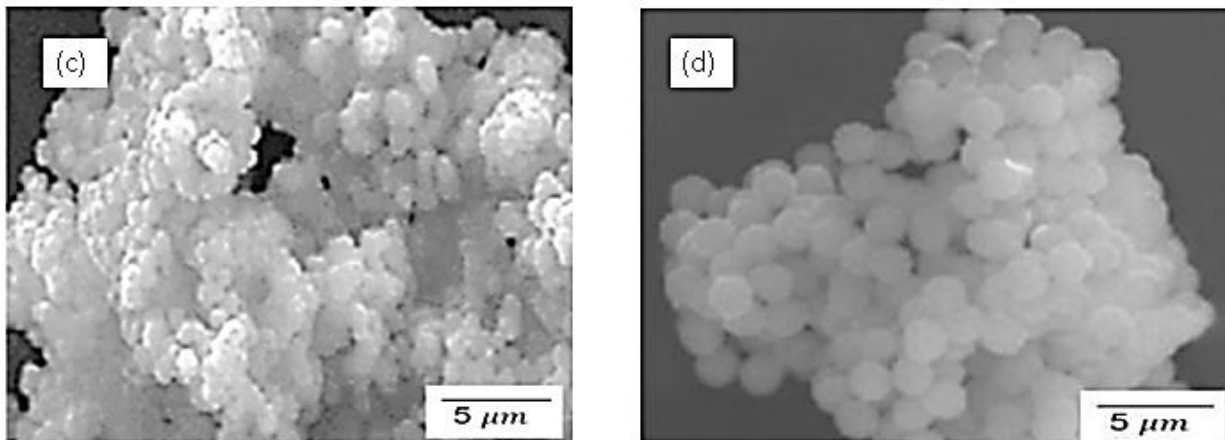**4.2.2.3. SEM for Pure and Sulfonated Silica Calcinated at 24h**

Figure 4.6. SEM for (a)s-SiO$_2$ Sol-gel (b) SiO$_2$ Sol-gel (c) SiO$_2$ Stober (d) s-SiO$_2$ Stober silica particles calcinated for 24h

The morphology of silica particles synthesized with different weight ratios and constant volume ratios of ethanol, water, ammonia, and tetraethyl-orthosilicate is shown in figure 4.6. The surface morphology of sulfonated silica in Figures 4.6(a) and 4.6(d) is almost round in structure and silica particles have a smooth surface, with a uniform particle size as well as little to no particle agglomeration. Pure silica particles in 4.6(b) and 4.6(c) created by sol-gel and Stober processes respectively show variety in size and shape of the particles, thus all the synthesis methods were unable to create silica particles that have uniform size distribution. Previous studies by (Hagar and Afifi, 2018) show the similar behavior of silica. These silica particles in (b) and (c) tend to agglomerate, and it is attributed to silica having high energy and surface tension. It can be concluded that both silica particles synthesized tend to agglomerate.

4.2.2.4. BET for Pure and Sulfonated Silica Calcinated at 24h

Table 4.2. BET for Silica Particles Calcinated for 24h

	Bet surface area (m^2/g)	Total pore volume (cm^3/g)	Average pore diameter (nm)
s-SiO$_2$(Sol-gel)	285	0.77	21.02
SiO$_2$(Sol-gel)	495	1.58	12.10
s-SiO$_2$ (Stober)	279	0.76	21.52
s-SiO$_2$ (Stober)	486	1.56	12.21

The samples' BET surface area and pore volume of the silica particles calcinated for 24h are demonstrated in table 4.2.2. High surface area and volume of sol-gel and Stober silica particles were recorded. Table 4.3.2 further indicates that, when silica was modified, the surface area decreased from the highest of 486 m^2/g to the lowest of 285 m^2/g with a corresponding total pore volume of 1.56 to 0.77 cm^3/g highest and lowest value, respectively. The decrease in surface area of modified silica particles was reduced by almost 50%. However, the pore volume increases with an increase in surface area and total pore volume. Large surface area is anticipated to play a role in assisting with the functionality of silica as a filler in the reduction of methanol permeability as silica tends to absorb methanol on its surface which will reduce the methanol permeability of the membrane. (Dhaneswara *et al.*, 2020) and (Usgodaarachchi *et al.*, 2021) reported a silica surface area of 236 m^2/g and 222 m^2/g respectively which are smaller than the ones found in this report. The decrease in surface area after sulfonation is caused by filling of the pores in the silica molecule and was also reported previously by (Tran *et al.*, 2013b) and (Alfawaz *et al.*, 2022). (Thi *et al.*, no date) also reported a decrease in the surface area of silica particles after sulfonation when

propanol solution and hydrogen peroxide were used as raw material and 3-mercatopropytrimethoxysilan (MPTMS) as a precursor. Silica particles calcinated for 24h show higher surface area and total pore volume compared to that calcinated for 2h. These improvements in surface area are a good factor in enhancing the performance of silica particles in the membranes to be modified in terms of increasing their chemical and mechanical properties (Rizzi *et al.*, 2021).

4.3. Conclusion

Synthesis of silica particles using tetraethyl-orthosilicate was successful. Silica particles' FTIR spectra of both samples indicate silica functional groups. Sulfonation of silica was confirmed by FTIR and this was seen by shifting of absorption peaks. Also, sulfonation caused the particles to move to low region on XRD and the particles diameter were also found to have decreased. The particles calcinated for 2h and 24h were found within the pore diameter range of 12 nm to 21 nm with the highest pore diameters recorded on silica calcinated for 24h. Silica particles for Stober and sol-gel calcinated for 2h and 24h have short-range ordering resulting in them having amorphous structures. Synthesized silica particles tend to agglomerate, and this was more visible in silica particles calcinated for 2h compared to the one calcinated for 24h using the same method and no visible agglomeration was discovered after surface modification of silica. Sol-gel method is the best method of synthesizing silica particles. Calcination of silica for 24h produced silica particles with high surface area.

4.4. References

Adam, F. and Fook, C.L. (2009) 'Chromium modified silica from rice husk as an oxidative catalyst', Journal of Porous Materials, 16(3), pp. 291–298.

Beganskiene, A., Sirutkaitis, V., Kurtinaitienė, M., Juškėnas, R. and Kareiva, A. (2004) 'FTIR, TEM and NMR Investigations of Stöber Silica Nanoparticles', Materials Science, 10(4), pp. 287–290.

Biswas, R.K., Khan, P., Mukherjee, S. and Mukhopadhyay, A.K. (2018) 'Study of the short-range structure of amorphous Silica from PDF using Ag radiation in lyaboratory XRD system, RAMAN, and NEXAFS', Journal of Non-Crystalline Solids, 488(January), pp. 1–9.

Büchner, C., Lichtenstein, L., Heyde, M. and Freund, H.J. (2015) 'The atomic structure of two-dimensional silica', NanoScience and Technology, 97, pp. 327–353.

Büchner, C. and Heyde, M. (2017) 'Two-dimensional silica opens new perspectives', Progress in Surface Science, 92(4), pp. 341–374.

Carol Deutsch1 Pengse Po1 Erin Delaney1, H.G.M.S.-K.L.S.L.T.A.K.E.J.P.Y.-M.H. (2017) '乳鼠心肌提取 HHS Public Access', Physiology & Behavior, 176(12), pp. 139–148.

Crundwell, F.K. (2017) 'On the Mechanism of the Dissolution of Quartz and Silica in Aqueous Solutions', ACS Omega, 2(3), pp. 1116–1127.

Deshmukh, P., Batt, J., Peshwe, J. and Pathak, S. (2012) 'Determination of silica activity index and XRD, SEM, and EDS studies of amorphous SiO_2 extracted from rice Husk Ash', Transactions of the Indian Institute of Metals, 65(1), pp. 63–70.

Elliston, J. (2018) 'Hydration of Silica and Its Role in the Formation of Quartz Veins-Part 1', An International Journal of the History of Chemistry, 2(2), pp. 43–71.

Farooq, M.A. and Dietz, K.J. (2015) 'Silicon as versatile player in plant and human biology: Overlooked and poorly understood', Frontiers in Plant Science, 6(NOVEMBER), pp. 1–14.

Ferreira, Y.K., Wallau, M. and Urquieta-González, E.A. (2003) 'Preparation of mesoporous solids by agglomeration of silica nanospheres', Studies in Surface Science and Catalysis, 146, pp. 197–200.

Hagar, M.E. and Afifi, T.H. (2018) 'Catalytic Activity of Sulfated and Phosphated Catalysts towards the Synthesis of Substituted Coumarin', (January).pp. `14-36.

Huber, L. (2020) 'The in fl uence of the ammonia concentration and the water content on the water sorption behavior of ambient pressure dried silica xerogels', Journal of Sol-Gel Science and Technology, pp. 197–206.

Javdani, (2020) 'Microporous and Mesoporous Materials Tannic acid-templated mesoporous silica nanoparticles as an effective treatment in acute ferrous sulfate poisoning', Microporous and Mesoporous Materials, 307(June).

Johansson, E.M. (2010) Controlling the Pore Size and Morphology of Mesoporous Silica [Elektronisk resurs],pp. 1-52.

Joseph, T.M., Kar Mahapatra, D., Esmaeili, A., Piszczyk, Ł., Hasanin, M.S., Kattali, M., Haponiuk, J. and Thomas, S. (2023). Nanoparticles: Taking a Unique Position in Medicine. Nanomaterials, [online] 13(3).

Kalaiselvimary, J., Sundararajan, M. and Prabhu, M.R. (2018) 'Preparation and characterization of chitosan-based nanocomposite hybrid polymer electrolyte membranes for fuel cell application', Ionics, 24(11), pp. 3555–3571.

Kohns, R., Meyer, R., Wenzel, M., Matysik, J., Enke, D. and Tallarek, U. (2020). In situ synthesis and characterization of sulfonic acid functionalized hierarchical silica monoliths. Journal of Sol-Gel Science and Technology, 96(1), pp.67–82.

Kumar, S., Malik, M.M. and Purohit, R. (2018) 'Synthesis of high surface area mesoporous silica materials using soft templating approach', Materials Today: Proceedings, 5(2), pp. 4128–4133.

Kusumastuti, E., Mahatmanti, W.F., Jumaeri, M.D. and Widiastuti. A . (2016) 'Modification of chitosan membranes with nanosilica particles as polymer electrolyte membranes', in AIP Conference Proceedings. American Institute of Physics Inc.

Martina, P., Gayathri, R., Pugalenthi, M.R., Cao, G., Liu, C. and Prabhu, M.R. (2020). Nanosulfonated silica incorporated SPEEK/SPVdF-HFP polymer blend membrane for PEM fuel cell application. Ionics, 26(7), pp.3447–3458.

Oh, K., Kwon, O., Son, B., Lee, D. and Shanmugam, S. (2019) 'Nafion-sulfonated silica composite membrane for proton exchange membrane fuel cells under operating low humidity condition', Journal of Membrane Science, 583(April), pp. 103–109.

Rahman, I.A. and Padavettan, V. (2012) 'Synthesis of Silica nanoparticles by Sol-Gel: Size-dependent properties, surface modification, and applications in silica-polymer nanocompositesa review', Journal of Nanomaterials, 2012. pp. 1-15.

Rangasamy, V.S., Thayumanasundaram, S. and Leuven, K.U.(2015) 'Vibrational spectroscopic study of pure and silica-doped sulfonated poly(ether ether ketone) membranes', Spectrochimica Acta - Part A: Molecular and Biomolecular Spectroscopy, 138, pp. 693–699.

Rizzi, F., Castaldo, S., Latronico, T., Lasala, P. and Fanizza, E. (2021) 'High surface area mesoporous silica nanoparticles with tunable size in the sub-micrometer regime: Insights on the size and porosity control mechanisms', Molecules, 26(14).pp. 4247.

Shi, R. and Tanaka, H. (2019) 'Distinct signature of local tetrahedral ordering in the scattering function of covalent liquids and glasses', Science Advances, 5(3), pp. 2–7.

Sompech, S., Dasri, T. and Thaomola, S. (2016) 'Preparation and Characterization of Amorphous Silica and Calcium Oxide from Agricultural Wastes'.pp. 1923-1928.

Sushko, P. V. (2005) 'Structure and properties of defects in amorphous silica: New insights from embedded cluster calculations', Journal of Physics Condensed Matter, 17(21).

Thahir, Wahab, A.W., La Nafie, L. and Raya, I. (2019) 'Synthesis of high surface area mesoporous silica SBA-15 by adjusting hydrothermal treatment time and the amount of polyvinyl alcohol', Open Chemistry, 17(1), pp. 963–971.

Thi, L., Tran, T.A., My, P.L. and Van Man, T. (no date) 'Synthesis of amorphous silica and sulfonic acid functionalized silica used as reinforced phase for polymer electrolyte membrane'.

Tiwary, A.K. and Rana, V. (2010) 'Cross-linked chitosan films: Effect of cross-linking density on swelling parameters', Pakistan Journal of Pharmaceutical Sciences, 23(4), pp. 443–448.

Trisunaryanti, W. Larasati, S. and Triyoyo, T. (2020) 'Selective production of green hydrocarbons from the hydrotreatment of waste coconut oil over Ni- And NiMo-supported on amine-functionalized mesoporous silica', Bulletin of Chemical Reaction Engineering & Catalysis, 15(2), pp. 415–431.

Tshavhungwe, A.M. (2010) 'esoporous ethanesilica materials with bimodal and trimodal pore - size distributions synthesised in the presence of cobalt ions', 106(3), pp. 6–10.

Wan, Y., Wang, L., Cheng, L.Y. and Shen, Z. (no date) Ionic conductivity of chitosan membranes.pp. 1-8.

Wang, X.-D., Shen, Z.-X., Sang, T., Cheng, X.-B., Li, M.-F., Chen, L.-Y. and Wang, Z.-S. (2010). Preparation of spherical silica particles by Stober process with a high concentration of tetra-ethyl-orthosilicate. Journal of Colloid and Interface Science, 341(1), pp.23–29.

Wazamtu, I., Sani, N.A. and Abdulsalam, A.K. (2013) 'Extraction and Quantification of Silicon From Silica Sand Obtained From Zauma River, Zamfara State, Nigeria', European Scientific Journal, 9(15), pp. 160–168.

Zeng, S., Zeng, X., Huang, L., Wu, H., Yao, Y., Zheng, X., and Zou, J. (2017). The formation mechanisms of porous silicon prepared from dense silicon monoxide. RSC Advances, 7(13), pp.7990–7995.

Zulfiqar, U., Subhani, T. and Husain, S.W. (2018) 'Synthesis and characterization of silica nanoparticles from clay Synthesis and characterization of silica nanoparticles from clay', Integrative Medicine Research, 4(1), pp. 91–96.

Chapter 5 Membrane Fabrication

5.1. Introduction

This chapter covers information on chitosan polymer membranes that were modified with silica nanoparticles. The nanoparticles were synthesized through Sol-gel and stober process both calcinated for 2h and 24h (refer to chapter 3). The polymer electrolyte membrane is a crucial component of the fuel cell (Smitha, Sridhar and Khan, 2005). Chitosan is the most abundant natural polymer and can be modified to achieve the desired properties of a good polymer used in a fuel cell. Polymer-based electrolytes are widely used in electrochemical devices (Kaczmarek *et al.*, 2019; Morin-Crini *et al.*, 2019; Podgorbunskikh *et al.*, 2022). Polymer electrolytes derived from renewable sources can be a cost-effective and environmentally friendly replacement for materials used in fuel cells (Carlson *et al.*, no date; Ramasubramanian *et al.*, 2022). According to current developments in membrane selection in PEMFC and DMFC applications, the primary options are organic membranes blended with inorganic membranes (Haragirimana *et al.*, 2020; Ramasubramanian *et al.*, 2022).

Based on the kind of chemical linkages that are established between the inorganic phase and the organic phase, organic-inorganic blended membranes can be divided into two main kinds. Weak links between organic and inorganic components, including hydrogen bonds, weak electrostatic interactions, and van der Waals forces, develop in Class 1 hybrid membranes. In contrast, Class 2 hybrid membranes are made of powerful covalent chemical connections which chemically fuse the inorganic and organic phases (Hattori *et al.*, 2015). Introducing inorganic materials like silica into organic polymers can prompt the membranes to function more effectively in comparison to the unmodified membrane, which also will improve the membranes' dimensional, thermal stability, and proton conductivity while reducing the methanol transport channel, which will decrease the membranes' methanol permeability, and improves the fuel cell performance (Wang and Wang, 2014). (Han *et al.*, 2020) used silica particles to modify the polymer membranes and the methanol permeability of those membranes was reduced by 50% while the fuel efficiency was increased by 10%. According to (Han *et al.*, 2020) work's functionalizing SiO_2 filler increased

composite membranes' proton conductivity to 2.90×10^{-2} S/cm. On the other hand (Purwanto *et al.*, 2021) reported a decrease in permeability when silica was added from 5% to 15% with suppression of methanol permeability from 3.96×10^{-4} to 2.42×10^{-4} cm^2/s and a decrease in IEC from 1.024 meq/g (5%) to 0.759 meq/g (15%).

5.2. Membrane Fabrication

5.2.1. Membrane Casting

Chitosan membranes were fabricated using chitosan flakes. The membranes were fabricated using the casting technique. Figure 5.1. show a summarized process of membranes fabtication.5g of chitosan flakes were added to 2% v/v of acetic acid solution and stirred for an hour. Taurine, DMSO, and Silica particles (0%, 2%, and 4%). The gel solution was dried at 70 ℃ for 5 h. The obtained dried membrane was cross-linked with 2M of sulfuric acid for 30 minutes and later immersed in NaOH after which the membrane surface was cleaned with deionized water to eliminate any excess acid. This procedure was also used for sulfonated silica-chitosan membranes.

| Chitosan + Acetic acid | → | Taurine+DMSO+Silica | → | Drying | → | Sulfonation | → | Washing and drying |
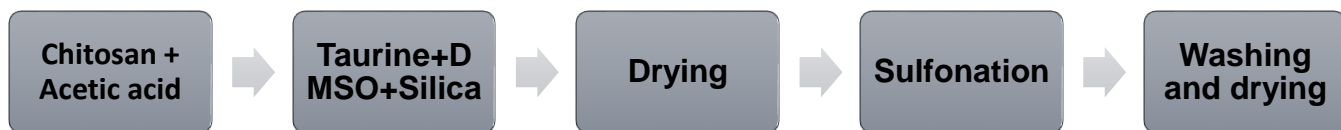
Figure 5.1. Casting method for membrane fabrication.

5.3. Results and Discussion

5.3.1. Membranes Synthesized by Sol-gel and Stober Processes (2h)

5.3.1.1. FTIR of Pure and Modified Chitosan Membranes with Silica Calcinated for 2h
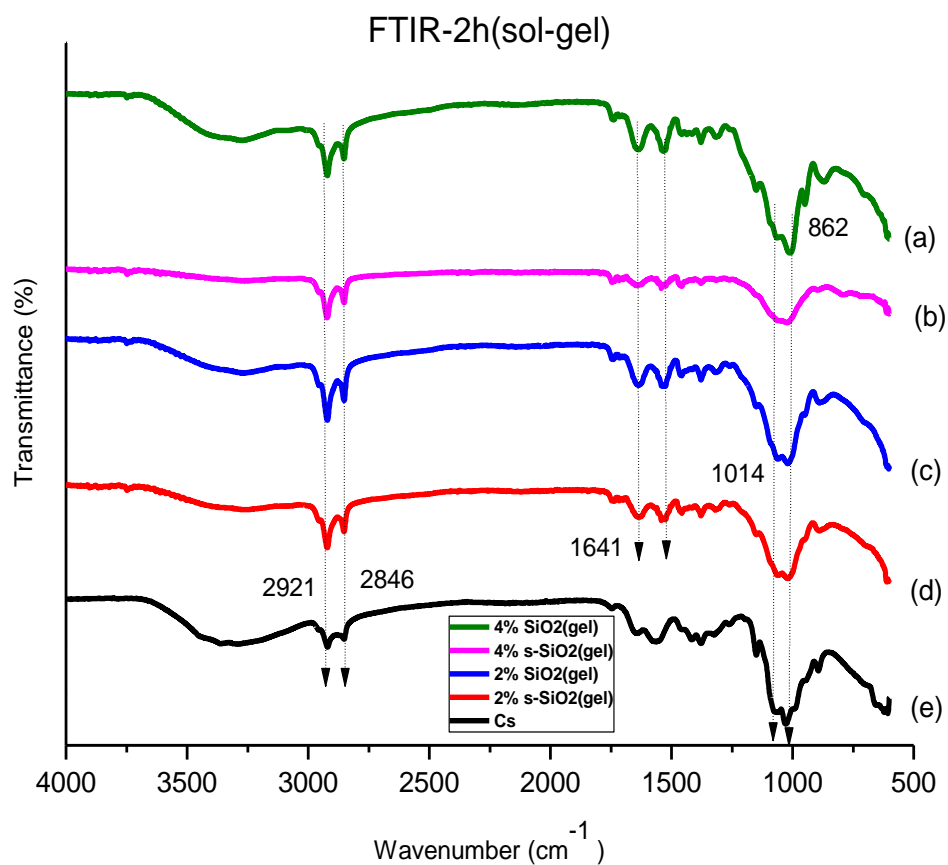
Figure 5.2.(i). FTIR of (a) 4% SiO_2 (b) 4% s-SiO_2 (c) 2% SiO_2 (d) 2% s-SiO_2 (e) Cs **- sol-gel (2h)**
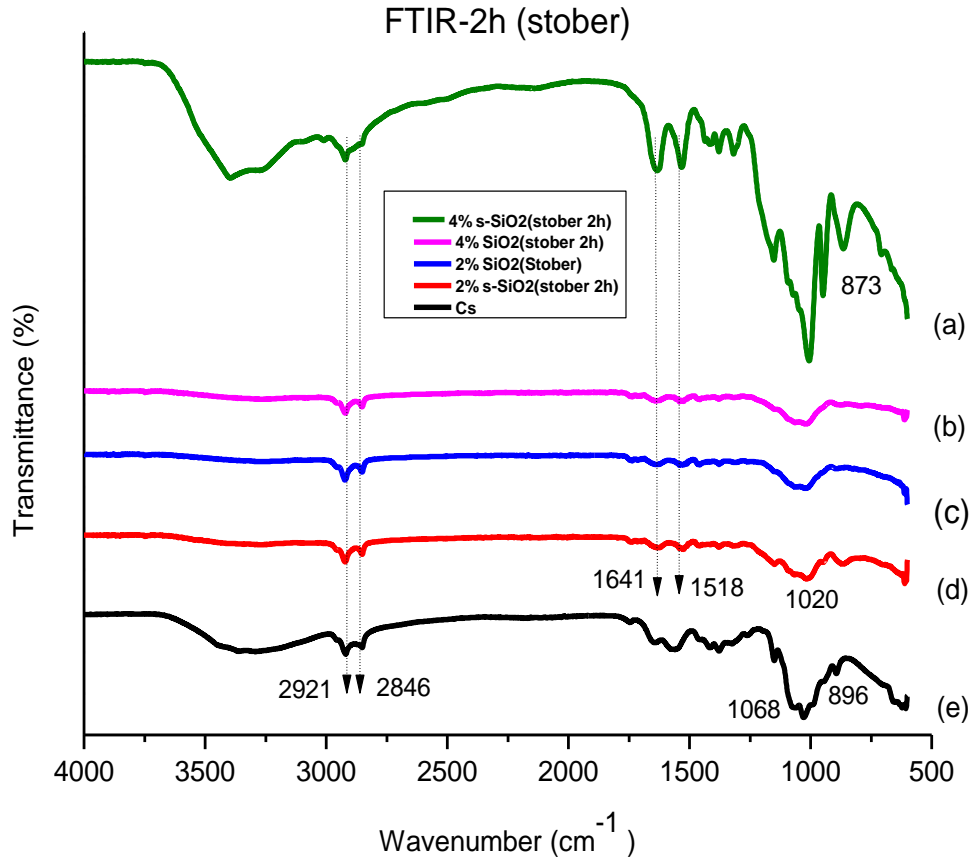
Figure 5.2. (ii). FTIR of (a) 4% s-SiO$_2$/Cs (b) 4% SiO$_2$/Cs (c) 2% SiO$_2$/Cs (d) 2% s-SiO$_2$/Cs (e) Cs **- (Stober 2h)**

Figure 5.2. (i and ii) shows FTIR spectra of pure chitosan, 2 % SiO$_2$, 2 % s-SiO$_2$, 4 % SiO$_2$, and 4 % s-SiO$_2$ membranes modified with silica synthesized through (i) sol-gel and (ii) the Stober process. A broad peak in Figure 5.2 (i and ii) can be seen at 3331 cm^{-1} on FTIR spectra of pure chitosan (e), this peak indicates the presence of an NH group that overlapped with the OH group's absorption (Lee *et al.*, 2009). There is a shift in this peak on modified chitosan membranes from 3331 cm^{-1} to (a and b) 3338 cm^{-1}, (c) 3294 cm^{-1}, and (d) 3333 cm^{-1} of Figure 5.2.i, and in Figure 5.2.i, and in Figure 5.2. (ii) it shifted to (a)3343 cm^{-1}, (b)3379 cm^{-1}, (c)3409 cm^{-1} and (d) 3428 cm^{-1}. The shift in this peak was also reported by (Thi *et al.*, no date) who reported a shift of this peak from 3429 to 3669 cm^{-1}. (Budnyak *et al.*, 2015) also reported similar results. Shifting of this peak indicates interaction between silica's O-H groups and chitosan's NH (Budnyak *et al.*, 2015). The

peak high intensity in Figure 5.2 around 3000 cm^{-1} indicates a highly developed interaction between chitosan and silica that resulted in an increase in ions' dissociation, which is crucial for raising conductivity. However, the was a reduction in the intensity of the peak in Figure 5.2. i (b) and 5.2. ii. (b, c, d) which is caused by the negatively charged single bond SiOH and the positively charged ammonium groups of the chitosan backbone interacting electrostatically. The peaks on the chitosan(e) spectrum at 2921 and 2846 cm^{-1} in Figure 5.2(i) and (ii) correspond to the C-H stretching and C-N vibrations respectively (Nur, Rohaeti and Darusman, 2017). The band at 1068 and 896 cm^{-1} is in Figure 5.2. (i) and (ii) correlate to chitosan (e) glucose rings' C-O-C vibrations and chitosan's glycosidic bond in the saccharide structure (Queiroz *et al.*, 2014).

The small peak at around 1500 cm^{-1} in both figures 5.2. (a, b, c, d, and e) can be attributed to the N-H bending of amide II. Comparing the FTIR spectra of the synthesized composite to the spectrum of the initial chitosan (e), Figure 5.2 shows a shift in the band 1518 cm^{-1} of -NH$_2$ deformation vibrations. It describes the interaction between the amine group of chitosan and the silanol group of the silica network. It also suggests that the CS nanocomposite structure has significant interactions between Si(OH) and amine and amide groups from chitosan as well as between Si(OH) and amine and amide groups as a result of electrostatic contact (Vijayalekshmi and Khastgir, 2018).The interaction between silica and chitosan can assists in reduction of membrane crystallinity while improving their ability to produce more protons. The presence of absorption bands at 1014 cm^{-1} and 1020 cm^{-1} Sol-gel (i) and Stober (ii) suggest the presence of Si-O-Si vibration, whereas Si-OH was revealed to be the cause of absorption at 862 cm^{-1} and 873 cm^{-1} in membranes synthesized by Sol-gel and Stober respectively (Diaconu *et al.*, 2010). A minor shift in this peak indicates a conjugation between the Si-OH group on the surface of silicon particles and the Si-OH functional group from cross-linked chitosan (Lee *et al.*, 2009). No new functional group is detected from the spectra, however, the membranes prepared by sol-gel have high-intensity peaks compared to those of the Stober method, and this is a result of the strong interaction between silica and chitosan. All the chitosan FTIR bands reported were also reported by others (Budnyak *et al.*, 2015; Santoso *et al.*, 2019; Bayoumy *et al.*, 2020).

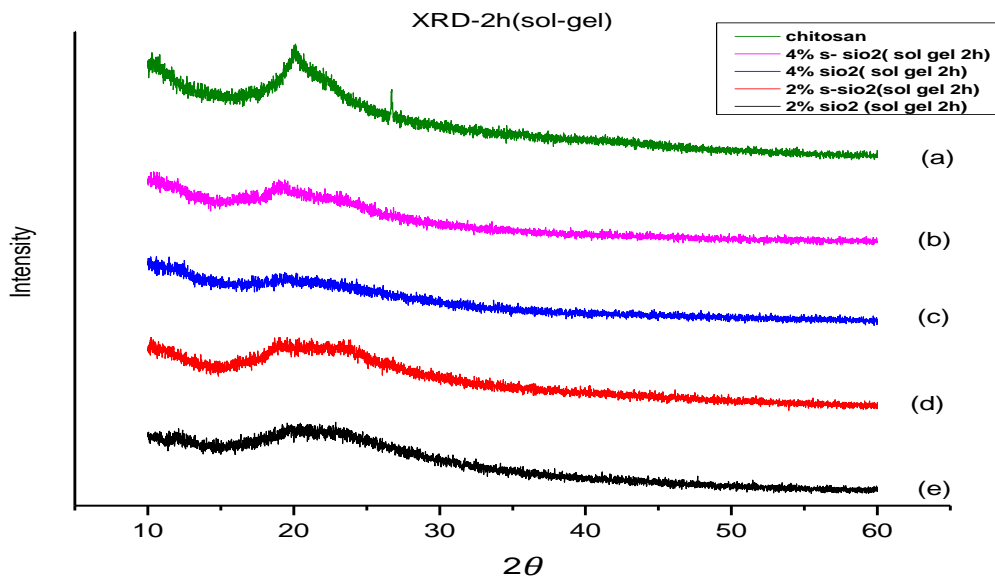5.3.1.2. XRD of Pure and Sulfonated Chitosan Membranes with Silica Calcinated for 2h

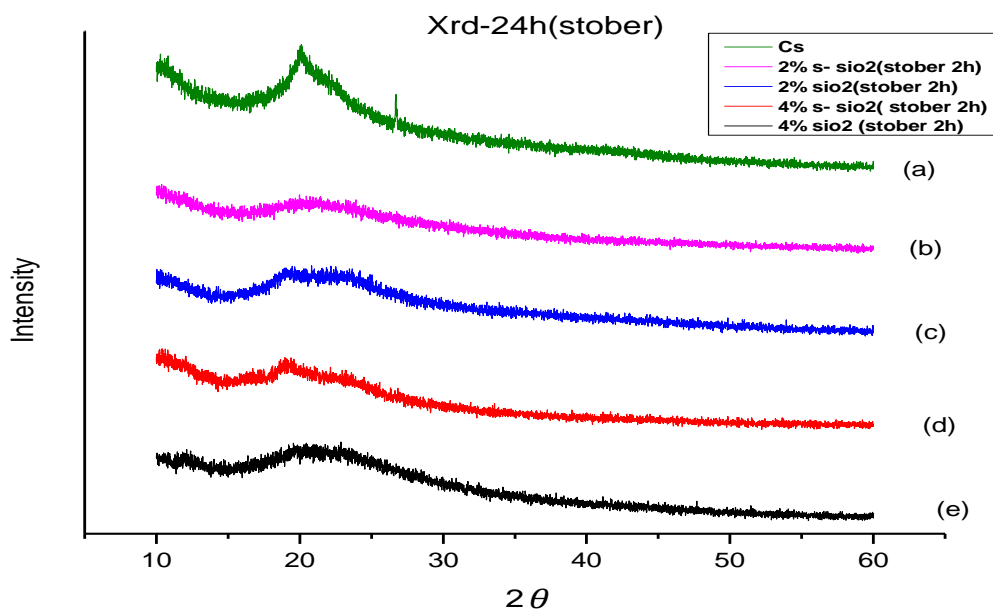Figure 5.3(i). XRD analysis of (a) Cs (b) 4% s-SiO$_2$ (c) 4% SiO$_2$ (d) 2% s-SiO$_2$ (e) 2% SiO$_2$ **- (Sol-gel 2h)**

Figure 5.3.(ii). XRD analysis of (a) Cs (b) 2% s-SiO$_2$ (c) 2% SiO$_2$ (d) 4% s-SiO$_2$ (e) 4% SiO$_2$ **- Stober (2h)**

Figure 5.3. Indicate XRD analysis of Cs, 2% s-SiO$_2$, 2% SiO$_2$, 4% s-SiO$_2$, and 4% SiO$_2$ membranes calcinated for 2h. The pure chitosan membrane has semi-crystalline properties. According to the XRD results shown in Figure 5.3 (i and ii) (a) a broad chitosan peak can be found around 19° and is situated exactly at 2θ=19. 94°. Figure 5.3(i) demonstrates that all the modified membranes are amorphous in structure with diffraction angles of 19.78°, 20.29°, 21.26° and 21,35° of membrane b, c, d, and e respectively, while those of corresponding membrane in Figure 5.3. (ii) are found at 20.8°,21.21°, 19.82°, and 20.93° respectively. There is a decrease in the diffraction peak of modified chitosan membranes in Figure 5.3. i. (b, c) and figure 5.3.ii (b, d) indicate crystallinity loss caused by the modification process. Similar results were found when (Gaabour, 2019) used amorphous particles (SiO$_2$ and s-SiO$_2$) to modify chitosan and the overall chitosan structure was amorphous with a diffraction angle between 17°- 30°. The results also agree with what is reported by (Saharan *et al.*, 2022; Zhong *et al.*, 2023). The amorphous structure of the modified membranes in Figure 5.3 can be attributed to the addition of amorphous silica sulfuric acid fragments that reduce crystalline areas of the membrane, lowering the total crystallinity of CS/s-SiO$_2$ (Thi *et al.*, no date).

Additionally, a considerable reduction in the crystalline phase was caused by hydrogen bonds that formed in films treated with silica where the latter is loosely organized among the chitosan molecules (Cui *et al.*, 2018). The segmented mobility of the polymer chain is much higher in amorphous regions than in crystalline regions, increasing the polymeric backbone's flexibility (Rosli *et al.*, 2021; Abdulwahid, Aziz and Kadir, 2022). The membranes in Figure 5.3. (Sol-gel and Stober) show the same behavior regardless of the method of preparation of the silica or s-silica particles filler. In this case, it can be said that the membrane crystallinity is merely affected by the method which was used in synthesizing particles as all membranes in Figure 5.3.i. (sol-gel) and figure 5.3. ii. (Stober) indicate the same behavior and are amorphous.

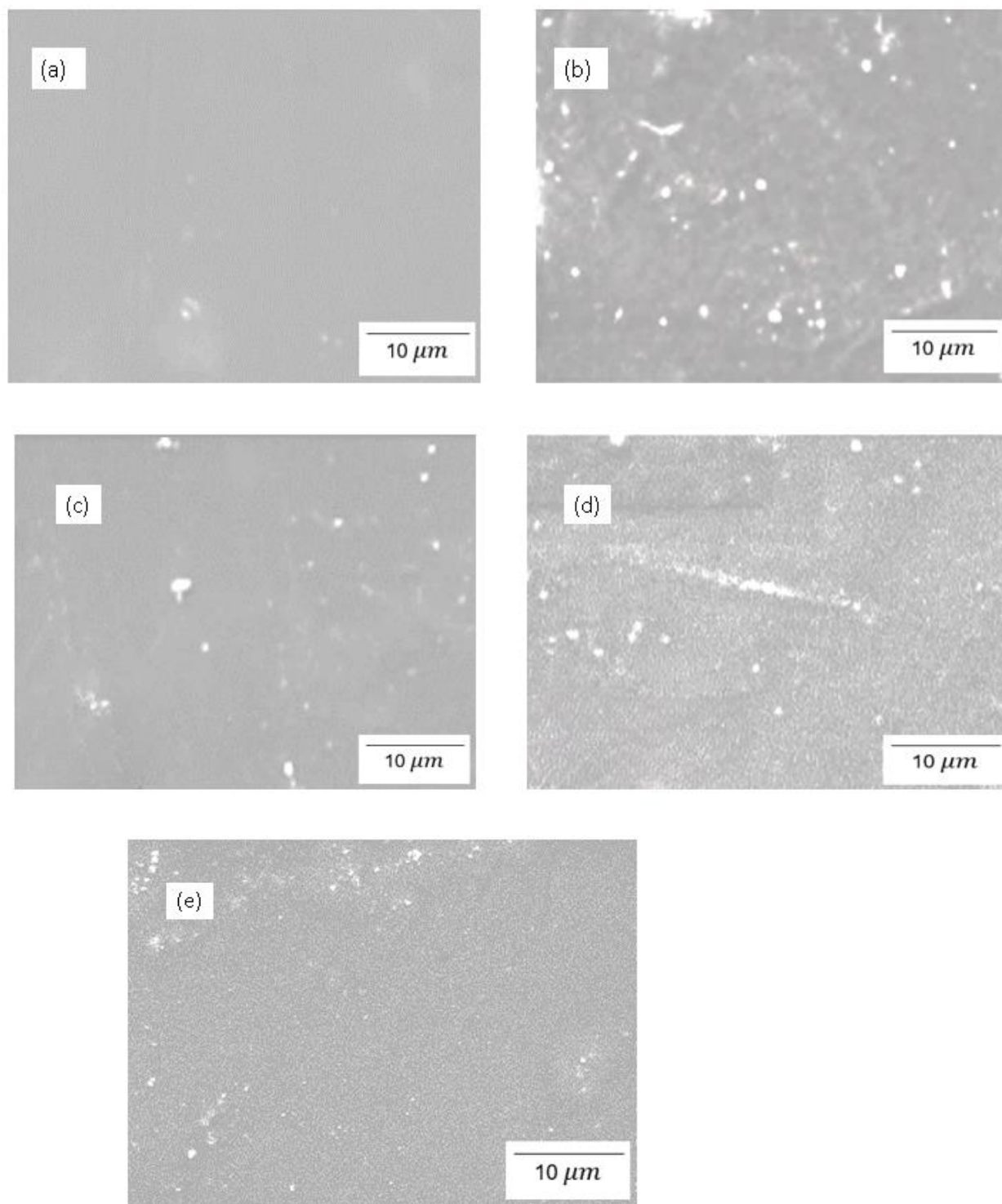## 5.3.1.3. SEM of Pure and Sulfonated Chitosan Membranes with Silica Calcinated for 2h

Figure 5.4(i). SEM of (a) Cs (b) 4% s-SiO$_2$/Cs (c) 4% SiO$_2$/Cs (d) 2% SiO$_2$ /Cs (e) 2% SiO$_2$/Cs **Sol-gel (2h)**
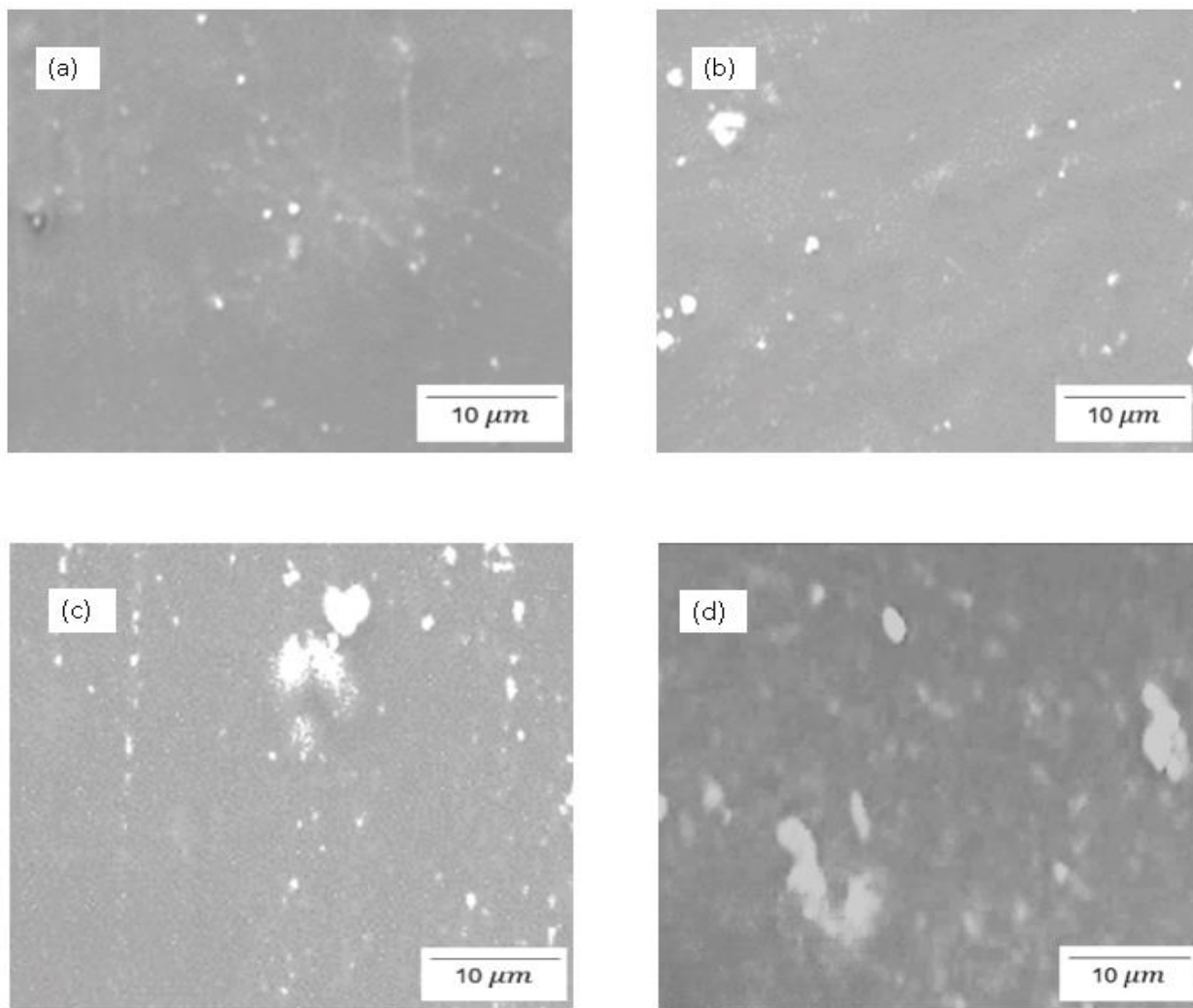

Figure 5.4.(ii). SEM of (a) 2% s-SiO$_2$/Cs (b) 2% SiO$_2$/Cs (c) 4% s-SiO$_2$/Cs (d) 4% SiO$_2$/Cs **Stober (2h)**

Figure 5.4. Indicate morphological characteristics of chitosan membranes synthesized by Sol-gel (figure 5.4. i) and Stober (figure 5.4. ii). The membrane morphologies were observed using SEM to evaluate the distribution of SiO$_2$ and s-SiO$_2$ in the CS matrix. Figure 5.4(i) revealed a complex and smooth surface with no visible pores on the pure chitosan membrane. The results agreed with those reported by (Rekik *et al.*, 2017) who discovered a homogenous, consistent, flat surface and uniform thickness of pure chitosan membrane. It is observable that the addition of silica to the

chitosan membrane in Figure 5.4. i (b, c, d, and e) and figure 5.4. ii. (a, b, c, and d) roughened its surface, and silica particles were not evenly distributed but dispersed. Despite silica particles being dispersed in Figure 5.4. (i) and (ii), the silica particles seem to aggregate in the polymer matrix, and the size of the aggregates grows as the silica content rises, this agrees with what was reported by (Liu *et al.*, 2016) and (Vijayakumar and Khastgir, 2018).Silica is known to agglomerate in the membrane, and this is evident in Figure 5.4. The degree of agglomeration was intense on the membrane incorporated with silica from the Stober process in Figure 5.4 (ii). (Liu *et al.*, 2016) reported that agglomeration is caused by silica's high energy level. The $-SO_3H/-SO_3H$ interaction may result in the association of silica-SO_3H particles that ought to interact ionically with Cs and be surrounded by Cs polymer chains causing the chains to act as separators, preventing the aggregation of silica-SO_3H particles (Su *et al.*, 2007).

5.3.1.4. Water Uptake of Pure and Sulfonated Chitosan Membranes with Silica Calcinated for 2h

(a) Effect of Silica on Water Uptake
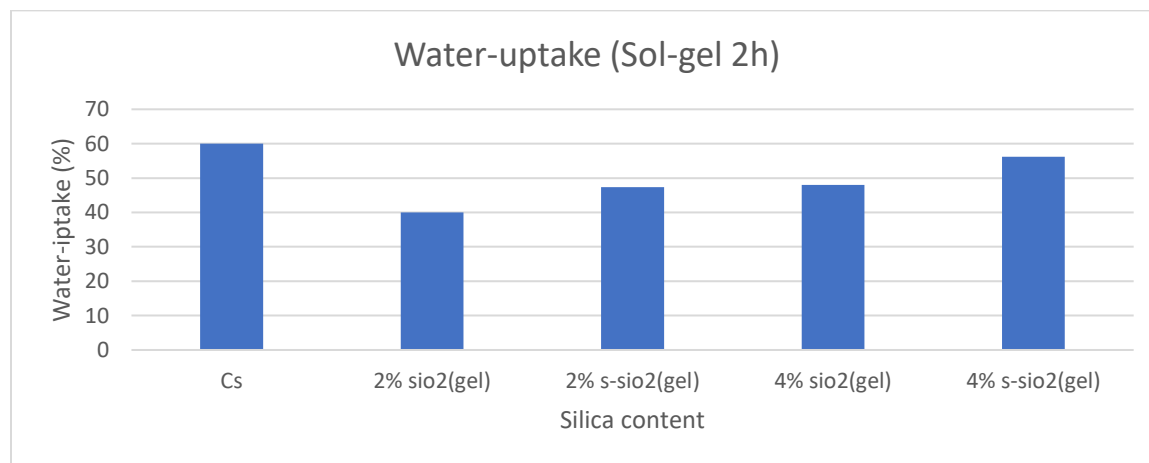
Figure 5.5.(i). Water-uptake of (a) Cs (b) 2% s-SiO_2/Cs (c) 2% SiO_2/Cs   (d) 4% s-SiO_2/Cs   (e) 4% SiO_2/Cs -**Sol-gel 2h)**

Water-uptake (stober 2h)
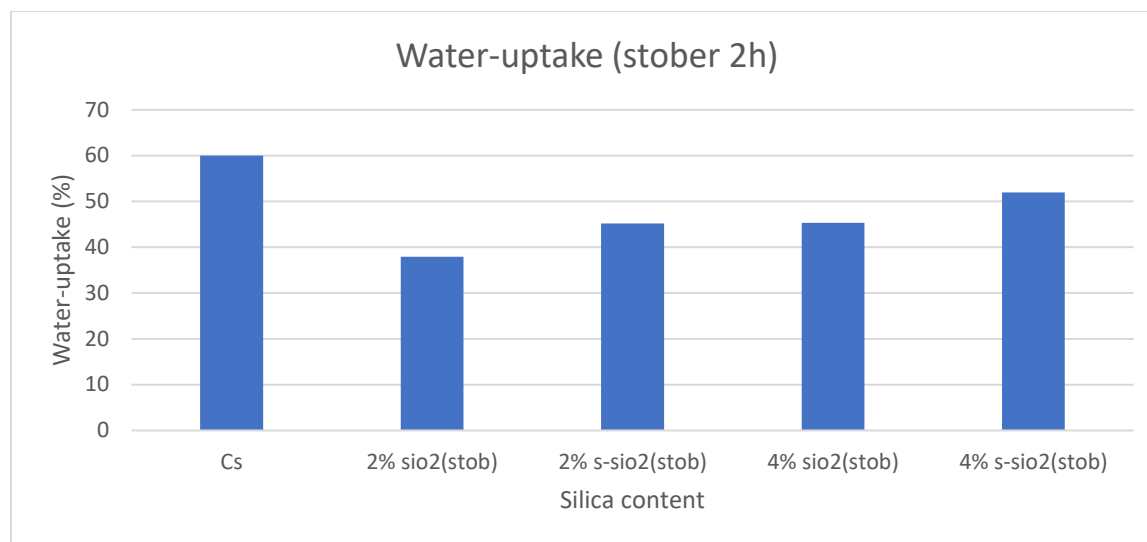
Figure 5.5.(ii). Water-uptake of (a) Cs (b) 2% s-SiO$_2$/Cs (c) 2% SiO$_2$/Cs (d) 4% s-SiO$_2$/Cs (e) 4% SiO$_2$/Cs **-(Stober 2h)**

Figure 5.5 (i and ii) indicate the relationship between silica content and water uptake. Figure 5.5 indicate that water uptake increase with the amount of both unmodified and modified nano-silica added into the chitosan membrane, this is due to silica's Si-OH groups' and chitosan hydrophilic qualities (Purwanto *et al.*, 2021), as chitosan is hydrophilic due to hydroxyl and amine groups present in its backbone. Similar results were reported by (Kusumastuti *et al.*, 2016a) with the highest water uptake of 63.56 % which is bigger than the 51.35 % reported in this research. The highest water uptake in Figure 5.5 is that of the 4% s-Sio$_2$ (Sol-gel) membrane of Figure 5.5. (i) and it is followed by 48.97% (4% s-SiO$_2$) Stober membrane in Figure 5.5. (ii). The increase in water uptake is caused by the polymer matrix's high silica content which is proportionate to the increase in the water charges caused by the quantity of Si-OH groups and the volume of water being absorbed. Additionally, adding more silica content and increasing temperature causes an increase in bonding interaction between silica's silanol group, acetyl, and amine groups of the chitosan which increases membrane hydrophobicity (Purwanto *et al.*, 2021). Also, silica's high hygroscopic affinity increases the membrane's potential to absorb water which serves as a medium for proton transport., but if the water content is too high, the membrane will be readily damaged and shorten its life span (Purwanto *et al.*, 2021).

(a) Effect of Temperature on Water Uptake

Figure 5.6 demonstrates the effect of temperature on water uptake. The membrane's water uptake was evaluated at temperatures of 40 ℃, 50 ℃, and 60 ℃. The membranes in Figure 5.6 show an increase in water uptake when temperature increases. All the membrane's water uptake values show a visible increment; however, the 2% s-SiO_2 membrane of Figure 5.6 (i) shows little variation in the water uptake at a temperature of 40 ℃ and 30 ℃. The minimal change in water uptake of this membrane may be due to the strong interaction between silica and chitosan which assisted the membrane in not absorbing excess moisture at these temperatures. The observed increase in water uptake as temperature increases in Figure 5.6 is due to hygroscopic characteristics and the water retention ability of the ammonium group found in the membrane. Membrane-free volume, chain mobility, and water diffusivity are likely the cause (Demina *et al.*, 2014). The increase in temperature causes membranes to swell due to the effect of the filler on water molecules of the chitosan chain (Liu, Su and Lai, 2004). (Vijayalekshmi and Khastgir, 2018; Rosli *et al.*, 2021) reported similar results. The overall water uptake capacity of membranes reported in Figure 5.6 (i and ii) show the highest water uptake to be that of membranes incorporated with sulfonated silica compared to that of the corresponding membrane made of pure silica.
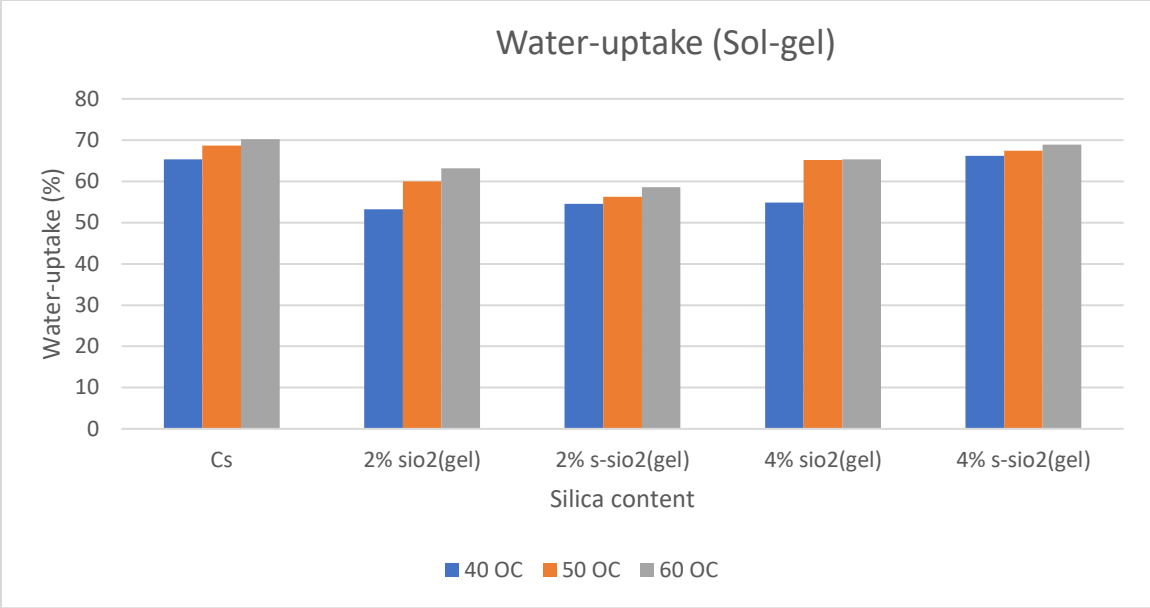
Figure 5.6.(i). Effect of temperature on water uptake of (a) Cs (b) 2% s-SiO$_2$ (c) 2% SiO$_2$ (d) 4% s-SiO$_2$ (e) 4% SiO$_2$ **- (Sol-gel 2h)**
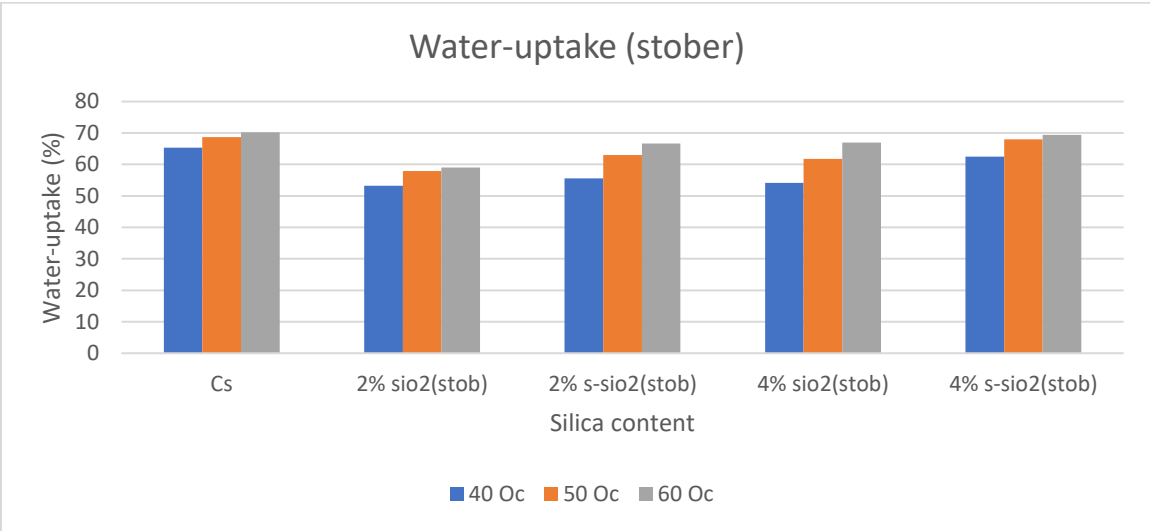
Figure 5.6.(ii). Effect of temperature on water-uptake of (a) Cs (b) 2% s-SiO$_2$ (c) 2% SiO$_2$ (d) 4% s-SiO$_2$ (e) 4% SiO$_2$ **- (Stober 2h)**

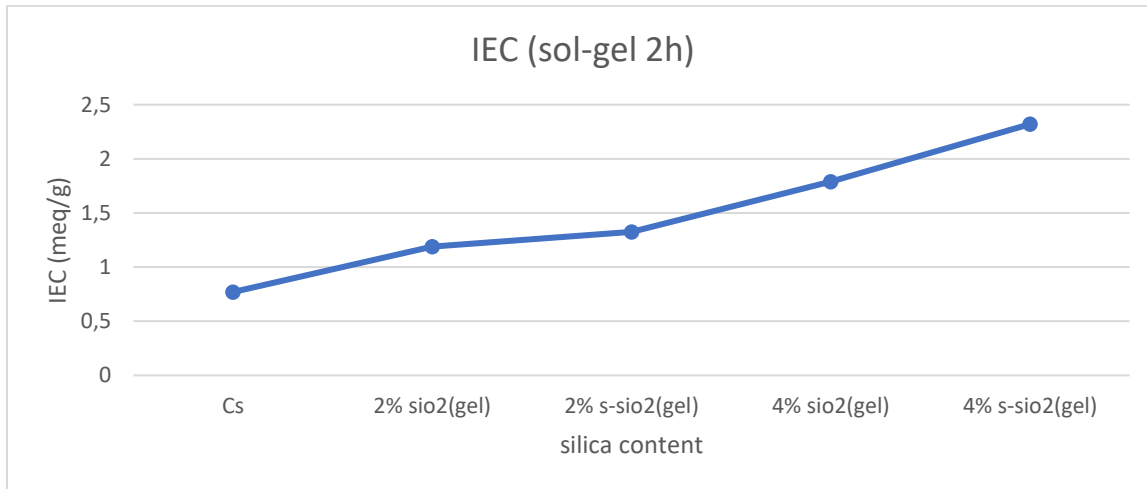5.3.1.5. Ion Exchange Capacity of Pure and Sulfonated Chitosan Membranes with Silica Calcinated for 2h.

Figure 5.7.(i). The ion exchange capacity of (a) Cs (b) 2% s-SiO$_2$ (c) 2% SiO$_2$ (d) 4% s-SiO$_2$ (e) 4% SiO$_2$ **- (Sol-gel 2h)**
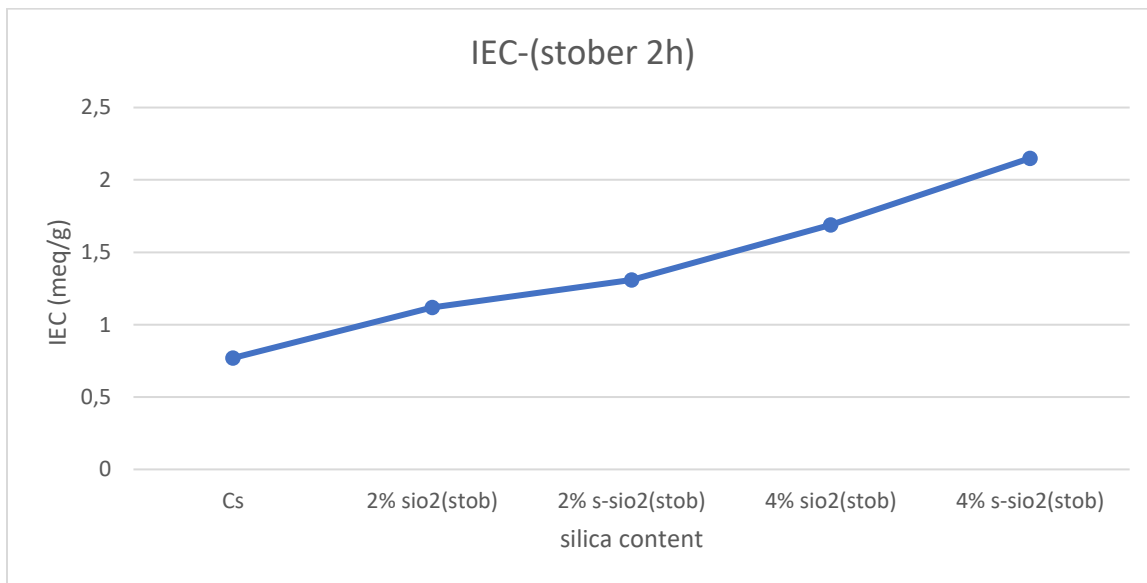
Figure 5.7.(ii). The ion exchange capacity (a) Cs (b) 2% s-SiO$_2$ (c) 2% SiO$_2$ (d) 4% s-SiO$_2$ (e) 4% SiO$_2$ - **(Stober 2h)**

Figure 5.7. Show the ion exchange capacity (IEC) of chitosan membranes modified with silica particles that were produced through the Sol-gel and Stober process. Ion exchange capacity is an indirect indicator of a polymer's proton conductivity because it refers to a group's capacity to bind protons in a solution. Ionic groups in chitosan promote the function of ion exchangers group NH_3^+ (Permana, Ahmad and Ramadhan, 2016). Ion exchange capacity through the membranes in Figure 5.7(i and ii) indicates an increase as the silica (SiO_2/s-SiO_2) content increases. The highest IEC value found is 2.32 meq/g from Figure 5.7(i) which corresponds to a 4% s-SiO_2 membrane prepared by the sol-gel method, followed by 2.15 meq/g of 4% s-SiO_2 Stober membrane of figure 5.7 (ii). The composite membranes' (s-SiO_2/Cs) higher IEC values were brought on by more acid groups, which were produced by the SiO_2-SO_3H particles' acidity (Septiawan *et al.*, 2018).

The ion exchange trend corresponds to what is reported in the literature by (Permana, Ahmad and Ramadhan, 2016) and (Septiawan *et al.*, 2018) who reported an increase in IEC from 1.1 meq/g to 2.18 meq/g, and 0.92 meq/g to 2.27 meq/g respectively. According to (Permana et al, 2016) membranes with high water uptake are likely to have improved ionic capacity because the ionic movement depends on water absorption and the number of silica groups in the polymer directly increases the localized water content. Additionally, IEC increases due to the hydrophilic polar functional groups in chitosan that boost the composite sheets' ability to absorb water (Permana, Ahmad and Ramadhan, 2016). The increase in ion exchange capacity corresponds to higher water uptake reported in Figure 5.5. Also, the amorphous nature of the material allows for the movement of more ions, increasing ionic mobility, which increases ionic conductivity (Peighambardoust, Rowshanzamir and Amjadi, 2010b; Lapicque *et al.*, 2012; Permana, Ahmad and Ramadhan, 2016).

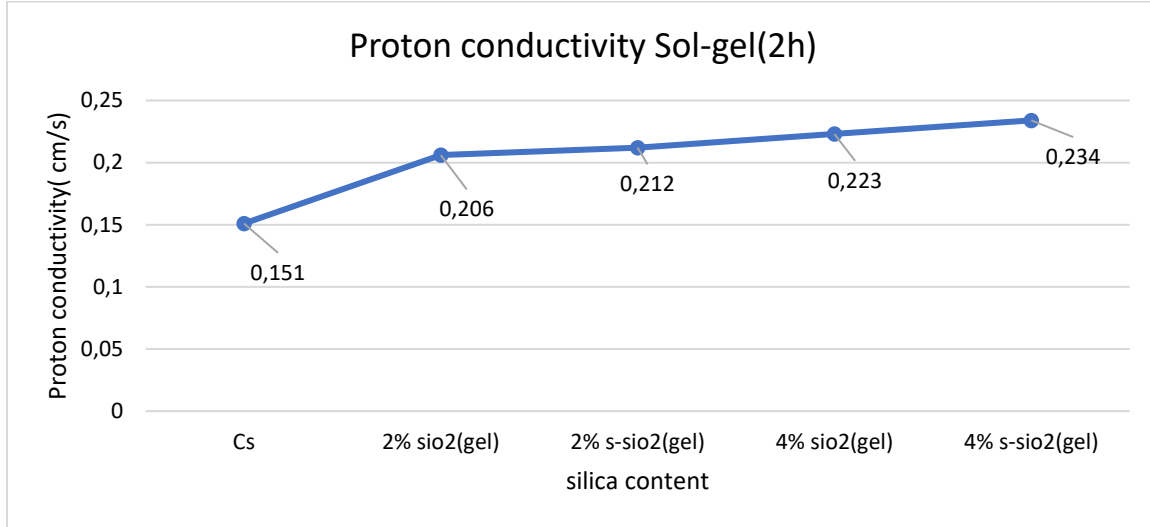5.3.1.6. Proton Conductivity of Pure and Sulfonated Chitosan Membranes with Silica Calcinated for 2h

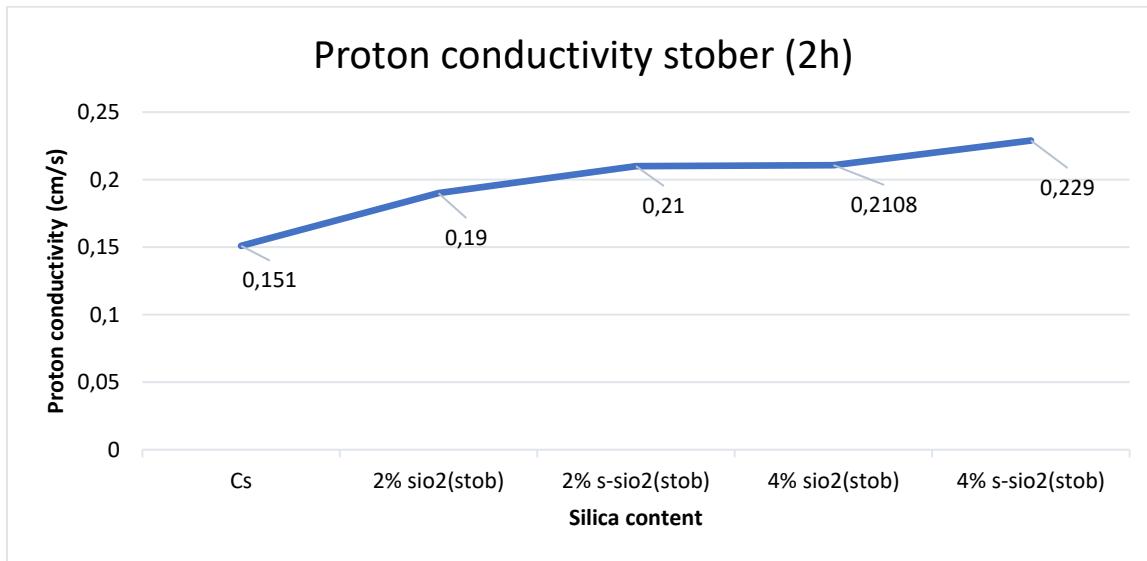Figure 5.8. (i). Proton conductivity of (a) Cs (b) 2% s-SiO$_2$ (c) 2% SiO$_2$ (d) 4% s-SiO$_2$ (e) 4% SiO$_2$ -**Sol-gel(2h)**

Figure 5.8.(ii). Proton conductivity of (a) Cs (b) 2% s-SiO$_2$ (c) 2% SiO$_2$ (d) 4% s-SiO$_2$ (e) 4% SiO$_2$) -(**Stober 2h**)

Figure 5.8 illustrates the proton conductivity of Cs, 2% s-SiO$_2$, 2% SiO$_2$, 4% s-SiO$_2$, and 4% SiO$_2$ composite membranes tested at room temperature. Reported Proton conductivity values in Figure 5.8 (ii) are lower than those observed in Figure 5.8 (i). It is observable in Figure 5.8 that proton conductivity increased when silica was added from 2% (0.206 S/cm) to 4% (0.223 S/cm) in Figure 5.8 (i) and from 0.19 S/cm to 0.2108 S/cm in figure 5.9(ii). The results in Figure 5.8 (i) further indicate an increase in proton conductivity from the lowest of 0.151 S/cm (pure chitosan) to the highest of 0.234 S/cm corresponding to 4% s-SiO$_2$ Sol-gel and that of membranes incorporated with silica from Stober in figure 5.9 (ii) was increased to 0.229 S/cm corresponding to 4% s-SiO$_2$ membrane. (Kusumastuti *et al.*, 2016a) reported the same behavior in the proton conductivity of chitosan membranes incorporated with silica particles and found the conductivity value of pure chitosan to be 0.174 S/cm and that of modified chitosan membrane highest to 0.234 S/cm when 5% silica was added in the chitosan membrane, this indicates an improvement in proton conductivity of membranes fabricated in this report.

The increase in proton conductivity of the membrane is due to the influence of ionic groups Si-OH which facilitate proton conduction (Narayanaswamy Venkatesan and Dharmalingam, 2013;Venkatesan *et al.*, 2012). The increase can also be attributed to the following major factors: (i) increase in water uptake which tends to increase proton carriers and H-networks; (ii) High IEC will increase the proton-hopping sites; (iii) which leads to tortuous transfer pathways for hydronium ions and protons; and (iv) promote chain mobility in the CS matrix which will decrease the hydronium ion and proton transfer resistance (O'Hayre, 2017). According to (Ramirez, no date) and (O'Hayre, 2017), water molecules subsumed in the membranes play a key role in proton conduction which facilitates the transport of protons. Particles can function as additional water clusters to enhance proton conduction. This is also supported by the water uptake results obtained reported in Figure 5.5.

The high proton conductivity of the s-SiO$_2$/Cs membrane in Figure 5.8 (i and ii) can be attributed to the formation of more open pathways owing to the existence of -SO$_3$ groups in the S-Cs. The high proton-conducting sulfonated groups that are anchored or stuck inside the routes of sulfonated polymer and sulfonated SiO$_2$ structure are most likely the cause of the excellent conductivity

(Yang *et al.*, 2010). The sulfonated groups of SO$_3$'s negative fixed charges make up the boundary walls of the channels. The proton could move through the periodic channels at the wall's surface moving from one SO$_3$ location to the next (Yang *et al.*, 2010;Luo *et al.*, 2022).

5.3.1.7. Methanol Permeability of Pure and Sulfonated Chitosan Membranes with Silica Calcinated for 2h.
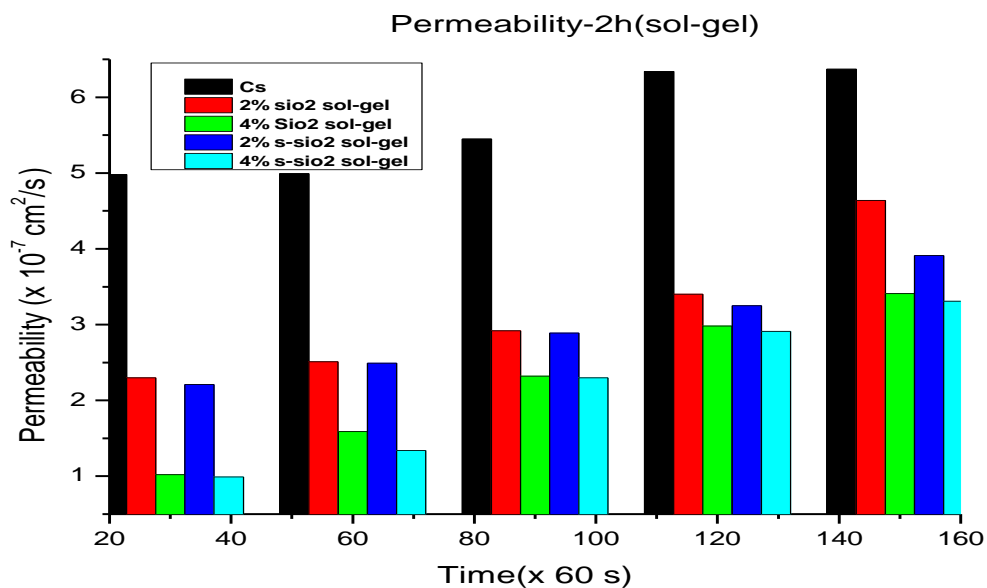

Figure 5.9. Methanol permeability of (a) Cs (b) 2% s-SiO$_2$ (c) 2% SiO$_2$ (d) 4% s-SiO$_2$ (e) 4% SiO$_2$ -**Sol-gel (2h)**
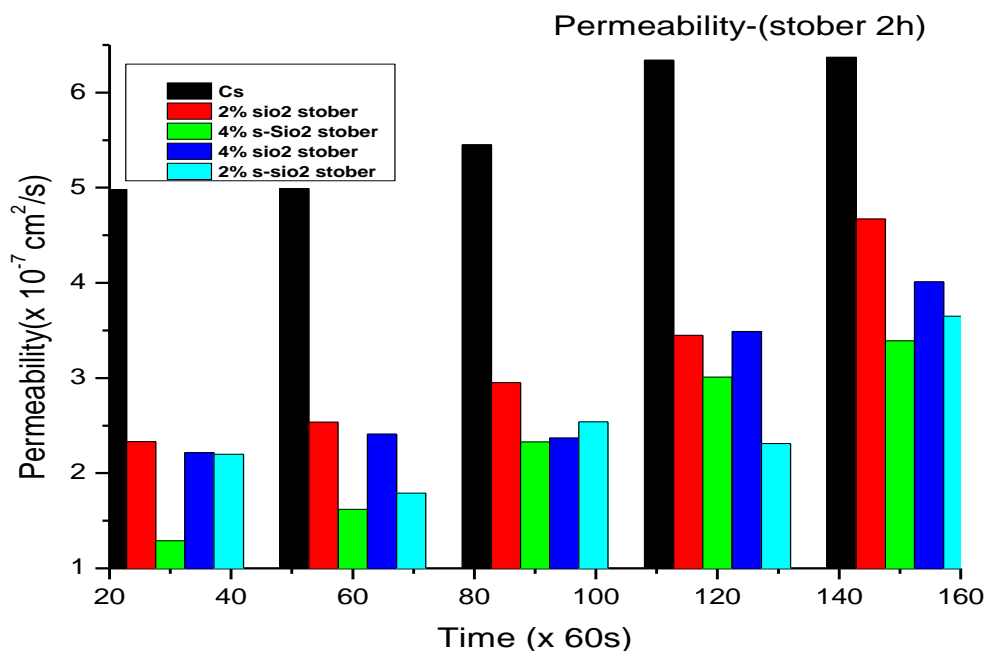
Figure 5.9. (ii). Methanol Permeability of (ii) (a) Cs (b) 2% s-SiO$_2$ (c) 2% SiO$_2$ (d) 4% s-SiO$_2$ (e) 4% SiO$_2$-Stober (2h)

Figure 5.9 displays the effect of silica content on the methanol permeability of chitosan composite membranes. The figures above, figure 5.9 (i and ii) indicate that an increase in adding silica particles reduces the methanol crossover in the membrane. Figure 5.9 indicate Cs' lowest methanol permeability of 4.98×10^{-7} cm^2/s at 30 minutes and highest permeability value of 6.37×10^{-7} cm^2/s at 150 minutes while figure 5.10(i) denotes the lowest methanol permeability of 0.99×10^{-7} cm^2/s at 30 minutes and highest of 3.31×10^{-7} cm^2/s at 60 minutes corresponding to 4% s-SiO$_2$. On the other hand, figure 5.9(ii) demonstrates the lowest methanol permeability of 1.29×10^{-7} cm^2/s of a 4% s-SiO$_2$ membrane followed by a 4% SiO$_2$ membrane with a permeability value of 2.2×10^{-7} cm^2/s at 30 minutes. It is observed that 4% s-SiO$_2$ chitosan (Sol-gel) in Figure 5.9 (i) has the lowest methanol permeability compared with other fabricated membranes in Figure 5.9 (i and ii). The results correspond to those reported by (Kusumastuti *et al.*, 2016b) and they show an improvement in lowering the methanol permeability of chitosan membrane modified with silica. Also, they comply with permeability requirements of less than 5.6 x 10^{-6} cm^2/s reported by (Kusumastuti *et al.*, 2016b). It can be noted that the permeability of the chitosan membrane incorporated with s-

SiO$_2$ particles in Figure 5.9 is lower than that of modified chitosan with pure silica, this is due to the strong -SO$_3$H/-SO$_3$H interactions between sulfonated-Cs that suppress polyelectrolyte chain motions, reducing the rate of methanol diffusion across the membranes. The membranes synthesized in this research indicate methanol permeability lower than that of commercial Nafion® membrane reported by (Lai *et al.*, 2007) and (Shaari *et al.*, 2018) who reported permeability measurements of 1.09×10^{-6} and 25.1×10^{-7} cm^2/s respectively. Low permeability values reported are attributed to the high aspect ratio of silica particles which allows for dispersal within CS polymer while suppressing chain mobility and free volume in a host polymer (Lue *et al.*, 2015). Also, the formation of a strong hydrogen bond network with chitosan, and ion-exchangeable acid groups promote proton conduction and successfully resists methanol permeability, thereby decreasing void volume (Su *et al.*, 2007). Figure 5.9 also indicates the relationship between time and permeability behavior on chitosan membranes. It is found that permeability increases with time, this is most likely caused by the elevated membrane swelling ratio and the greater mobility of methanol over a long period.

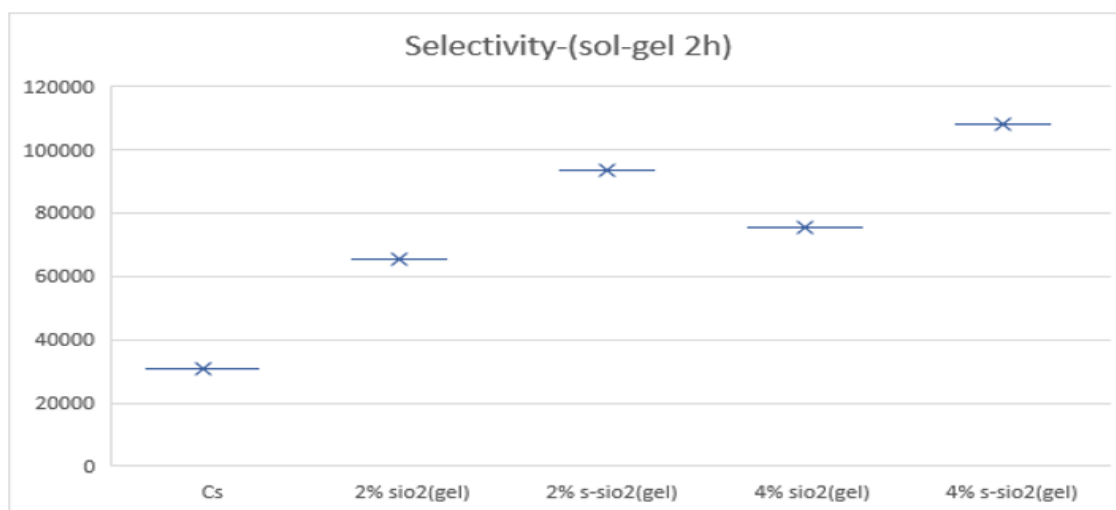5.3.1.8. Membrane Selectivity of Pure and Sulfonated Chitosan Membranes with Silica Calcinated for 2h.

Figure 5.10. Membrane selectivity of (a) Cs (b) 2% s-SiO$_2$ (c) 2% SiO$_2$ (d) 4% s-SiO$_2$ (e) 4% SiO$_2$) -Sol-gel (2h)
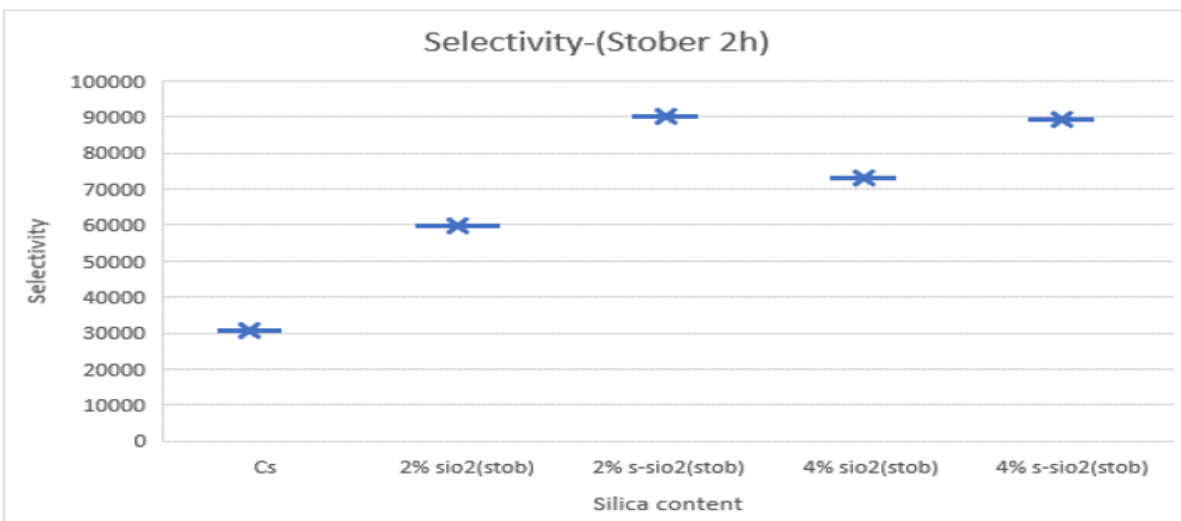
Figure 5.10.(ii) Membrane selectivity of (a) Cs (b) 2% s-SiO$_2$ (c) 2% SiO$_2$ (d) 4% s-SiO$_2$ (e) 4% SiO$_2$-Stober(2h)

Figure 5.10 presents the membrane selectivity of chitosan, 2% SiO$_2$, 2% s-SiO$_2$, 4% SiO$_2$, and 4% s-SiO$_2$ membranes. Figure 5.10(i) has membrane selectivity between 3.0 x 10^4 and 1.08 x 10^5 while selectivity values of membranes in Figure 5.11(ii) range between 3.0 x 10^4 and 9.0 x 10^5. It is observed in Figure 5.10(i) that, 4% s-SiO$_2$ (sol-gel) exhibits the highest selectivity of 1.08 x 10^5 followed by that of Figure 5.10(ii) 2% s-SiO$_2$ (Stober) with a selectivity of 9.0 x 10^5. Membranes with sulfonated silica pose high selectivity compared to those modified with pure silica. The high selectivity value of the membranes corresponds to high proton conductivity values and low methanol uptake as selectivity is the ratio between proton conductivity and methanol permeability. Figure 5.10(i) indicates that with 4% s-SiO$_2$ addition, the chitosan-silica membrane exhibits the best membrane selectivity, and this makes it to be suitable for application in a fuel cell.

5.3.1.9. Mechanical Strength of Pure and Sulfonated Chitosan Membranes with Silica Calcinated for 2h
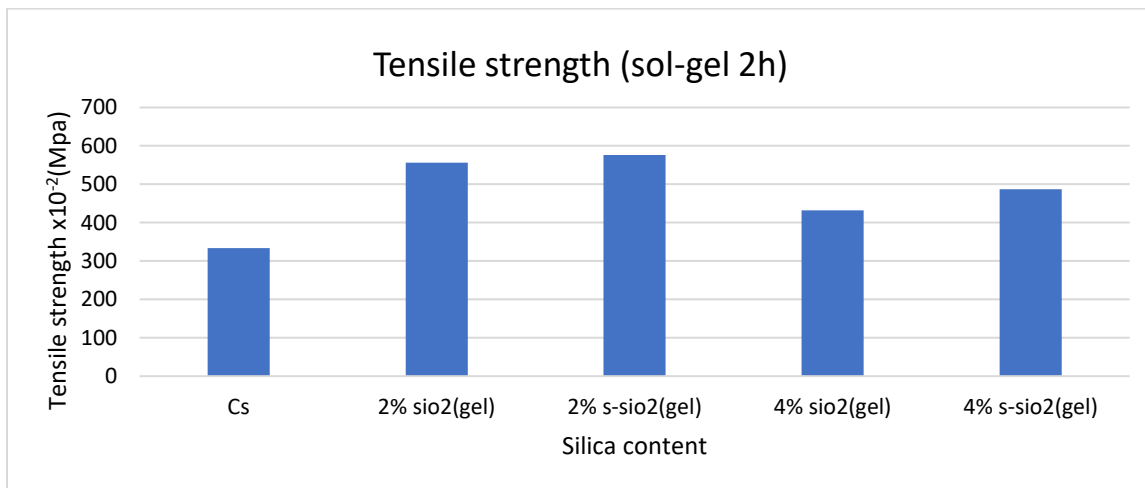

Figure 5.11.(i) Tensile strength of (a) Cs (b) 2% s-SiO$_2$ (c) 2% SiO$_2$ (d) 4% s-SiO$_2$ (e) 4% SiO$_2$ - **Sol-gel (2h)**
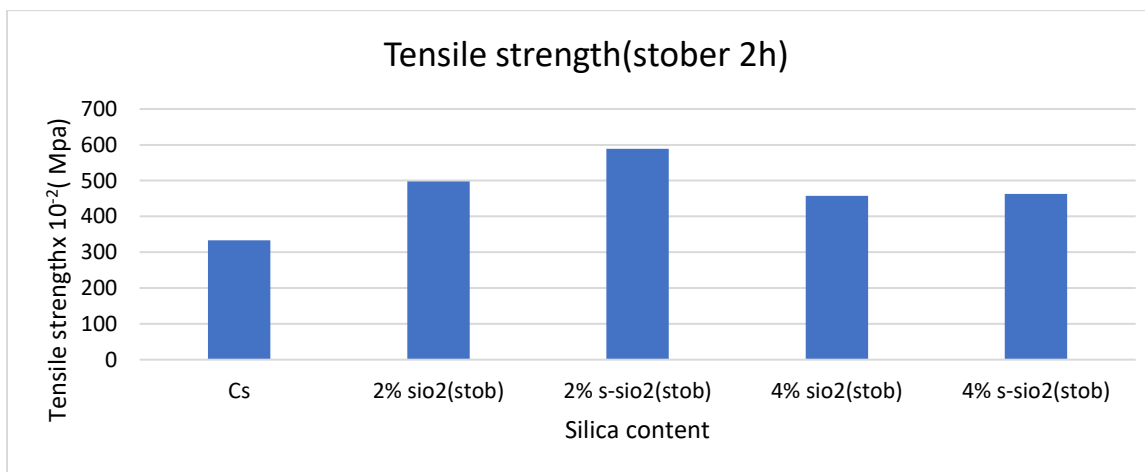

Figure 5.11. (ii). Tensile strength of (a) Cs (b) 2% s-SiO$_2$ (c) 2% SiO$_2$ (d) 4% s-SiO$_2$ (e) 4% SiO$_2$ -**Stober (2h)**

Figure 5.11 indicates the mechanical property of chitosan membranes in terms of tensile strength. The results in Figure 5.11 (i and ii) indicate an improvement in chitosan tensile strength when the inorganic filler was added, however, its mechanical strength weakened when more filler was added. Chitosan tensile strength of 3.33 Mpa was improved by the addition of silica particles to the highest value of 5.83 Mpa corresponding to 2% s-SiO$_2$ in figure 5.11(ii) followed by 5.76 Mpa of 2% s-SiO$_2$ of figure 5.12 (i). This is a clear indication that the sulfonation of particles is a contributing factor on increase in tensile strength of sulfonated chitosan membranes as membranes with s-SiO$_2$ possess excellent mechanical strength. When the filler content was increased to 4% a decline in strength was noticed and the lowest value was that of 4% SiO$_2$ (4.32 Mpa) found in Figure 5.11(i). The decrease in strength as filler content is added corresponds to what was reported by (Widhi Mahatmanti, Nuryono and Narsito, 2014) as high silica content is believed to harden the membrane. (Widhi Mahatmanti, Nuryono and Narsito, 2014) and (Film, 2021) also used silica particles to modify chitosan and the modified membranes show a decrease in tensile strength when silica filler was added in high concentration.

5.2.2. Membranes- 24h

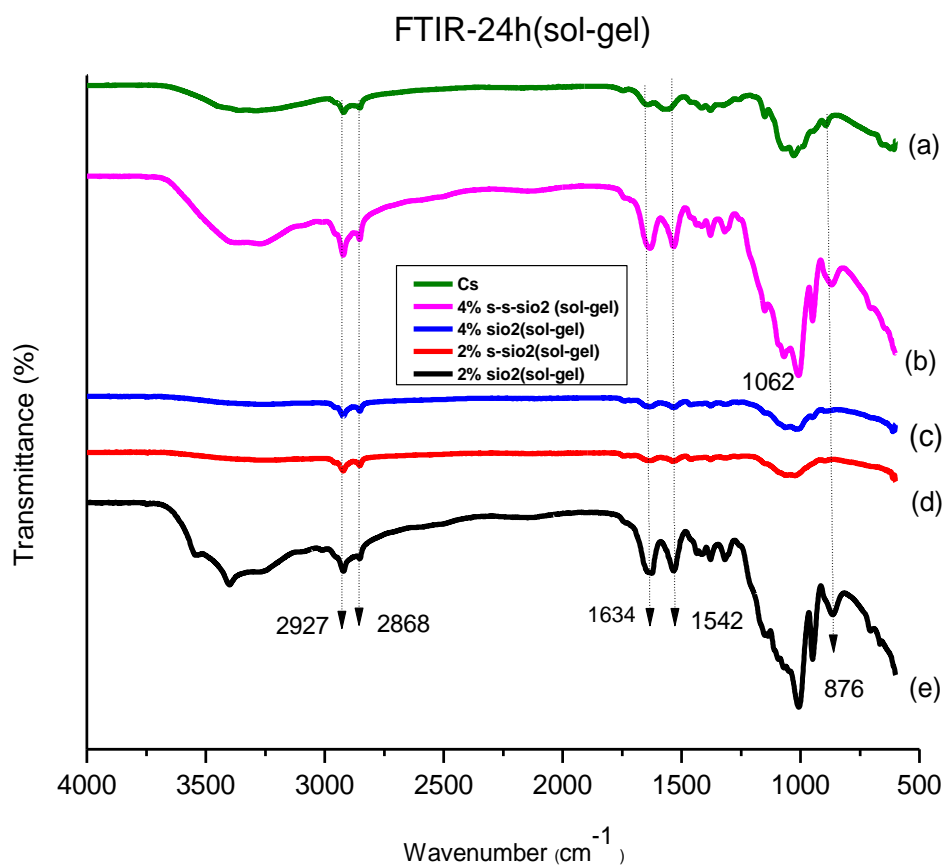5.2.2.1 FTIR of Pure and Sulfonated Chitosan Membranes with Silica Calcinated for 24h

FTIR-24h(sol-gel)

Figure 5.12.(i). FTIR of (a) Cs (b) 2% s-SiO$_2$ (c) 2% SiO$_2$ (d) 4% s-SiO$_2$ (e) 4% SiO$_2$ **- (sol-gel 24h)**
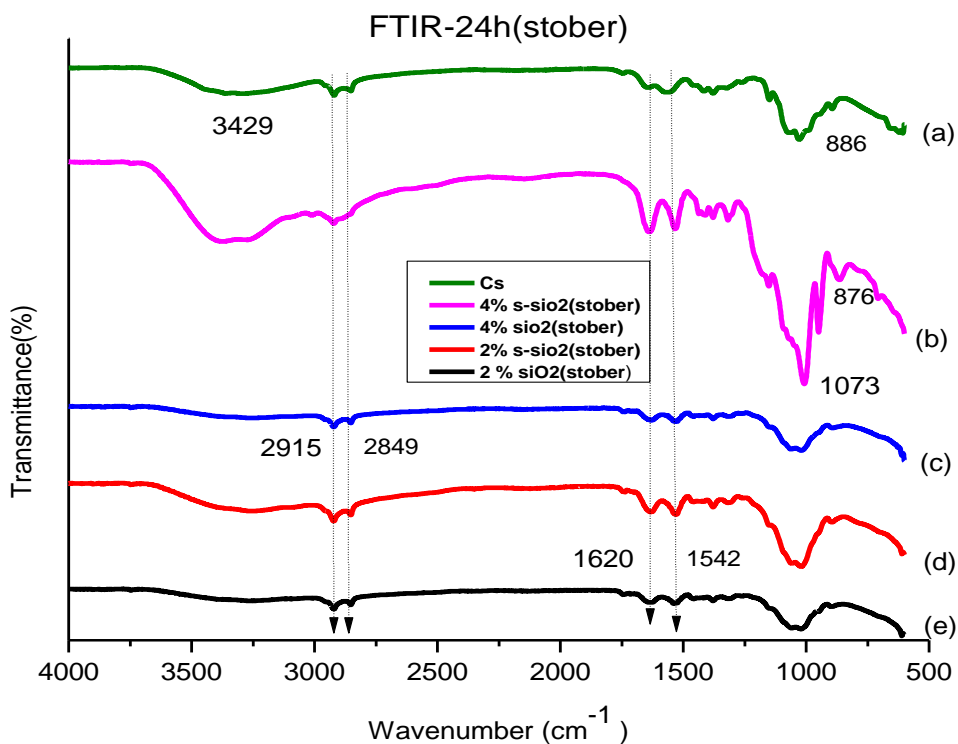
Figure 5.12.(ii)FTIR of (a) Cs (b) 2% s-SiO$_2$ (c) 2% SiO$_2$ (d) 4% s-SiO$_2$ (e) 4% SiO$_2$ **-Stober (24h)**

Figure 5.12 indicates Fourier transform spectroscopy spectra of chitosan membranes incorporated with 0%, 2%, and 4% pure and sulfonated silica particles calcinated for 24 h. The band at 3429 cm^{-1} in the FTIR spectrum of chitosan in Figure 5.12 (e) pertains to the stretching of hydroxyl groups attached to carbon atoms. The band at 1542 cm^{-1} directly correlates to the deformation vibrations of N-H$_2$ on the pure chitosan membrane (e), and that of C-H bending vibration is denoted by wavenumber 1420 cm^{-1}. Figure 5.12 (e) has bending vibrations at 1380 cm^{-1} which can be ascribed to C-H. The asymmetric stretching vibration of C-O-C is observed at 1309 cm^{-1} and that of Si-O-Si stretching vibration at 1012 cm^{-1} (Rupiasih, Suharta and Sumadiyasa, 2021). The increase in band intensity seen in Figure 5.12 (b, c, d, e) at about 850-1200 cm^{-1} is caused by the overlap of IR peaks brought about by the bending of the chitosan matrix's silica. The presence of the Si-OH network in the chitosan matrix is demonstrated by the shoulders that appear around 800 cm^{-1} on membranes b, c, d, and e of Figure 5.12. The FTIR spectra of this section compared with those reported in 5.3.2.1 have the same functional groups present in the fabricated membranes,

however, they were not located in the same wavenumbers as this was affected by how chitosan interacts with incorporated silica particles. The shifting in functional groups was observed in both FTIR spectra of chitosan modified with pure and sulfonated silica and it indicates successful modification.

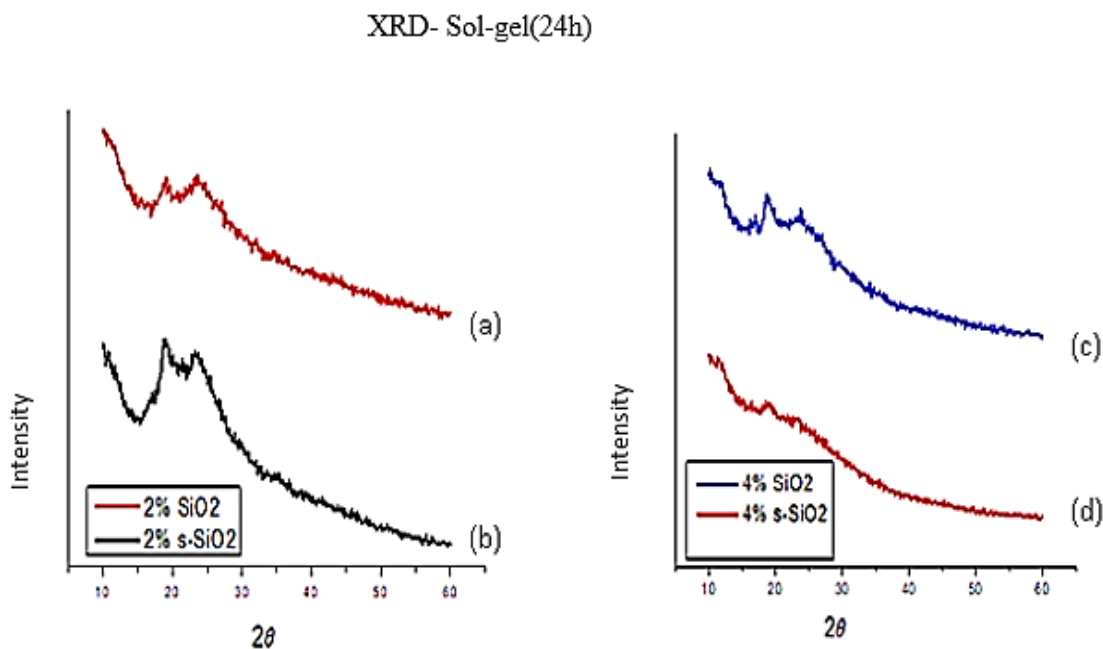5.3.2.2. XRD of Pure and Sulfonated Chitosan Membranes with Silica Calcinated for 24h

Figure 5.13.(i) XRD analysis of (a) 2% s-SiO$_2$ (b) 2% SiO$_2$ (dc) 4% s-SiO$_2$ (d) 4% SiO$_2$ **-sol-gel (24h)**
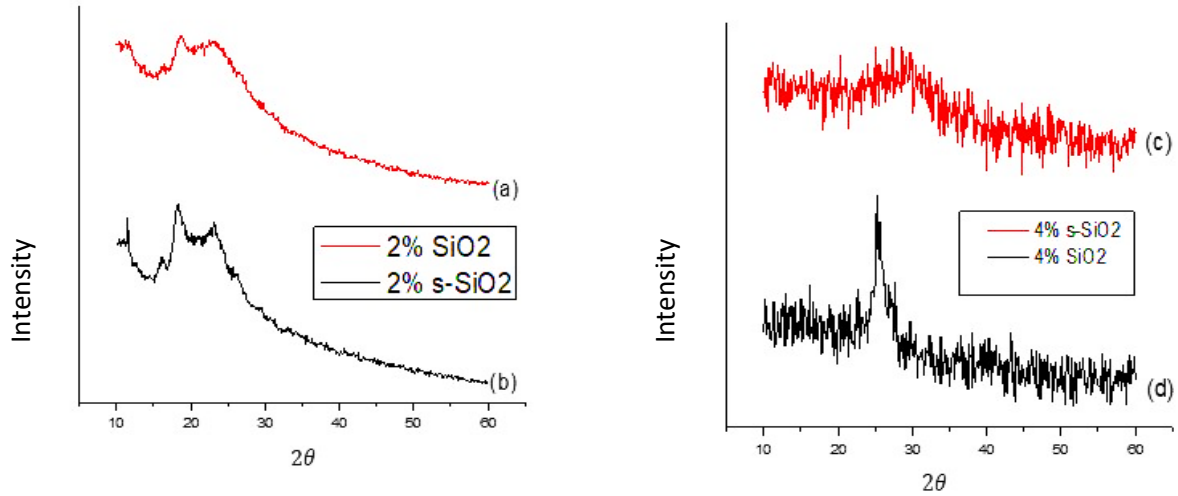
Figure 5.13.(ii). XRD analysis of (a) 2% SiO_2 (b) 2% s-SiO_2 (c) 4% s-SiO_2 (d) 4% SiO_2 **- Stober (24h)**

Figure 5.13 illustrates the XRD pattern of 2% s-SiO_2, 2% SiO_2, 4% s-SiO_2, and 4% SiO_2 membranes with thickness of 0.041 cm. One can notice that membranes in Figure 5.13 (i) have one characteristic band at 21.0^0, 21.7^0, 21, 40, and 20.4^0 corresponding to 2% s-SiO_2, 2% SiO_2, 4% s-SiO_2, and 4% SiO_2 membrane respectively. Stober membranes in Figure 5.13(ii) display two peak bands at 15.8^0, 21.2^0 (2% SiO_2), and 15.9^0 and 20.5^0 (2% s-SiO_2) which is attributed to the semi-crystalline structure of chitosan membranes (Qiao *et al.*, 2021). However, 4% s-SiO_2 and 4% SiO_2 membranes show amorphous characteristics of chitosan with diffraction peaks at 29.9^0 and 25.7^0. It is known that s-SiO_2 chitosan membranes are more amorphous than SiO_2 due to partial reconstitution of the crystal region of SiO_2 during the modification process (Muraishi, 1989; Gutzow *et al.*, 2014; Gaabour, 2019).

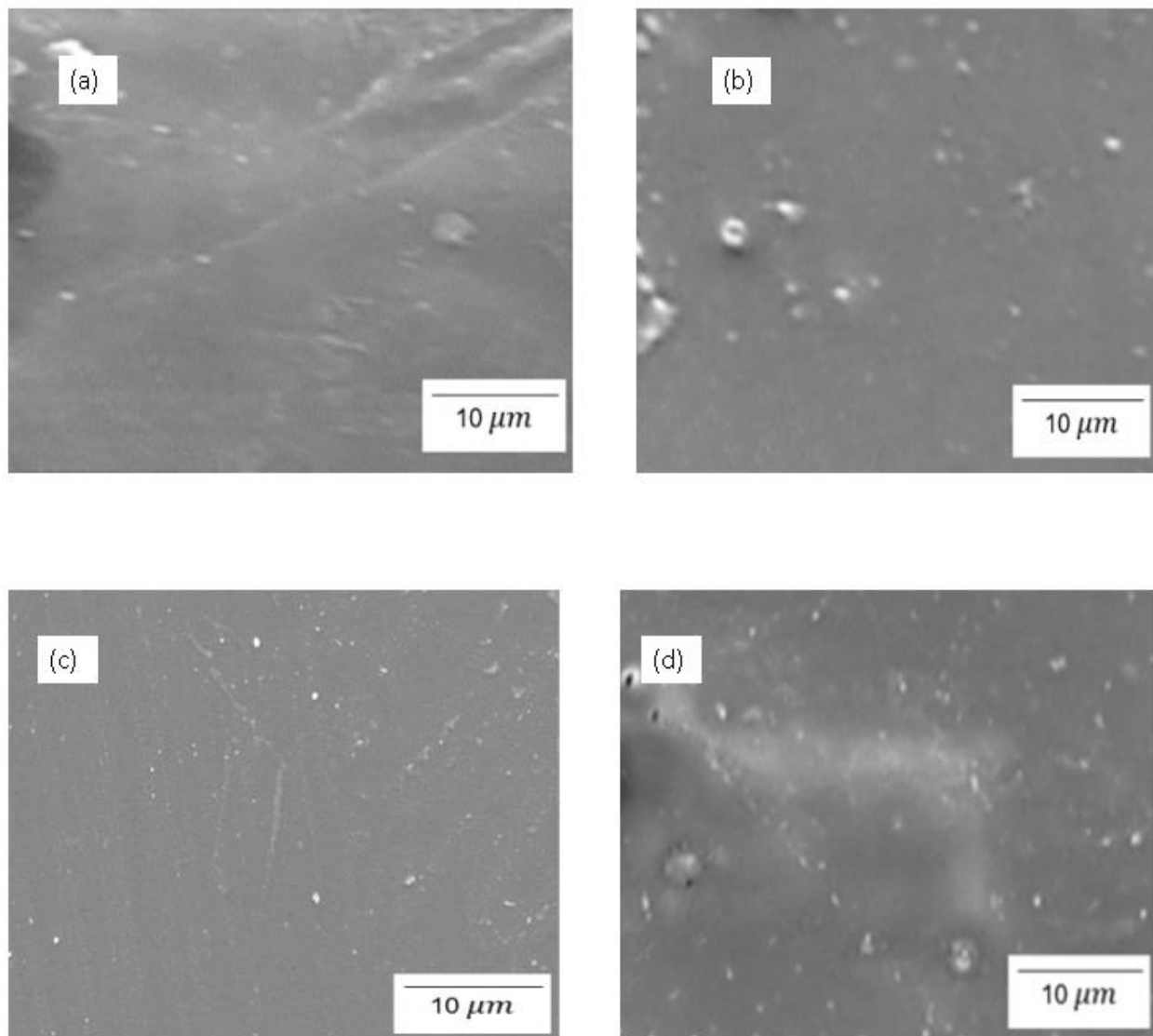## 5.3.2.3. SEM of Pure and Sulfonated Chitosan Membranes with Silica Calcinated for 24h

Figure 5.14.(i). SEM of (a) 2% SiO_2 (b) 2% s-SiO_2 (c) 4% s-SiO_2 (d) 4% SiO_2 -**Sol-gel (24h)**
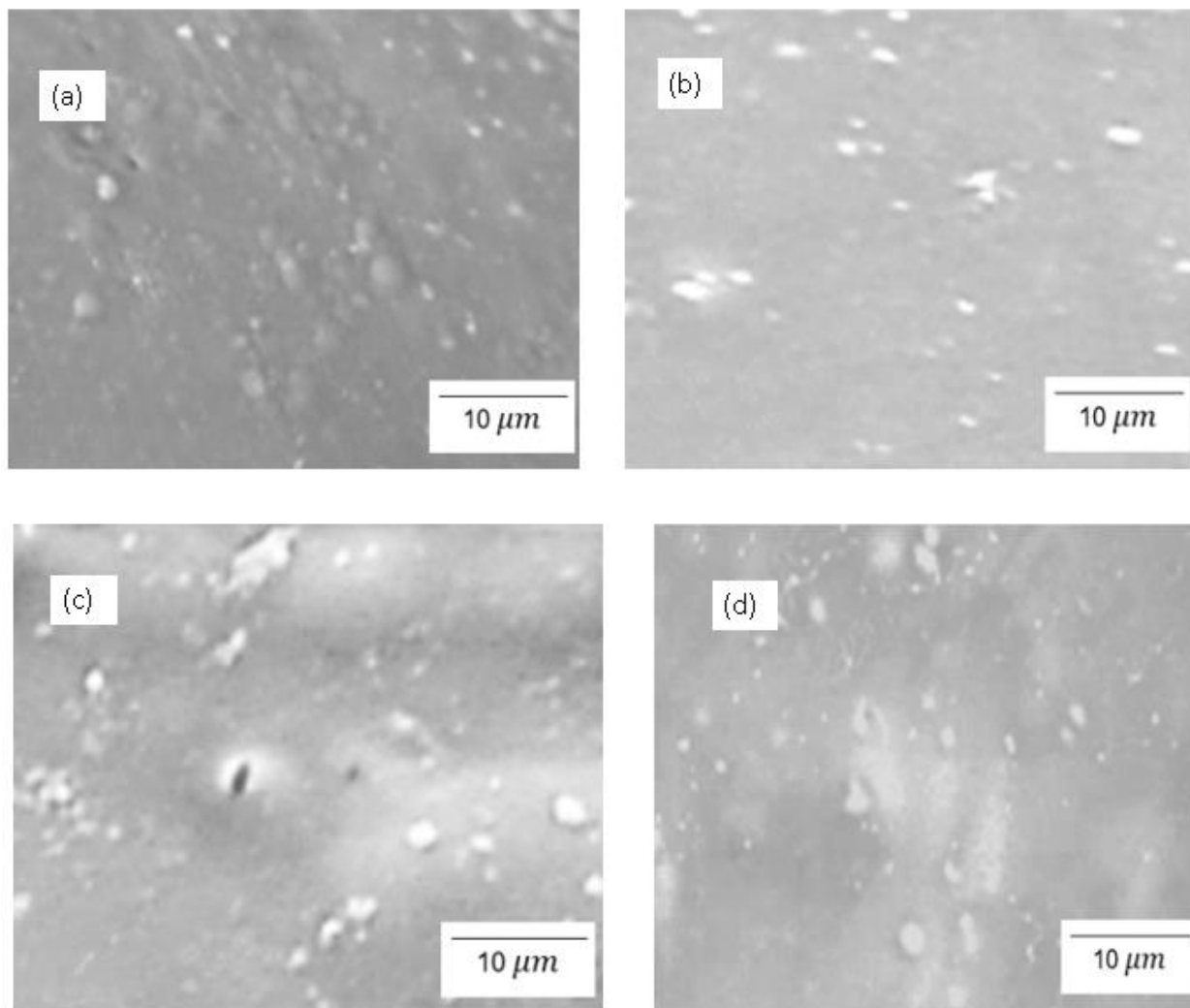
Figure 5.14.(ii) SEM of (a) 2% SiO$_2$ (b) 2% s-SiO$_2$ (c) 4% SiO$_2$ (d) 4% s-SiO$_2$-**Stober (24h)**

Figure 5.14 indicates the physical morphology of 2% SiO$_2$, 2% s-SiO$_2$, 4% SiO$_2$, and 4% s-SiO$_2$ membranes incorporated with silica calcinated for 24h. Figure 5.14 indicates that all membranes in figure 5.14 (i and ii) are hard in the structure causing the membrane's morphology to be seemed as lumpy, with membranes in figure 5.14 (ii) having the toughest and grumpy surface. Silica agglomeration was less visible in membrane (c) of Figure 5.14(i) which demonstrates good interaction between chitosan and nano-silica, resulting in dispersion and successful incorporation of silica on the membranes, this is due to the introduction of acid groups in the silica which may have lowered silica energy level (Han *et al.*, 2020). Figure 5.14(ii) indicates lumps on the surface of the membrane (a), the lumps may be caused by the hardness properties of the membrane, the

results agree with what was reported by (Zungu, 2021) who reported similar results regarding chitosan morphology. It can be said that in Figure 5.14 (ii) agglomeration is high in the membrane (b), (c) and (d) as silica particles appear as large agglomerates or particles compared to those of Figure 5.15 (i), this can be attributed to silica particles in figure 5.15 (ii) having more energy than that of figure 5.14 (i). However, though silica particles agglomeration was high in Figure 5.14 (ii) the particles were dispersed on the membranes.

5.3.2.4. Water Uptake of Pure and Sulfonated Chitosan Membranes with Silica Calcinated for 24h
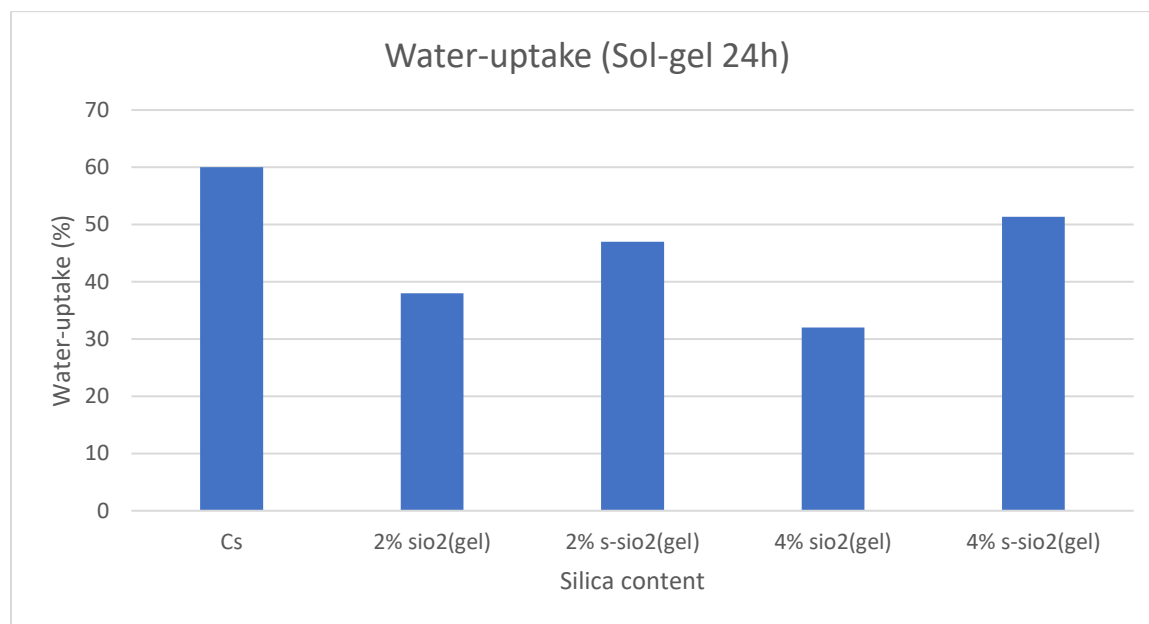
(a) Effect of Silica Content on Water-Uptake

Figure 5.15.(i). Effect of silica content on water-uptake of (a) 2% SiO_2 (b) 2% s-SiO_2 (c) 4% SiO_2 (d) 4% s-SiO_2 - **(Sol-gel 24h)**
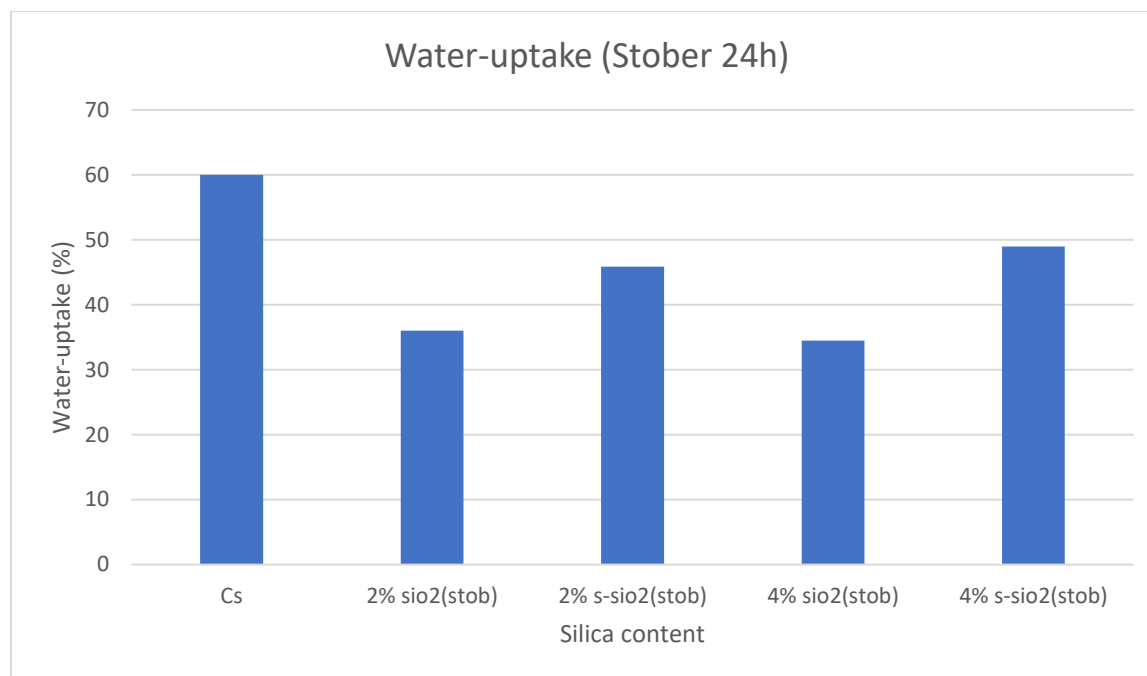
Figure 5.15.(ii) Effect of silica content on water-uptake of (a) Cs (b) 2% s-SiO$_2$ (c) 2% SiO$_2$ (d) 4% s-SiO$_2$ (e) 4% SiO$_2$ –Stober(24h)

Figure 5.15 indicates the water uptake of chitosan membranes at room temperature. Figure 5.15 demonstrates that water uptake of silica particles synthesized by Stober (ii), and Sol-gel (i) increases as the silica particle content increases. The membranes showing the lowest water uptake are that of 2% both pure and sulfonated silica in Figure 5.15 (i and ii). However, the highest uptake recorded is 56.21% corresponding to 4% s-SiO$_2$ in Figure 5.15 (i) followed by 4% s-SiO$_2$ from Figure 5.15 (ii) having an uptake of 48.92%. (Science, 2021) reported similar results with water uptake of about 62% on a 4% SiO$_2$/Cs membrane which is higher than the one reported in this research. The increase in acidic formation in the membrane may be the main reason behind the increase in water uptake values for membranes modified with silica (Huang, Chen and Lin, 2017; Vijayalekshmi and Khastgir, 2018; Rosli *et al.*, 2021) . Though the modified membranes indicate an increase as filler increases, they were able to suppress the water uptake lower than of pure chitosan which is 60%. The increase in water uptake can be explained in terms of the bond formation between the amine and acetyl groups from chitosan and the silanol groups from silica. Also, it is caused by the improved hydrophilic -SO$_3$H functional groups of the s-SiO$_2$ filler.

Additionally, the increased water uptake of chitosan membranes can be explained by silica nano filler's hygroscopic properties that enhance high-water absorption of the Cs/SiO_2 and Cs/ s-SiO_2 membranes, which is advantageous for the de-protonation of acid molecules into protons and ensuing mobility of those protons (Jiao and Li, 2011; Huber, 2020; Nakayama *et al.*, 2020).

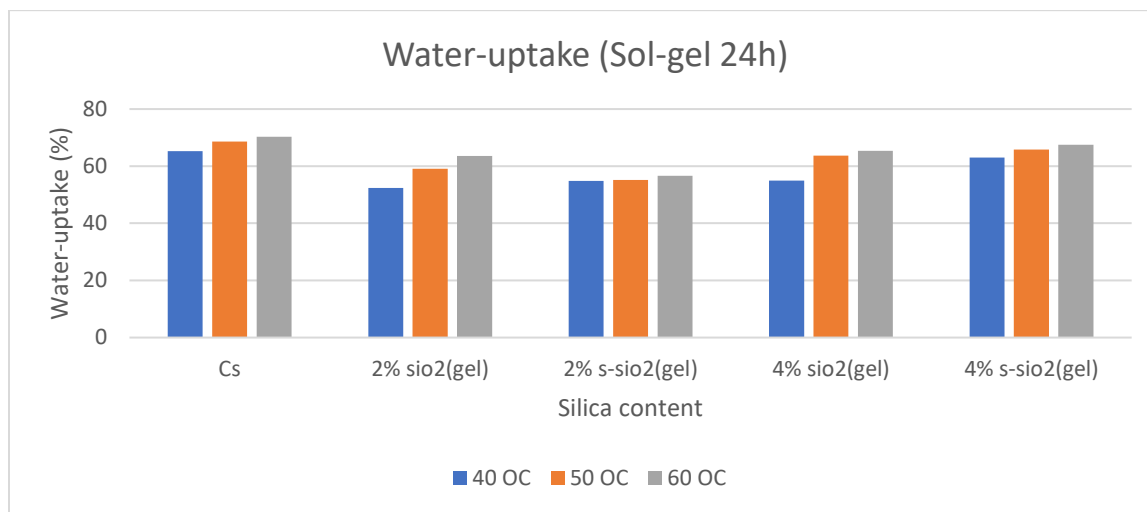(b) Effect of temperature on water-uptake

Figure 5.16.(i). Effect of temperature on water-uptake of (a) Cs (b) 2% s-SiO_2 (c) 2% SiO_2 (d) 4% s-SiO_2 (e) 4% SiO_2 -Sol-gel (24h)
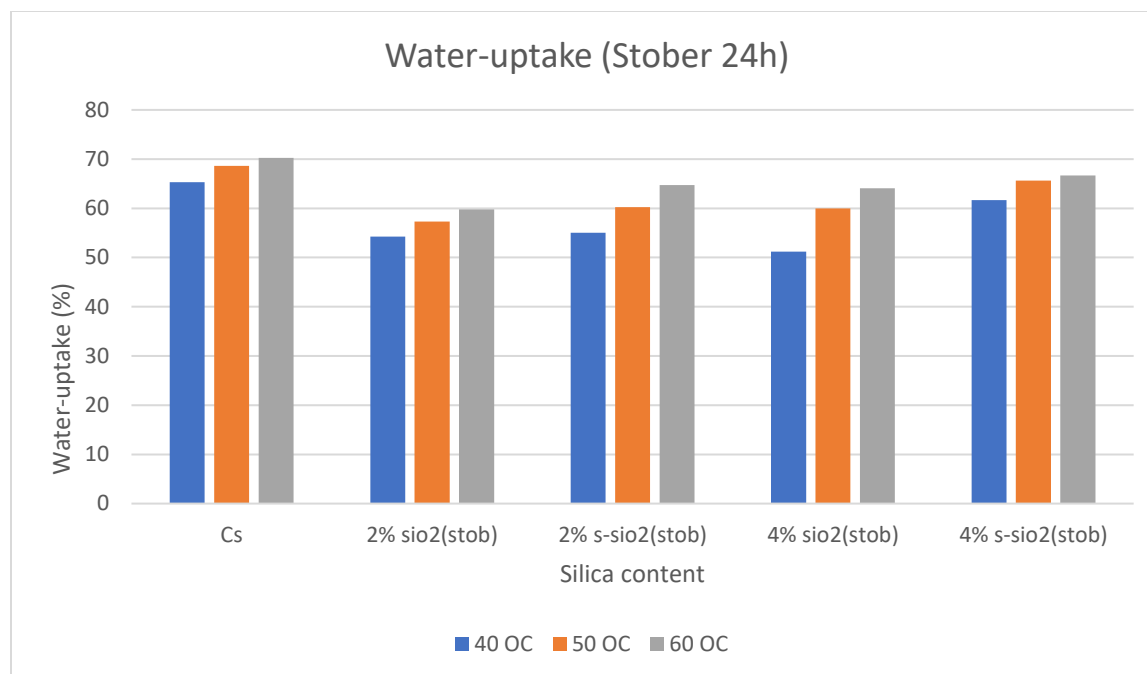
Figure 5.16.(ii). Effect of temperature on water-uptake (a) Cs (b) 2% s-SiO$_2$ (c) 2% SiO$_2$ (d) 4% s-SiO$_2$ (e) 4% SiO$_2$ -Stober (24h)

Figure 5.16 indicate the effect of temperature on chitosan, 2% SiO$_2$, 2% s-SiO$_2$, 4% SiO$_2$, and 4% s-SiO$_2$ membranes at temperatures of 40℃, 50 ℃, and 60℃. Regarding the influence of temperature on water uptake, all membranes in Figure 5.16 (i and ii) displayed a rising trend in water content as the temperature rose. Water molecules and chitosan polymer chains often travel more quickly at higher temperatures, which makes water easily permeate into membranes, and the presence of silanol groups from silica also contributes to the high hydrophilic properties of chitosan at elevated temperatures (Srinophakun *et al.*, 2017; Walkowiak-Kulikowska, Wolska and Koroniak, 2017). An increase in water properties on membranes at elevated temperatures was also reported by (Tsen, 2020).

5.3.2.5. IEC of Pure and Sulfonated Chitosan Membranes with Silica Calcinated for 24h

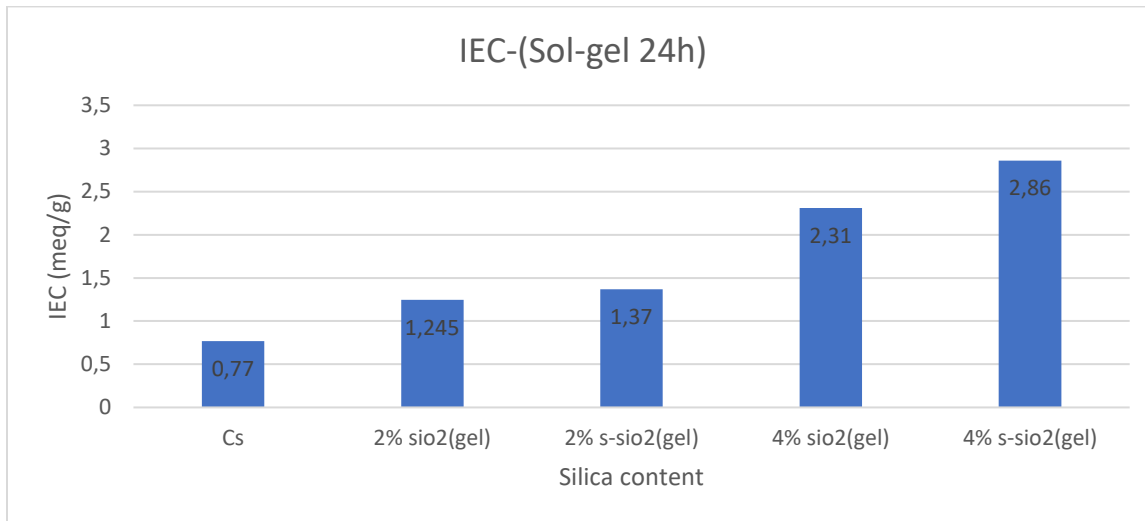Figure 5.17.(i). The ion exchange capacity of (a) Cs (b) 2% s-SiO$_2$ (c) 2% SiO$_2$ (d) 4% s-SiO$_2$ (e) 4% SiO$_2$ - (**Sol-gel 24h)**
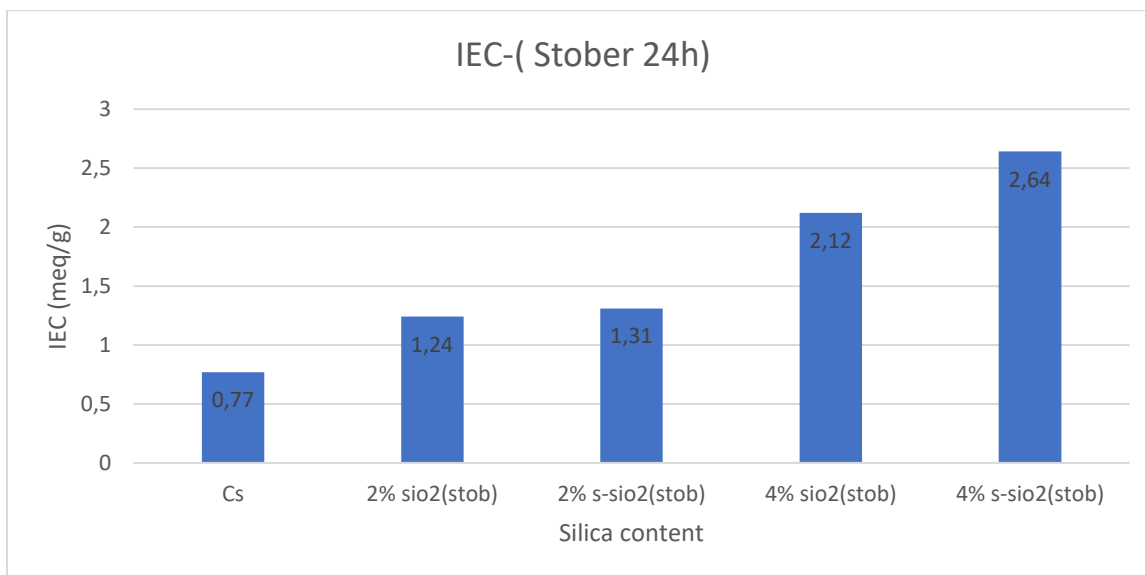

Figure 5.17.(ii). The ion exchange capacity of (a) Cs (b) 2% s-SiO$_2$ (c) 2% SiO$_2$ (d) 4% s-SiO$_2$ (e) 4% SiO$_2$ -(Stober 24h)

Figure 5.17 represents the ion exchange capacity of chitosan, 2 % SiO_2, 2 % s-SiO_2, 4 % SiO_2, and 4 % s-SiO_2 membranes modified with silica calcinated for 24h. The number of sulfonic acid groups in the polymer served as the theoretical basis for the calculated IEC values, which were then measured using the titrimetric method, and IEC values were obtained using the equation of IEC in Chapter 3. Figure 5.17 indicate a rising IEC value when silica is added with pure chitosan having an IEC of 0.77 meq/g which was improved by adding silica particles in the chitosan matrix and the IEC was elevated to the highest of 2.86 meq/g corresponding to 4 % s-SiO_2 sol-gel membrane in figure 5.18(i).

It is noticeable in Figure 5.18 that the IEC value increased as the amount of silica increased, and the highest ionic capacity is recorded in membranes with sulfonated silica. The noticed increase in IEC is due to sulfate ions in the structure of the polymer that serves as proton exchange sites, also the presence of silica created a strong connection with chitosan, resulting in an environment that is favorable for the ion exchange phenomena in the membrane (Vijayakumar and Khastgir, 2018).(Purwanto *et al.*, 2015) reported similar IEC results of chitosan membranes. The IEC values of membranes prepared by the sol-gel method (figure 5.17. i) have high values compared with those of membranes modified with silica synthesized by the Stober process (figure 5.18.ii). The same behavior was reported in membranes fabricated with silica synthesized for 2h. However, the best ion exchange values recorded are of membranes modified with silica calcinated for 24 h compared to those with silica calcinated for 2h.

5.3.2.6. Proton conductivity of pure and sulfonated chitosan membranes with silica calcinated for 24h

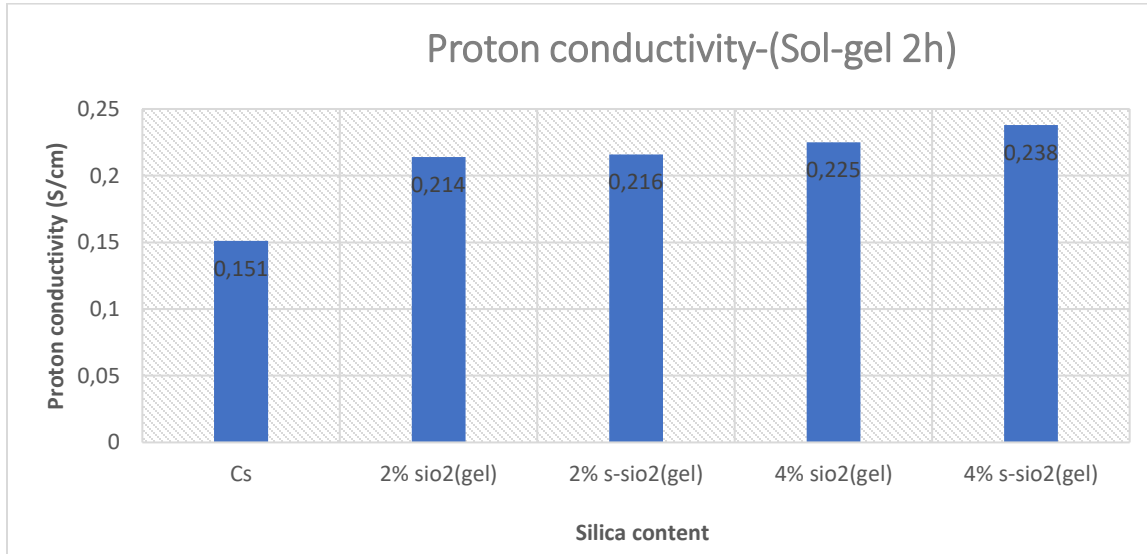Figure 5.18.(i). Proton conductivity of (a) Cs (b) 2% s-SiO$_2$ (c) 2% SiO$_2$ (d) 4% s-SiO$_2$ (e) 4% SiO$_2$ - (Sol-gel 24h)
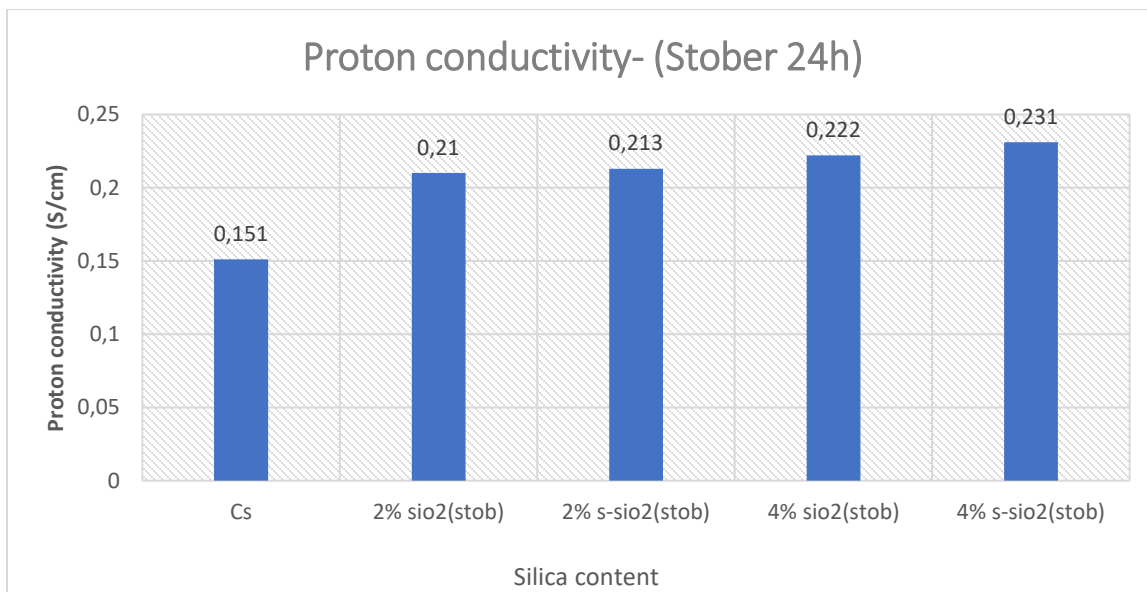

Figure 5.18.(ii). Proton conductivity of (a) Cs (b) 2% s-SiO$_2$ (c) 2% SiO$_2$ (d) 4% s-SiO$_2$ (e) 4% SiO$_2$ $_2$-Stober (24h)

Figure 5.18 the proton conductivity of membranes made of Cs/SiO_2 and $Cs/s-SiO_2$ with 2% and 4% examined in figure 5.18. The results indicate that the proton conductivity of membranes in Figure 5.18 is higher than that of pure chitosan which is 0.151 S/cm. The results show the highest proton conductivity of 0.238 S/cm (4 % $s-SiO_2$) in Figure 5.19 (i) followed by 0.225 S/cm of 4 % SiO_2 membrane. The lowest proton conductivity is 0.214 S/cm corresponding to 2 % SiO_2. On the other hand, figure 5.19 (ii) reported the highest conductivity of 0.231 S/cm and the lowest of 0.21 S/cm belonging to 4 % $s-SiO_2$ and 2 % SiO_2. Similar results were reported by (Kusumastuti *et al.*, 2016b) and (Liu *et al.*, 2016), however proton conductivity values reported in the literature were lower than the ones reported in this research as (Liu *et al.*, 2016) found highest conductivity value of 0.025 S/cm and lowest value of 0.02 S/cm corresponding to 4% SiO_2 and 2% SiO_2 respectively and (Kusumastuti *et al.*, 2016b) reported proton conductivity of 0.234 S/cm on 5% membrane.

Improved proton conduction is a result of the structural characteristic as well as better filler dispersion. Proton conduction in the CS membrane is primarily caused by hopping between the NH_2 and the nearby NH_3^+ groups and the presence of filler may make proton hopping between adjacent sites easier. In the case of these membranes, the addition of $s-SiO_2$ acts as a bridge to connect and reduce the path length for proton hopping. As a result, $CS/s-SiO_2$ membranes attain greater conductivity than CS/SiO_2 membranes. The increased mobility of water molecules and polymer chains is the main cause of the increased proton conductivity that is seen with an increase in silica addition (Yang, Lue and Shih, 2011). Protons can then be transported quickly and continuously using the Grotthuss mechanism after being dissociated from the activated state and combined with a nearby water molecule to create a new activated state (Feng *et al.*, 2010;Yang, Lue and Shih, 2011).

5.3.2.7. Methanol Permeability of Pure and Sulfonated Chitosan Membranes with Silica Calcinated for 24h

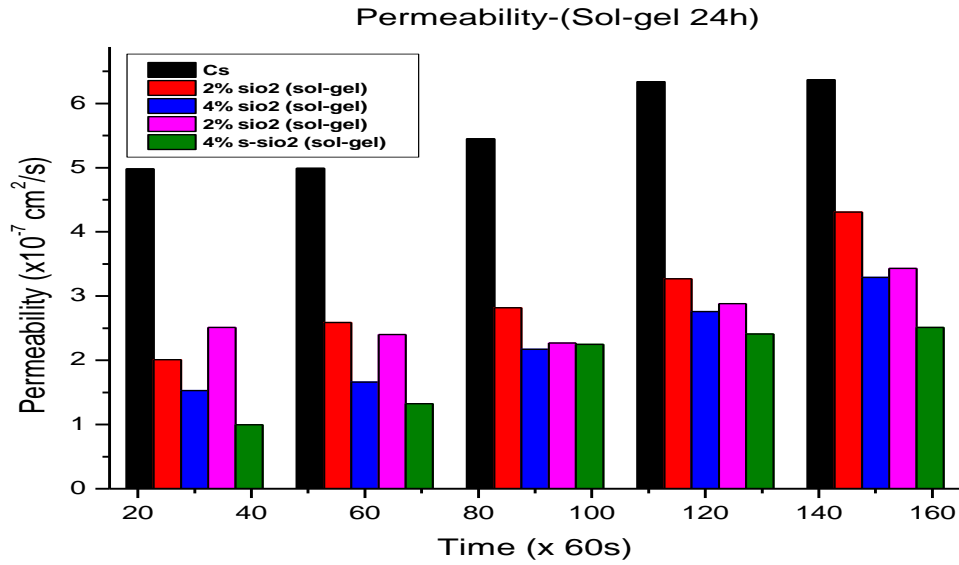Figure 5.19.(i).(a) Methanol permeability of Cs (b) 2% s-SiO$_2$ (c) 2% SiO$_2$ (d) 4% s-SiO$_2$ (e) 4% SiO$_2$ **- (Sol-gel 24h)**
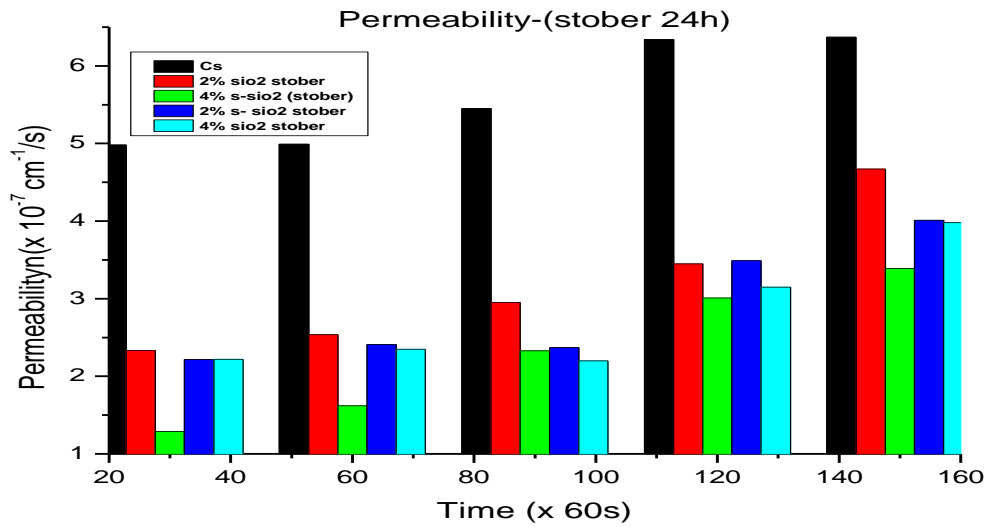

Figure 5.19.(ii). Methanol permeability of (a) Cs (b) 2% s-SiO$_2$ (c) 2% SiO$_2$ (d) 4% s-SiO$_2$ (e) 4% SiO$_2$ -Stober (24h)

Figure 5.19 represents Methanol permeability of chitosan, 2 % SiO_2, 2 % s-SiO_2, 4 % SiO_2 and 4 % s-SiO_2 membranes at room temperature. A decrease in methanol permeability was observed when silica particles were added to the chitosan. Methanol crossover was suppressed from 4.98 1.53 x 10^{-7} cm^2/s of pure chitosan membrane to the lowest of 1.53 x 10^{-7} cm^2/s of 4% SiO_2 membrane, and 0.995 x 10^{-7} cm^2/s of 4% s-SiO_2 membrane in figure 5.19 (i). On the other hand, the lowest methanol permeability of modified chitosan membranes in Figure 5.20 (ii) was reported to be 1.29 x 10^{-7} cm^2/s followed by 2.217 x 10^{-7} cm^2/s which belongs to 4% s-SiO_2 and 2% s-SiO_2 at 30 minutes. The decrease was made possible by the interaction between chitosan and nano-silica as nano-silica particles act as coupling agents, and disseminate over the chitosan matrix, finally covering the membrane pores effectively thus suppressing methanol by reducing its diffusion into the membrane (Liu, Su and Lai, 2004). (Kusumastuti *et al.*, 2016a) reported the same decrease in methanol permeability with the addition of silica, and permeability was reduced to the lowest of 7.75X10^{-7} cm^2/s.

A decreasing trend in methanol permeability can also be caused by the closely packed internal structure of the material and the longer diffusion path that was created by increased filler loading (Su *et al.*, 2007; Hanna Rosli *et al.*, 2020; Ng *et al.*, 2022). The lack of adequate chemical interaction between methanol and the ionic clusters presented in the matrix of polymeric membranes can also be used to explain this decrease (Vaghari *et al.*, 2013a; S. *et al.*, 2020). However, methanol permeability in Figure 5.19 increases with time, this is caused by a lack of free space along the membrane, as the membrane will stop absorbing methanol on its surface when it is (Yan and Jen, 2008; Kim, 2010; Awang, Jaafar and Ismail, 2018). It can be concluded that modification of chitosan with silica particles successfully reduces methanol permeability.

5.3.2.8. Selectivity of pure and sulfonated chitosan membranes with silica calcinated for 24h

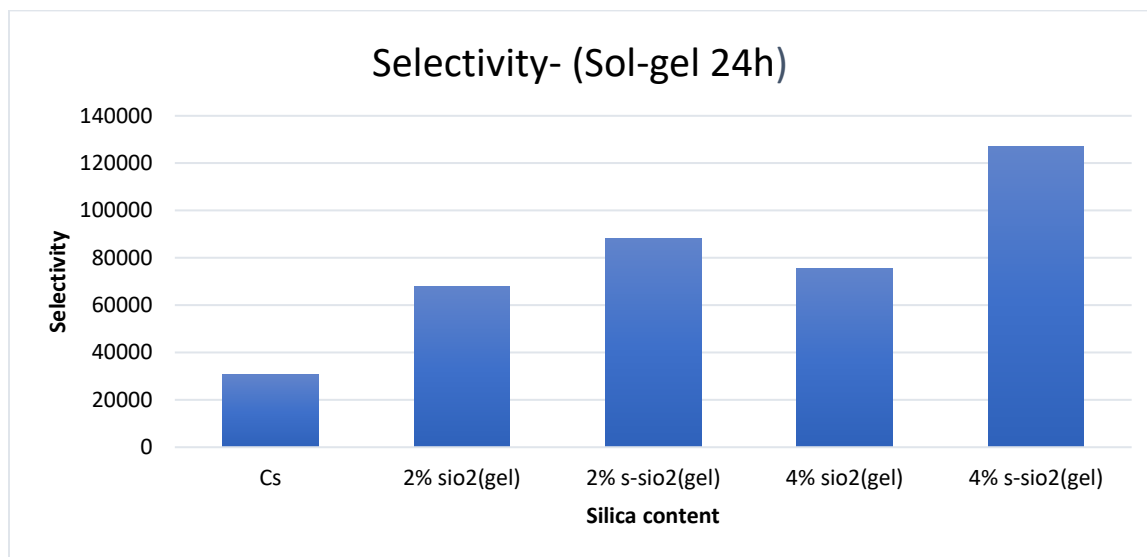Figure 5.20.(i). Membrane selectivity of (a) Cs (b) 2% s-SiO$_2$ (c) 2% SiO$_2$ (d) 4% s-SiO$_2$ (e) 4% SiO$_2$ -Sol-gel (24h)
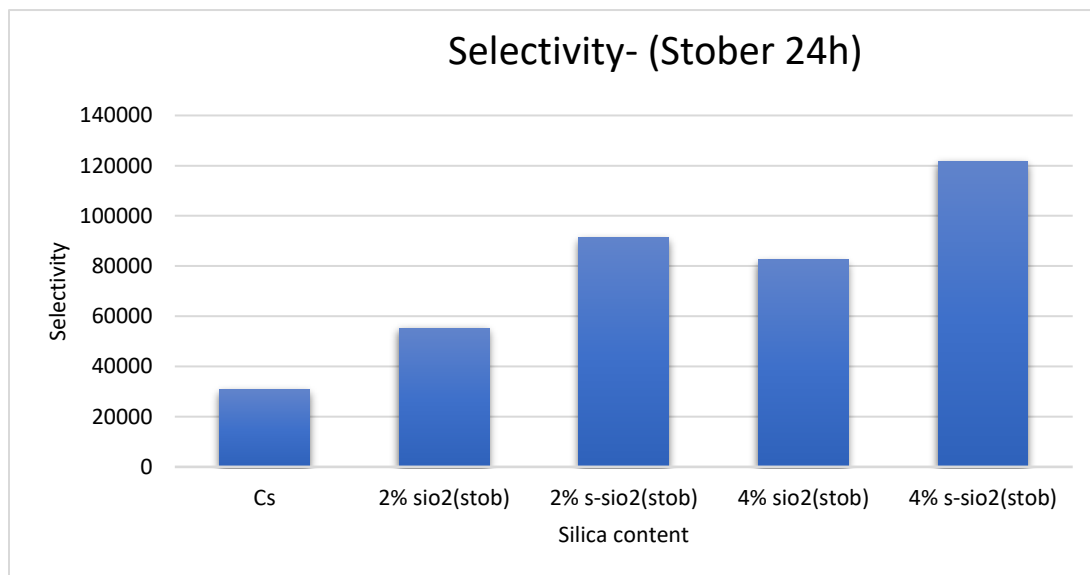

Figure 5.20.(ii). Membrane selectivity of (a) Cs (b) 2% s-SiO$_2$ (c) 2% SiO$_2$ (d) 4% s-SiO$_2$ (e) 4% SiO$_2$ -Stober (24h)

Figure 5.20 represents the membrane selectivity of chitosan membranes incorporated with silica calcinated for 24h. Membrane selectivity can be defined by the Nernst-Plank equation and Fick's law, which describe the proton and methanol flux, respectively, it can be used to determine the expression of the ratios of methanol absorption to ionic conductivity. Figure 5.20 indicates pure chitosan membrane selectivity of 3.067×10^4 and that of modified membranes highest selectivity of 1.269×10^5 and lowest of 5.527×10^4 corresponding to 4% s-SiO$_2$ of figure 5.20 (i) and 2% SiO$_2$ of figure 5.20 (ii) respectively. It is evident in Figure 5.20 that membranes incorporated with sulfonated silica possess high membrane selectivity, this is due to their high proton conductivity and low methanol permeability. The addition of -SO$_3$H groups improved the proton conductivity of the s-SiO$_2$/Cs and the improvement in the organic and inorganic phases' compatibility raised the methanol resistance of the membranes, which in turn led to higher selectivity than SiO$_2$/Cs. These modified silica-chitosan hybrid membranes, in particular the s-SiO$_2$/Cs membranes, present an intriguing promise for the development of DMFC due to their high selectivity, cheap cost, environmental friendliness, and ease of production (Wu *et al.*, 2007).

5.3.2.9. Tensile strength of pure and sulfonated chitosan membranes with silica calcinated for 24h
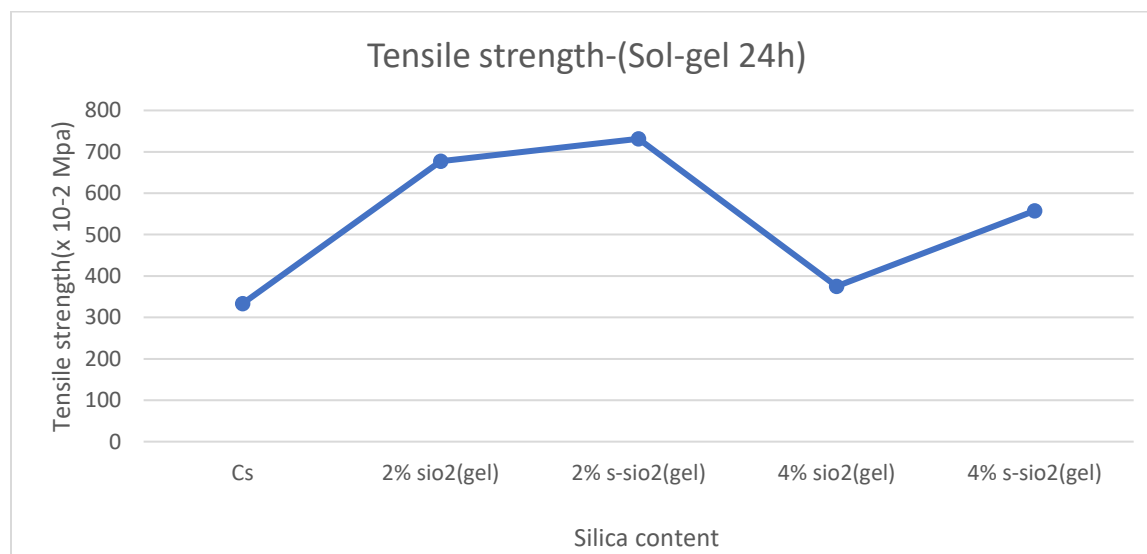
Figure 5.21.(i) Tensile strength of (a) Cs (b) 2% s-SiO$_2$ (c) 2% SiO$_2$ (d) 4% s-SiO$_2$ (e) 4% SiO$_2$ **- (Sol-gel 24h)**

Tensile strength-24h
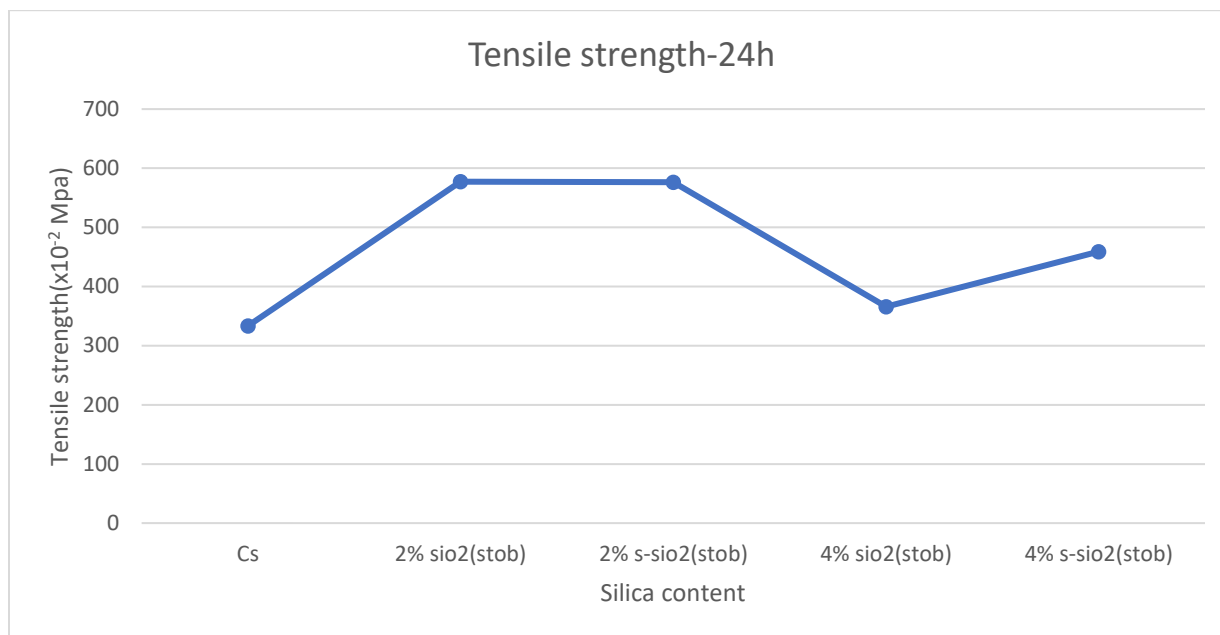
Figure 5.21.(ii). Tensile strength of (a) Cs (b) 2% s-SiO$_2$ (c) 2% SiO$_2$ (d) 4% s-SiO$_2$ (e) 4% SiO$_2$ –Stober (24h)

Figure 5.21 presents the tensile strength of membranes modified with silica from the Sol-gel and Stober process. Figure 5.21 indicates that chitosan's tensile strength reduces at greater silica levels. The optimal ratio that has the highest tensile strength is 7.3 Mpa of 2% s-SiO$_2$ (Sol-gel) followed by 5.77 Mpa of 2% s-SiO$_2$ (Stober) membrane. The decrease in tensile strength of these synthesized membranes agrees with what was reported by (Film, 2021), and the reported strength in the literature is lower than the one recorded in this research. Membranes with the addition over 4% of silica lend support to the hypothesis that silica may harden and toughen chitosan. The obtained results are like those reported in section 5.3.1.9 as both results indicate a drastic decrease in tensile strength with the addition of 4% nano-silica. The optimum strength of the membranes between those modified with silica for 2h and 24h is that of 2% s-Sio$_2$ (sol-gel) and the value is 7.1 Mpa. It was observed that the membranes modified with sulfonated silica have higher tensile strength which proves that modifying silica with sulfuric acid contributed to this increase.

Table 5.1. Chapter 5 Summary

	Sol-gel	Stober
Water-uptake	Increases as silica content increases	Increases as silica content increases
Proton conductivity	Increases as silica content increases	Increases as silica content increases
Ion exchange capacity	Increases as silica content increases	Increases as silica content increases
Methanol permeability	Decreases as silica content increase	Decreases as silica content increase
Mechanical Strength	High at low silica content, low at high silica 4%	High at low silica content, low at high silica 4%

5.3. Conclusion

The fabricated chitosan membranes modified with 0%, 2%, and 4% SiO_2 and s-SiO_2 calcinated for 2h and 24h were compared to their morphology, water uptake, proton conductivity, IEC, selectivity, and tensile strength. The FTIR indicates shift in peaks which indicate successful interaction of chitosan and silica. The membranes were found to have high water uptake and proton conductivity with suppressed methanol permeability which makes them an ideal choice for use in fuel cells. The water uptake, IEC, and proton conductivity were found to increase with higher filler content. It was found that modified membranes have water uptake lower than pure chitosan membranes. Optimum proton conductivity in s-SiO_2 membranes was found to be 0.238 S/cm of 4% s-SiO_2 (sol-gel 24h) membrane and that of SiO_2 membranes to be 0.225 S/cm (4% s-SiO_2). The membranes are in line with the properties of a fuel cell application. The membranes with silica calcinated for 24h show exceptional results in terms of proton conductivity and methanol permeability. It can be concluded that the Sol-gel method is the best method to synthesize silica particles.

5.5. References

Abdulwahid, R.T., Aziz, S.B. and Kadir, M.F.Z. (2022) 'Insights into ion transport in biodegradable solid polymer blend electrolyte based on FTIR analysis and circuit design', Journal of Physics and Chemistry of Solids, 167(April).

Amoura, M., Nassif, N., Roux, C., Livage, J. and Coradin, T. (2007). Sol–gel encapsulation of cells is not limited to silica: long-term viability of bacteria in alumina matrices. Chemical Communications, (39), pp.4015-4017.

Awang, N., Jaafar, J. and Ismail, A.F. (2018) 'Thermal stability and water content study of void-free electrospun SPEEK/Cloisite membrane for direct methanol fuel cell application', Polymers, 10(2).

Removal of pharmaceuticals from aquatic environment using modified biomaterials. (2020). Biointerface Research in Applied Chemistry, 10(4), pp.5986–5993.

Budnyak, T.M., Plypchuk, L.V. and Kolodynska.D. (2015) 'Synthesis and adsorption properties of chitosan-silica nanocomposite prepared by sol-gel method', Nanoscale Research Letters, 10(1).pp.1-10.

Carlson, A. (no date) Electrochemical properties of alternative polymer electrolytes in fuel cells.pp. 311-352.

Cui, L., Gao, S., Song, X., Huang, L., Dong, H., Liu, J., Chen, F. and Yu, S. (2018). Preparation and characterization of chitosan membranes. RSC Advances, 8(50), pp.28433–28439.

Demina, T.S., Gilman, A.B., Akopova, T.A. and Zelenetskii, A.N. (2014). Modification of the chitosan structure and properties using high-energy chemistry methods. High Energy Chemistry, 48(5), pp.293–302.

Diaconu, M., Tache, A., Eremia, A.V.M. and Gatea, A. (2010) 'Structural characterization of chitosan coated silicon nanoparticles -A FT-IR approach', UPB Scientific Bulletin, Series B: Chemistry and Materials Science, 72(3), pp. 115–122.

Feng, S., Shang, Y.M., Liu, G.S., Dong, W.Q., Xie, X.F., Xu, J.M. and Mathur, V.K (2010) 'Novel modification method to prepare crosslinked sulfonated poly(ether et.her ketone)/silica hybrid membranes for fuel cells', Journal of Power Sources, 195(19), pp. 6450–6458.

Film, S.C. (2021) 'Enhanced Mechanical Properties of Organic-Inorganic Chitosan/Nano Journal of Advanced Manufacturing Technology (JAMT) Silica Composite Film', 15(2), pp. 1–10.

Gaabour, L.H. (2019) 'Influence of silica nanoparticles incorporated with chitosan/polyacrylamide polymer nanocomposites', Journal of Materials Research and Technology, 8(2), pp. 2157–2163.

Gutzow, I., Pascova, R., Jordanov, N., Gutzov, S., Penkov, I., Markovska, I., Schmelzer, J.W.P. and Ludwig, F.-P. (2014). 3. Crystalline and Amorphous Modifications of Silica: Structure, Thermodynamic Properties, Solubility, and Synthesis. Glass, pp.137–196.

Han, S., Gu, B., Kim, S., Mun, D. and Kim, W. (2020) 'Effect of Sulfur Variation on the Vulcanizate Structure of Silica-Filled Styrene-Butadiene Rubber Compounds with a Sulfide – Silane Coupling Agent'.

Rosli, N.A.H., Loh, K.S., Wong, W.Y., Yunus, R.M., Lee, T.K., Ahmad, A. and Chong, S.T. (2020). Review of Chitosan-Based Polymers as Proton Exchange Membranes and Roles of Chitosan-Supported Ionic Liquids. International Journal of Molecular Sciences, 21(2).

Rosli, N.A.H., Loh, K.S., Wong, W.Y., Yunus, R.M., Lee, T.K., Ahmad, A. and Chong, S.T. (2020). Review of Chitosan-Based Polymers as Proton Exchange Membranes and Roles of Chitosan-Supported Ionic Liquids. International Journal of Molecular Sciences, 21(2).pp 619-632

Haragirimana, A., Li, N., Ingabire, P.B., Hu, Z. and Chen, S. (2020). Multi-component organic/inorganic blend proton exchange membranes based on sulfonated poly(arylene ether sulfone)s for fuel cells. Polymer, 210, pp. 123123-123015.

Hattori, M., Yamaura, S., Zhang, W., Sakamoto, W. and Yogo, T. (2015). Proton-conductive inorganic–organic hybrid membranes synthesized from a trimethoxysilylmethylstyrene–fluorophenylvinyl acid copolymer. Journal of Membrane Science, 488, pp.166–172.

Huang, S.L., Chen, M.L. and Lin, Y.S. (2017) 'Chitosan–silica anion exchange membrane for the vanadium redox flow energy storage battery applications', Reactive and Functional Polymers,119(July),pp.1–8.

Huber, L. (2020) 'The in fl uence of the ammonia concentration and the water content on the

water sorption behavior of ambient pressure dried silica xerogels', Journal of Sol-Gel Science and Technology, pp. 197–206.

Jiao, K. and Li, X. (2011) 'Water transport in polymer electrolyte membrane fuel cells', Progress in Energy and Combustion Science, pp. 221–291.

Kaczmarek, M.B., Struszczyk-Swita, K., Li, X., Szczęsna-Antczak, M. and Daroch, M. (2019). Enzymatic Modifications of Chitin, Chitosan,and Chitooligosaccharides. Frontiers in Bioengineering and Biotechnology, [online].pp. 1-13.

Ke, C.-C., Li, X.-J., Shen, Q., Qu, S.-G., Shao, Z.-G. and Yi, B.-L. (2011). Investigation on sulfuric acid sulfonation of in-situ sol–gel derived Nafion/SiO2 composite membrane. International Journal of Hydrogen Energy, 36(5), pp.3606–3613.

Kim, H. (2010) 'High Energy Density Direct Methanol Fuel Cells'.

Kusumastuti, E., Siniwi, W.T., Mahatmanti, F.W., Jumaeri, Atmaja, L. and Widiastuti, N. (2016). Modification of chitosan membranes with nanosilica particles as polymer electrolyte membranes.

Lai, Y.H., Kuo, M.C., Huang, J.C. and Chen, M. (2007). On the PEEK composites reinforced by surface-modified nano-silica. Materials Science and Engineering: A, 458(1-2), pp.158–169.

Lapicque, F., Bonnet, C., Huang, B.T. and Chatillon, Y. (2012). Analysis and Evaluation of Aging Phenomena in PEMFCs. Fuel Cell Engineering, pp.265–330.

Lee, E.-J., Shin, D.-S., Kim, H.-E., Kim, H.-W., Koh, Y.-H. and Jang, J.-H. (2009). Membrane of hybrid chitosan–silica xerogel for guided bone regeneration. Biomaterials, 30(5), pp.743–750.

Liu, H., Gong, C., Wang, J., Liu, X., Liu, H., Cheng, F., Wang, G., Zheng, G., Qin, C. and Wen, S. (2016). Chitosan/silica coated carbon nanotubes composite proton exchange membranes for fuel cell applications. Carbohydrate Polymers, 136, pp.1379–1385.

Liu, Y.-L., Su, Y.-H. and Lai, J.-Y. (2004). In situ crosslinking of chitosan and formation of chitosan–silica hybrid membranes with using γ-glycidoxypropyltrimethoxysilane as a crosslinking agent. Polymer, 45(20), pp.6831–6837.

Lue, S.J., Pai, Y.-L., Shih, C.-M., Wu, M.-C. and Lai, S.-M. (2015). Novel bilayer well-aligned

Nafion/graphene oxide composite membranes prepared using spin coating method for direct liquid fuel cells. Journal of Membrane Science, 493, pp.212–223.

Luo, Y., Liu, Y., Shen, J. and Van der Bruggen, B. (2022). Application of Bipolar Membrane Electrodialysis in Environmental Protection and Resource Recovery: A Review. Membranes, 12(9).

Morin-Crini, N., Lichtfouse, E., Torri, G. and Crini, G. (2019). Fundamentals and Applications of Chitosan. Sustainable Agriculture Reviews 35, [online] pp.49–123.

Muraishi, H. (1989) 'Crystallization of silica gel in alkaline solutions at 100 to 180°C: characterization of SiO2-Y by comparison with magadiite', American Mineralogist, 74(9–10), pp. 1147–1151.

Nakayama, R., Katsumata, K., Niwa, Y. and Namiki, N. (2020). Dependence of Water-Permeable Chitosan Membranes on Chitosan Molecular Weight and Alkali Treatment. Membranes, 10(11).

Narayanaswamy Venkatesan, P. and Dharmalingam, S. (2013) 'Characterization and performance study on chitosan-functionalized multi walled carbon nano tube as separator in microbial fuel cell', Journal of Membrane Science, 435, pp. 92–98.

Ng, W.W., Thiam, H.S., Pang, Y.L., Chong, K.C. and Lai, S.O. (2022). A State-of-Art on the Development of Nafion-Based Membrane for Performance Improvement in Direct Methanol Fuel Cells. Membranes, 12(5).

Nur, Y., Rohaeti, E. and Darusman, L.K. (2017) 'Optical sensor for the determination of Pb2+ based on immobilization of dithizone onto Chitosan-Silica membrane', Indonesian Journal of Chemistry, 17(1), pp. 7–14.

O'Hayre, R.P. (2017) 'Fuel cells for electrochemical energy conversion', EPJ Web of Conferences, 148, pp. 1–16.

Peighambardoust, S.J., Rowshanzamir, S. and Amjadi, M. (2010) 'Review of the proton exchange membranes for fuel cell applications', in International Journal of Hydrogen Energy, pp. 9349–9384.

Permana, D., Ahmad, L.Od. and Ramadhan, L.O.A.N.N. (2016) 'Enhanced Conductivity and

Ion Exchange Capacity of Chitosan Membranes through Modification with Lithium for Lithium Polymer Battery Application | Request PDF', WSEAS Transactions on Power Systems, 11, pp. 183–189.

Podgorbunskikh, E., Kuskov, T., Rychkov, D., Kuskov, B. and Byshkov, A. (2022) 'Mechanical Amorphization of Chitosan with Different Molecular Weights', Polymers, 14(20).

Purwanto, M. Atmaja, A., Mohamed, A.M., Salleh, M.A. amd Widstatuti, N. (2015) 'Biopolymer – based electrolyte membranes from chitosan incorporated with montmorillonite-crosslinked GPTMS for direct methanol fuel cell'.pp. 2314-2322.

Purwanto, M., Widiastuti, N., Saga, B.H. and Gusmawan, H. (2021). Synthesis of Composite Membrane Based Biopolymer Chitosan With Silica From Rice Husk Ash For Direct Methanol Fuel Cell Application. IOP Conference Series: Earth and Environmental Science, 830(1).

Fernandes Queiroz, M., Melo, K., Sabry, D., Sassaki, G. and Rocha, H. (2014). Does the Use of Chitosan Contribute to Oxalate Kidney Stone Formation? Marine Drugs, 13(1), pp.141–158.

Ramasubramanian, B., Rao, R.P., Chellappan, V. and Ramakrishna, S. (2022). Towards Sustainable Fuel Cells and Batteries with an AI Perspective. Sustainability, 14(23), pp.16001-16014.

Ramirez, L.M. (no date) 'Personal information sheet', pp. 6–7.

Rekik, S.B., Gassara, S., Bouaziz, J., Deratani, A. and Baklouti, S. (2017). Development and characterization of porous membranes based on kaolin/chitosan composite. Applied Clay Science, 143, pp.1–9.

Rosli, N.A.H., Loh, K.S., Wong, W.Y., Lee, T.K. and Ahmad, A. (2021). Hybrid Composite Membrane of Phosphorylated Chitosan/Poly (Vinyl Alcohol)/Silica as a Proton Exchange Membrane. Membranes, 11(9).

Rupiasih, N.N., Suharta, W.G. and Sumadiyasa, M. (2021) 'Tailored Manufacture Of Chitosan-Silver Nanoparticles (Agnp) Composite Membranes : Preparation , Characterization , And Antibacterial Agent', 8(6), pp. 3868–3879.

S., A.B., Handika, G., Purwanto, M., Pramono, E. and Linaya R., C. (2019). Electrolyte Membrane Composite from Modified Chitosan-Vanillin and Zeolite Filler for Direct Methanol Fuel Cell Application. Proceedings of the 1st International Conference on Industrial Technology.

Santoso, A.V. Susanto, A., Irawaty, W., Hadisoewignyo, L. and Hartono, S.B. (2019) 'Chitosan modified mesoporous silica nanoparticles as a versatile drug carrier with pH dependent properties', AIP Conference Proceedings, 2114(June 2019).

Science, E. (2021) 'Synthesis of Composite Membrane Based Biopolymer Chitosan With Silica From Rice Husk Ash For Direct Methanol Fuel Cell Application Synthesis of Composite Membrane Based Biopolymer Chitosan With Silica From Rice Husk Ash For Direct Methanol Fuel Cell Appli'.

Septiawan, M.R., Permana, D., Sabarwati, S.H., Ahmad, L.O. and Ramadhan, L.O.A.N. (2018). Functionalization of Chitosan with Maleic Anhydride for Proton Exchange Membrane. Indonesian Journal of Chemistry, 18(2), pp.313-320.

Shaari, N., Kamarudin, S.K., Basri, S., Shyuan, L.K., Masdar, M.S. and Nordin, D. (2018). Enhanced Proton Conductivity and Methanol Permeability Reduction via Sodium Alginate Electrolyte-Sulfonated Graphene Oxide Bio-membrane. Nanoscale Research Letters, 13(1).pp.345-350

Smitha, B., Sridhar, S. and Khan, A.A. (2005) 'Solid polymer electrolyte membranes for fuel cell applications - A review', Journal of Membrane Science, 259(1–2), pp. 10–26.

Srinophakun, P., Thanapimmetha, A., Plangsri, S., Vetchayakunchai, S. and Saisriyoot, M. (2017). Application of modified chitosan membrane for microbial fuel cell: Roles of proton carrier site and positive charge. Journal of Cleaner Production, 142, pp.1274–1282.

Su, Y.-H., Liu, Y.-L., Sun, Y.-M., Lai, J.-Y., Wang, D.-M., Gao, Y., Liu, B. and Guiver, M.D. (2007). Proton exchange membranes modified with sulfonated silica nanoparticles for direct methanol fuel cells. Journal of Membrane Science, [online] 296(1), pp.21–28.

Tran, T.N., Anh Pham, T.V., Phung Le, M.L., Thoa Nguyen, T.P. and Tran, V.M. (2013). Synthesis of amorphous silica and sulfonic acid functionalized silica used as reinforced phase for polymer electrolyte membrane. Advances in Natural Sciences: Nanoscience and

Nanotechnology, 4(4), pp.045007-045012.

Toskas, G., Cherif, C., Hund, R.-D., Laourine, E., Mahltig, B., Fahmi, A., Heinemann, C. and Hanke, T. (2013). Chitosan(PEO)/silica hybrid nanofibers as a potential biomaterial for bone regeneration. Carbohydrate Polymers, 94(2), pp.713–722.

Tsen, W.C. (2020) 'Composite proton exchange membranes based on chitosan and phosphotungstic acid immobilized one-dimensional attapulgite for direct methanol fuel cells', Nanomaterials, 10(9), pp. 1–15.

Vaghari, H., Jafarizadeh-Malmiri, H., Berenjian, A. and Anarjan, N. (2013). Recent advances in application of chitosan in fuel cells. Sustainable Chemical Processes, 1(1), pp.1-16.

Venkatesan, J., Ryu, B., Sudha, P.N. and Kim, S.-K. (2012). Preparation and characterization of chitosan–carbon nanotube scaffolds for bone tissue engineering. International Journal of Biological Macromolecules, 50(2), pp.393–402.

Vijayakumar, V. and Khastgir, D. (2018) 'Hybrid composite membranes of chitosan/sulfonated polyaniline/silica as polymer electrolyte membrane for fuel cells', Carbohydrate Polymers, 179(January), pp. 152–163.

Vijayalekshmi, V. and Khastgir, D. (2018) 'Fabrication and comprehensive investigation of physicochemical and electrochemical properties of chitosan-silica supported silicotungstic acid nanocomposite membranes for fuel cell applications', Energy, 142, pp. 313–330.

Walkowiak-Kulikowska, J., Wolska, J. and Koroniak, H. (2017) 'Polymers application in proton exchange membranes for fuel cells (PEMFCs)', Physical Sciences Reviews. De Gruyter. pp. 293-348.

Wang, J. and Wang, L. (2014) 'Preparation and properties of organic-inorganic alkaline hybrid membranes for direct methanol fuel cell application', Solid State Ionics, 255, pp. 96–103.

Widhi Mahatmanti, F., Nuryono and Narsito (2014) 'Physical characteristics of chitosan based film modified with silica and polyethylene glycol', Indonesian Journal of Chemistry, 14(2), pp. 131–137.

Wu, H., Zheng, B., Zheng, X., Wang, J., Yuan, W. and Jiang, Z. (2007). Surface-modified Y zeolite-filled chitosan membrane for direct methanol fuel cell. Journal of Power Sources,

173(2), pp.842–852.

Yan, T.Z. and Jen, T.C. (2008) 'Two-phase flow modeling of liquid-feed direct methanol fuel cell', International Journal of Heat and Mass Transfer, 51(5–6), pp. 1192–1204.

Yang, C.C., Lue, S.J. and Shih, J.Y. (2011) 'A novel organic/inorganic polymer membrane based on poly(vinyl alcohol)/poly(2-acrylamido-2-methyl-1-propanesulfonic acid/3-glycidyloxypropyl trimethoxysilane polymer electrolyte membrane for direct methanol fuel cells', Journal of Power Sources, 196(10), pp. 4458–4467.

Yang, Z. Peng, H. and Liu, T. (2010) 'Crystallization behavior of poly(ε-caprolactone)/layered double hydroxide nanocomposites', Journal of Applied Polymer Science, 116(5), pp. 2658–2667.

Zungu, N.P. (2021) 'Development of Sulfonated Chitosan Membranes Modified with Inorganic Nanofillers and Organic Materials for Fuel Cell Applications'.

Chapter 6 Conclusion and future work

Silica particles were synthesized by Sol-gel and Stober method and calcinated for 2h and 24h. The synthesis method used to produce silica particles and calcination time has a crucial impact on the physical characteristics of the particles such as the size. It can be concluded that the addition of sulfur reduces the surface area of silica particles as sulfonated silica particles have surface areas 271-280 m^2/g with Sol-gel having larger surface areas than that of Stober. Pure silica particles produced by sol-gel calcinated for 2h have a small surface area of 398 m^2/g compared to that of the Stober process with a surface area of 487 m^2/g. The XRD results of both pure and modified silica particles calcinated for 2h and 24h are amorphous and it can be concluded that the calcination time of silica particles has no impact on the structure of silica as both silica particles are amorphous. The FTIR shows the same functional groups and the modification of silica with the sulfonic group was successful. The Morphologies of synthesized silica calcinated for 2h and 24h through Sol-gel and Stober processes were confirmed to be amorphous with different shapes and sizes and the particles agglomerated due to silica's high energy level. The influence of the incorporation of silica particles in chitosan membranes was discussed in Chapter 5. According to the FTIR spectra, there is no chemical interaction between chitosan and silica particles (pure and modified); instead, only a physical interaction result. As silica content increases the characteristics of the modified silica-chitosan membrane such as water uptake, IEC, and proton conductivity increase while methanol permeability is reduced making it appropriate for use in the fuel cell. Water uptake of chitosan membrane incorporated with silica was found to increase with the addition of silica from 2% to 4% SiO_2 (Sol gel-24h) while that of modified silica increased from 46.97% to 51.35% and that of Stober sulfonated silica indicate an increase of 48.97% on 4% membrane. On the other hand, membranes with silica calcinated for 2h show an increase in water uptake from 40% to 56.21% Sol-gel and 37.9% to 51.97 Stober. Exceptional results regarding IEC and proton conductivity were found on the 4% s-SiO_2 membrane from sol-gel and Stober membranes having the highest IEC of 2.86 and 2,64 meq/g and high proton conductivities of 0.238 and 0.231 S/cm 4% s-SiO_2 Sol-gel(24h) and Stober(24h) respectively. The Proton conductivity of membranes incorporated with s-SiO_2/Cs is higher than that of the membranes incorporated with pure silica with 4% SiO_2/Cs having the highest proton conductivity of 0.234 S/cm Sol-gel (2h) and 0.238 S/cm Sol-gel (24h), and that of Stober having highest proton conductivity of 0.229 S/cm

Stober (2h) and 0.231 S/cm Stober (24h). Though the proton conductivity of membranes incorporated with pure silica was lower than that of those modified with sulfonated silica, their proton conductivity was higher than that of pure chitosan (0.151 S/cm) with the highest conductivity of 0.225 S/cm of 4% SiO_2 Sol-gel (24h) followed by 0.223 S/cm Sol-gel (2h). Developed membranes showed a decrease in methanol permeability when silica was added from 2% to 4% with lowest values of 1.53 x 10^{-7} cm^2/s of 4% SiO_2 membrane, and 0.995 x 10^{-7} cm^2/s of 4% s-SiO_2 by Sol-gel(24h) and that of Stober (24h) membranes having lowest values of 1.29 x 10^{-7} cm^2/s followed by 2.217 x 10^{-7} cm^2/s corresponding to 4% s-SiO_2 and 2% s-SiO_2 with lowest methanol permeability of 0.99 × 10^{-7} and 1.29 × 10^{-7} cm^2/s of 4% s-SiO_2 membrane. The 4% s-SiO_2 membranes give optimum results and can be used in fuel cell applications. Synthesized membranes can be used in fuel cell applications. It can be concluded that the addition of silica particles in chitosan suppresses methanol permeability.

For future work, synthesized membranes must be investigated for thermal stability using TGA. Proton conductivity and methanol permeability at high temperatures must also be evaluated. Evaluation of Fuel cell performance must also be done. High silica loading membrane must also be fabricated.